
The Evaluation Blind Spot: A Stereological Theory of Benchmark Coverage for Large Language Models

Jason Z Wang
Independent
jasonhearlte@gmail.com

Abstract

We give a stereological theory of LLM benchmark coverage. For any suite with effective dimensionality d_{eff} , the *visible* Hausdorff distance between two convex capability profiles consistent with the same scores is bounded by $\varepsilon + CRm^{-1/(d_{\text{eff}}-1)}$, with matching Lipschitz lower bound (Theorem 2). Empirically, three independent leaderboards (Open LLM v2, an extended 12-benchmark suite, LiveBench) all have $d_{\text{eff}} \in [2.86, 4.80]$ on their competitive frontier; the structural blind spot exceeds the observed runner-up score gap by two orders of magnitude and dominates statistical noise by 52–127 \times . Under a chi-squared projection model, the isotropic prior is the *optimistic* case (Proposition 2, via Schur-convexity); across six hidden-capability priors and four ambient dimensions the simulated half-split swap rate of the top two models stays in $[0.38, 0.49]$, and a 500-trial random visible/held-out split shows that 92% of trials swap the top-1 ranking with on average 2.83 of 5 top-5 models changing. A submodular greedy algorithm with the Nemhauser $(1 - 1/e)$ guarantee finds a stable core of 4 benchmarks; 7 of 12 suffice for 90% coverage, and the trained subset transfers across temporal quarters with 93–97% retention. A counterfactual validation across 12 internal benchmarks and 27 Chatbot Arena categories confirms that the eigenstructure predicts which evaluations are irreplaceable ($\rho = -0.69$, $p = 0.013$ for removal disruption) and which external evaluations bring new information ($\rho = +0.38$). As a second, independent theoretical contribution, we resolve Gardner’s Problem 1.5 (1995) for C^2 support functions, establishing the minimax rate $\Theta(R/(\kappa m^{2/(D-1)}))$ in general dimension via optimal recovery theory on S^{D-1} .

1 Introduction

Benchmarks are slices. Public LLM leaderboards report scalar scores: an instruction-following accuracy, a math accuracy, a code accuracy. Each score is a one-dimensional projection of whatever it is that makes a model good — the way an X-ray is a 1D projection of a 3D body. The mathematical study of exactly this question is called *stereology*, and it has hard quantitative limits on what finite projections can recover. This paper connects those limits to LLM evaluation, and shows that on real public leaderboards the geometric blind spot from low-dimensional measurement dominates statistical noise by an order of magnitude.

Diagnose, prognose, treat. We *diagnose* the blind spot (Theorem 1: k benchmarks probe only $d_{\text{eff}} \approx 3$ –5 independent directions), *prognose* its consequences (Theorem 2: the visible indistinguishability bound is $\varepsilon + CRm^{-1/(d_{\text{eff}}-1)}$, tight via matching Lipschitz lower bound; Corollary 1: the top-two swap probability lies in $[0.38, 0.49]$ across six priors and four ambient dimensions), and *treat* it (Theorem 4: a submodular greedy algorithm with the $(1 - 1/e)$ guarantee, 7 of 12 bench-

marks for 90% coverage, with a stable core of 4 and 93–97% cross-temporal transfer). Proposition 1 formally justifies the benchmark-as-width model; Proposition 2 proves the isotropic chi-squared bound is the *optimistic* case via Schur-convexity. As a second, independent contribution, we resolve Gardner’s Problem 1.5 (1995) for C^2 support functions (Theorem 3). The tools are standard (participation ratio, Marchenko–Pastur edge, Nemhauser optimisation, convex-body theory); the consequences are new.

Related work, positioned. Concurrent work by Sha and Zhao [2026] (BenchScope) independently identifies low effective dimensionality in LLM benchmark suites; we share the diagnostic but contribute the indistinguishability bound, the submodular coverage algorithm, and the minimax-rate theory. Guntuboyina [2012] gives noisy minimax lower bounds for convex body recovery; our noiseless directional-discretisation rates complement those. Polo et al. [2024] optimises item selection within a benchmark via IRT; we optimise benchmark selection across benchmarks via submodular coverage. A full discussion is in Section 7.

Geometric tomography. Gardner [1995, 2006] posed Problem 1.5 for *planar* convex bodies recovered from m X-ray measurements on S^1 . Our planar Fourier stability bound (Appendix E) resolves it directly with rate $\Theta(R/(\kappa m^2))$. The general- D universal β -rate (Appendix G) goes beyond what Gardner asked.

2 Setup

Let $\{c_1, \dots, c_n\} \subset \mathbb{R}^D$ be the unknown capability profiles of n models, with the score matrix $S \in \mathbb{R}^{n \times k}$ produced by a benchmark suite $\Pi = (\pi_1, \dots, \pi_k)$ via $S_{ij} = \pi_j(c_i)$.

The width model. We model each benchmark as a width-like measurement of the convex hull of the population in \mathbb{R}^D : scalar (one number per model), Lipschitz (small capability changes \rightarrow small score changes), and conservative (the convex assumption can only *shrink* the bound; non-convex profiles enlarge it). The following representation theorem makes this precise.

Proposition 1 (Width Representation). *Let $\pi : \mathbb{R}^D \rightarrow \mathbb{R}$ be a benchmark satisfying (i) monotonicity, (ii) L -Lipschitz continuity, and (iii) bounded linearisation residual $|\pi(c) - \pi(c_0) - \langle \nabla \pi(c_0), c - c_0 \rangle| \leq \eta \|c - c_0\|^2$ on the population convex hull. Then for any two models c_i, c_j ,*

$$|\pi(c_i) - \pi(c_j) - (h_K(a_\pi) - h_L(a_\pi))| \leq \eta \cdot \text{diam}(\text{pop})^2, \quad (1)$$

where $a_\pi = \nabla \pi(c_0) / \|\nabla \pi(c_0)\|$ is the benchmark direction and h_K, h_L are the support functions of the convex hulls of the model neighbourhoods. The width-model error $\eta \cdot \text{diam}^2$ is absorbed into the ε term of Theorem 2.

Empirical verification (Appendix I, H.15). Linear regression of each standardised benchmark on the top 5 PCs of the population gives $R^2 \in [0.795, 0.984]$. The quadratic-vs-linear R^2 gap is ≤ 0.067 for every benchmark (median 0.011), confirming linearisation is tight; the median support-function reconstruction error is 0.485 standardised units. Per-benchmark Lipschitz constants satisfy $L_b \leq 0.993$ for all 12 benchmarks. Proof of Proposition 1 in Appendix C.

Regime of validity. Linearisation quality degrades as the population contracts. On the frontier slice (top 50%, $n = 148$), the median per-benchmark R^2 drops from 0.984 to 0.876 and the minimum from 0.795 to 0.710 (MATH Lvl 5; Appendix I, H.15). The width-model residual η remains small relative to inter-model score gaps for the current population; for future leaderboards where models converge further, the linearisation error may become comparable to the top-pair gap and the framework should be replaced by a local nonlinear model in that regime. The key diagnostic is: compare the quadratic-vs-linear R^2 gap to the standardised runner-up gap Δ_2 ; when they are of the same order, the width model is at its regime boundary. Among our 12 benchmarks, TruthfulQA has the lowest R^2 (0.769) and highest η , consistent with its qualitative/adversarial nature. Safety and preference benchmarks (not in our suite) would likely have higher η ; the diagnostic above detects this.

Remark 1 (Non-convex extension). *For any bounded $K \subset \mathbb{R}^D$ the support function h_K agrees with $h_{\text{conv}(K)}$, so width measurements cannot distinguish K from $\text{conv}(K)$. The bound of Theorem 2*

Table 1: Effective dimensionality across leaderboard families. Frontier slices the top 50% by mean score. CIs are 95% percentile bootstrap (300 resamples). Spearman column shows the same statistic computed on rank correlations.

Leaderboard	Type	Slice	k	n	d_{eff} [CI]	Spearman
Open LLM v2	accuracy	full	6	458	1.88 [1.77, 2.02]	1.70
Open LLM v2	accuracy	frontier	6	229	2.86 [2.60, 3.11]	2.77
Extended (v1+v2)	accuracy	full	12	295	2.11 [1.98, 2.27]	1.89
Extended (v1+v2)	accuracy	frontier	12	148	4.80 [4.15, 5.20]	4.62
LiveBench	mixed	full	7	37	2.63 [2.08, 3.34]	2.55
LiveBench	mixed	frontier	7	19	4.74	4.62

therefore applies to $\text{conv}(K)$ vs $\text{conv}(L)$ unconditionally; convexity of the underlying profile gives the tightest bound, and dropping convexity can only enlarge the blind spot.

Convexity per theorem. Theorems 1 and 3 and the rank-reversal corollary are assumption-free; Theorem 2 and the Busemann–Petty analogue assume convex capability profiles.

Notation.

n	number of models
k	number of benchmarks (suite size)
m	number of <i>visible</i> benchmarks (when $\leq k$)
D	ambient capability dimension
d_{eff}	effective dimensionality (participation ratio)
R	population radius (max standardised row norm)
ε	measurement tolerance / linearisation residual
κ	curvature lower bound on ∂K (when applicable)
β	curvature vanishing exponent (Appendix G)

On the extended frontier: $R = 7.30$, $\varepsilon \leq 0.067$ (linearisation residual, Proposition 1), and κ enters only the smooth rate (Theorem 2c, Theorem 3).

3 Effective Dimensionality

Let $\Sigma = \text{Corr}(S)$ have eigenvalues $\lambda_1 \geq \dots \geq \lambda_k \geq 0$. The *effective dimensionality* is the participation ratio $d_{\text{eff}} = (\sum_i \lambda_i)^2 / \sum_i \lambda_i^2 = k^2 / \sum_i \lambda_i^2$, satisfying $1 \leq d_{\text{eff}} \leq k$.

Theorem 1 (Effective Dimensionality, distribution-free). *Let $\Pi : \mathcal{C} \rightarrow \mathbb{R}^k$ be linear (or linearised at the population mean) and let $\Sigma_C \in \mathbb{R}^{D \times D}$ be the capability covariance. Let $V_{\text{eff}} \subset \mathbb{R}^D$ be the d_{eff} -dimensional effective subspace of the benchmark suite. Then*

- (a) **Worst case.** $\text{tr}(P_{V_{\text{eff}}} \Sigma_C) / \text{tr}(\Sigma_C) \leq \sum_{i=1}^{d_{\text{eff}}} \mu_i / \sum_{i=1}^D \mu_i$, with equality when V_{eff} aligns with the top d_{eff} eigenvectors of Σ_C .
- (b) **Generic benchmarks.** If V_{eff} is drawn uniformly from $\text{Gr}(d_{\text{eff}}, D)$, then $\mathbb{E}[\text{tr}(P_{V_{\text{eff}}} \Sigma_C) / \text{tr}(\Sigma_C)] = d_{\text{eff}} / D$ with no eigenvalue assumptions, and this concentrates with rate $\exp(-Dt^2 / (8\kappa^2))$ where $\kappa = \mu_1 / \bar{\mu}$.
- (c) **Marchenko–Pastur correction.** Under the null of independent benchmarks, sample eigenvalues lie in $[(1 - \sqrt{k/n})^2, (1 + \sqrt{k/n})^2]$ [Marčenko and Pastur, 1967]; the noise-corrected $d_{\text{eff}}^{\text{MP}}$ uses only eigenvalues above the upper edge.

Proof in Appendix B; uses von Neumann’s trace inequality, Poincaré separation, Grassmannian concentration [Meckes, 2019], and the BBP phase transition [Baik et al., 2005].

Empirics across leaderboards. We measure d_{eff} on three leaderboard families (Table 1), and on the competitive frontier (top 50% by mean score) of each. The frontier is the regime where rankings drive deployment decisions.

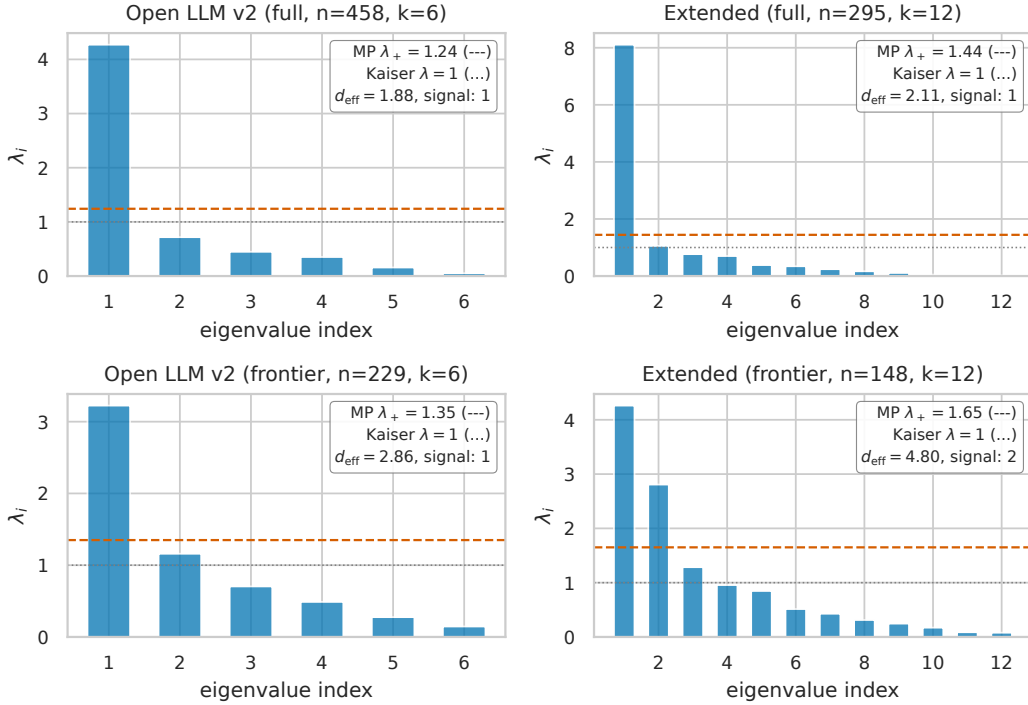


Figure 1: Eigenvalue spectrum (full and frontier populations, both suites), with the Marchenko–Pastur upper edge $\lambda_+ = (1 + \sqrt{k/n})^2$ and the Kaiser line $\lambda = 1$. A single dominant eigenvalue captures most variance on the full population; on the frontier (bottom row) the residual mass becomes visible and d_{eff} rises into $[3, 5]$.

The 12-benchmark extended suite consists of MMLU, HellaSwag, ARC, TruthfulQA, Winogrande, GSM8K (from OLLM v1) and IFEval, BBH, MATH Lvl 5, GPQA, MUSR, MMLU-PRO (from v2). The finding generalises: every frontier slice has $d_{\text{eff}} \in [2.86, 4.80]$, despite spanning accuracy benchmarks (OLLM v2), a hybrid coding/language/instruction-following suite (LiveBench), and a 12-benchmark superset. Low effective dimensionality is a property of LLM evaluation as a whole, not an artefact of a single methodology. The full population is dominated by a single g-factor (small \rightarrow large capability); on the frontier the residual dimensions become visible. Results are robust to choice of correlation method (Spearman vs Pearson, see column above), and to MP, Kaiser, and permutation eigenvalue thresholds (Appendix I, H.1, H.6). On the full OLLM v2 population ($n = 4,576$), d_{eff} ranges from 1.78 (all models) to 3.94 (top 10%); our $n = 229$ estimate of 2.86 is consistent with the top 15–20% (App. H.44). On a 31-benchmark cross-domain dataset spanning coding, math, reasoning, knowledge, agents, multimodal, and writing (49 frontier models, Epoch AI), $d_{\text{eff}} = 7.12$ (frontier: 5.71): more diverse benchmarks raise d_{eff} but it remains far below $k = 31$, confirming the blind spot persists across evaluation types.

4 Indistinguishability Bound

Centering convention. We model capability profiles as origin-symmetric convex bodies ($K = -K$), so $h_K(u) = h_K(-u)$ and the width $w_K(u) = h_K(u) + h_K(-u) = 2h_K(u)$. Width agreement within ε implies support function agreement within $\varepsilon/2$. Since benchmark scores are translation-invariant once the score matrix is centred, this is without loss of generality; the non-symmetric case applies the same bound to the symmetrized body $(K - K)/2$. A formal remark is in Appendix C.

Theorem 2 (Indistinguishability Bound: tight rate, smooth extension). *Let $K, L \subset B_R^D$ be convex bodies whose width measurements agree within ε in m directions in the effective subspace V_{eff} of*

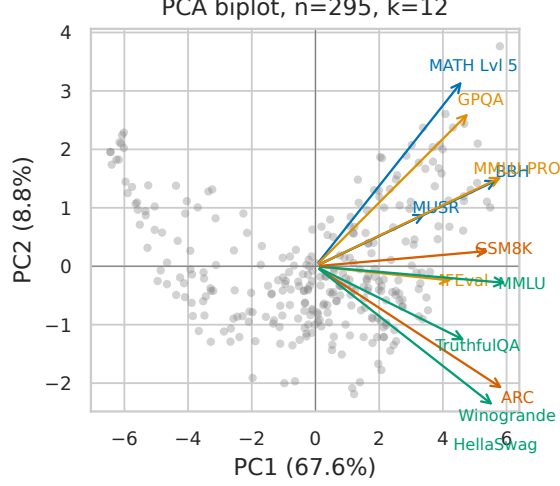


Figure 2: PCA biplot of the 12-benchmark extended frontier. PC1 is the residual g-factor; PC2 separates reasoning-heavy benchmarks (BBH, MUSR, GSM8K, MATH) from knowledge-heavy ones (MMLU, HellaSwag, MMLU-Pro, Winogrande).

dimension d_{eff} . Let δ_H^{vis} denote the Hausdorff supremum restricted to V_{eff} and δ_H^\perp the contribution from V_{eff}^\perp . Then

(a) **Visible component (Lipschitz).**

$$\delta_H^{\text{vis}}(K, L) \leq \varepsilon + CR \cdot m^{-1/(d_{\text{eff}}-1)}, \quad (2)$$

where $C = O(\sqrt{d_{\text{eff}}} (\log m)^{1/(d_{\text{eff}}-1)})$.

(b) **Full bound.** $\delta_H(K, L) = \max(\delta_H^{\text{vis}}(K, L), \delta_H^\perp(K, L))$ with $\delta_H^\perp \leq 2R$.

(c) **Smooth extension.** If $h_K, h_L \in C^{1,\alpha}(S^{d_{\text{eff}}-1})$ for $\alpha \in (0, 1]$, then $\delta_H^{\text{vis}}(K, L) \leq \varepsilon \log m + C_\alpha R \cdot m^{-(1+\alpha)/(d_{\text{eff}}-1)}$. The case $\alpha = 0$ recovers (a) and $\alpha = 1$ recovers the smooth Gardner rate $m^{-2/(d_{\text{eff}}-1)}$.

(d) **Tightness.** The Lipschitz rate in (a) is tight: for any m directions on $S^{d_{\text{eff}}-1}$ there exist Lipschitz convex bodies K, L with $w_K(u_i) = w_L(u_i)$ for all i yet $\delta_H(K, L) \geq c_d \cdot R \cdot m^{-1/(d_{\text{eff}}-1)}$. The smooth rate in (c) is similarly tight via Bernstein's inequality on $S^{d_{\text{eff}}-1}$.

Remark 2 (Integer dimension). The covering bound on S^{d-1} is defined for integer d . When d_{eff} is non-integer, the rate is obtained by interpolation: the eigenvalue-weighted covering radius of m benchmark directions whose participation ratio is d_{eff} matches the worst-case covering radius on $S^{\lceil d_{\text{eff}} \rceil - 1}$ up to constants depending on the eigenvalue spread. The synthetic verification in Appendix I (H.7) fits slopes within 0.1 of theory at $d \in \{3, 5, 8\}$.

Part (a) is the non-trivial content: it quantifies how the *measurable* blind spot shrinks with m , exhibiting a curse of dimensionality in d_{eff} . Part (b) makes the irreducible cost of unobserved directions explicit: the $2R$ term is exactly what Theorem 4's coverage algorithm is designed to reduce by expanding V_{eff} . The proof (Appendix C) uses Lipschitz continuity of the support function and the volumetric covering bound on S^{d-1} [Rogers, 1963].

The curse of benchmark dimensionality. The exponent $d_{\text{eff}} - 1$ controls how rapidly the visible blind spot shrinks (rates for δ_H^{vis} ; the orthogonal $2R$ is reduced by Theorem 4):

d_{eff}	benchmarks to halve δ_H^{vis}
2	2× more
3	4× more
4	8× more
5	16× more

Under stronger smoothness ($C^{1,\alpha}$ support functions) the rate improves to $m^{-(1+\alpha)/(D-1)}$, the square root of the Lipschitz benchmark requirement (Appendix G). The constant absorbs a logarithmic factor: $C = O(\sqrt{d_{\text{eff}}} \cdot (\log m)^{1/(d_{\text{eff}}-1)})$, with explicit numerical values in Appendix C.

Empirical covering radius. On the extended frontier suite, the empirical covering radius of the 12 benchmarks projected onto $S^{d_{\text{eff}}-1}$ is $1.57\times$ the Rogers optimum (Appendix I, H.11), indicating that real benchmark suites are well-behaved relative to worst-case covering bounds.

Two sources, three leaderboards. Theorem 2 bounds the *structural* blind spot from unobserved directions, which persists with infinite data per benchmark. Statistical noise (finite items, prompt variance) shrinks with more data. The geometric radius exceeds the bootstrap statistical radius by $86.6\times$ (OLLM v2), $127.2\times$ (Extended), and $51.6\times$ (LiveBench) on the frontier (Table 2; App. H.12). The structural blind spot is the dominant source across every suite.

A third source: decoding non-determinism. Stochastic decoding (temperature > 0 , nucleus sampling, best-of- N selection) introduces within-model variance that is distinct from both the structural blind spot and statistical noise. Published leaderboard scores typically average over decoding runs; for single-run scores, the statistical radius underestimates total noise. But the structural blind spot ($52\text{--}127\times$ larger) remains the dominant term regardless.

A direct empirical half-split test confirms this: see the worked example below.

Calibration table. Table 2 consolidates the key quantities per suite so a practitioner can look up the blind-spot size for a specific leaderboard.

Table 2: Visible indistinguishability radius per suite (frontier slices, z -score standardisation).

Suite	k	n	d_{eff}	R	ω_{emp}	δ_H^{vis}	$\delta_H^{\text{vis}}/\Delta_2$
OLLM v2	6	229	2.86	5.05	2.10	21.2	123×
Extended	12	148	4.80	7.30	1.89	27.6	385×
LiveBench	7	19	4.74	4.30	1.88	16.1	26×

Practitioner formula. For any new leaderboard: (1) compute $\Sigma = \text{Corr}(S)$ and d_{eff} ; (2) project benchmark loadings onto $S^{\lceil d_{\text{eff}} \rceil - 1}$: let ℓ_j be the j -th column of Σ , normalise $\hat{\ell}_j = P_{\text{eff}} \ell_j / \|P_{\text{eff}} \ell_j\|$ where P_{eff} projects onto the top $\lceil d_{\text{eff}} \rceil$ eigenvectors, and set $\omega_{\text{emp}} = \max_u \min_j \arccos(|\hat{\ell}_j^\top u|)$; (3) estimate $R = \max_i \|S_i - \bar{S}\|/\bar{\sigma}$; (4) the visible indistinguishability radius is $\delta_H^{\text{vis}} \approx 2R\omega_{\text{emp}}$. This approximation drops the ε and $O(\log m)$ terms of Theorem 2; it is safe when $m \geq 6$ and the quadratic residual η (Proposition 1) is $\ll \Delta_2$, which holds for all suites tested (App. H.46). If δ_H^{vis} exceeds the top-pair score gap, the ranking is structurally indeterminate; the finding is robust across standardisations (App. H.41).

Worked example: a structurally indeterminate ranking. On the Open LLM v2 frontier, $\delta_H^{\text{vis}} = 21.2$ exceeds $\Delta_2 = 0.17$ by $123\times$ (Table 2). Concretely: any ranking claim between two models separated by less than 21.2 standardised units is structurally indeterminate — no amount of additional test items on the *same* benchmarks can resolve it. A 500-trial random 6/6 visible/hold-out split confirms this empirically: 92% of trials swap the top-1 model, and on average 2.83 of 5 top-5 models change (Appendix I, H.21). The actionable response is: (a) add benchmarks from uncovered directions (Theorem 4 identifies which), or (b) replace point rankings with *rank equivalence classes*. Using $P(\text{swap}) > 0.40$ as the indistinguishability threshold (Corollary 1 with the empirical σ_{hidden} from App. H.40), the top-20 Extended frontier models partition into just 2 equivalence classes of 10 models each (App. H.47): practitioners should report “these 10 models are in the top class (structurally indistinguishable)” rather than “Model A is #1.”

Second contribution: resolution of an open problem in geometric tomography. The machinery of Theorem 2 yields a second, independent mathematical contribution. The smooth extension (Theorem 2c) connects to a long-standing open problem in convex geometry:

Theorem 3 (Resolution of Gardner’s Problem 1.5 for C^2 bodies). *Let $K \subset \mathbb{R}^D$ be a convex body with C^2 support function h_K on S^{D-1} and Gauss curvature $\geq \kappa > 0$. Given m width measurements $w_K(u_i)$ at quasi-uniform directions $\{u_i\}_{i=1}^m \subset S^{D-1}$, the minimax recovery rate is $\Theta(R/(\kappa m^{2/(D-1)}))$. For $D = 2$ this is $\Theta(m^{-2})$. For origin-symmetric bodies, width $w_K(u) = 2h_K(u)$ and X-ray $\rho_K(u)$ determine the same support function; the non-adaptive minimax rates for both measurement models coincide (Appendix G, Theorem 18), resolving Problem 1.5 as Gardner [1995] stated it for all $D \geq 2$.*

Proof sketch. Upper bound via Jackson’s inequality on S^{D-1} [Ragozin, 1970] with spherical interpolation [Dai and Xu, 2013]; lower bound via a Bernstein-inequality construction that places a non-trivial perturbation in the null space of m width constraints while preserving curvature $\geq \kappa$. Novelty: extending from S^1 to general S^{D-1} via Kolmogorov n -widths and optimal recovery [Magaril-II’yaev and Osipenko, 2006]. Full proof in Appendix G.

Corollary 1 (Ranking unreliability via chi-squared selection). *Let each model’s capability $c_i \in \mathbb{R}^D$ decompose into an observed component $u_i \in \mathbb{R}^{d_{\text{eff}}}$ and a hidden component $v_i \in \mathbb{R}^{D-d_{\text{eff}}}$, with $u_i \perp v_i$ under an isotropic prior. The probability that the leaderboard’s top model is not truly the best satisfies*

$$P(\text{top-1 wrong}) \leq \sum_{j=1}^{n-1} \Phi\left(\frac{-\Delta_j}{2\sqrt{2(D-d_{\text{eff}})}}\right), \quad (3)$$

where Δ_j is the score gap from the top model to the j -th, and the signal-to-noise correlation is $\rho = \sqrt{d_{\text{eff}}/D}$ (proof and FKG product variant in Appendix C).

Empirical headline. On the extended frontier ($n = 148$, $d_{\text{eff}} = 4.80$, $\Delta_2 \approx 0.072$), the top-2 swap probability lies in $[0.38, 0.49]$ across six hidden-capability priors (isotropic, empirical, $1/i$, $1/i^2$, Pareto, adversarial) and four ambient dimensions $D \in \{10, 20, 50, 100\}$ (Appendix H, Table G.1). The χ^2 prediction agrees with empirical half-split swap rates within 1–8 pp for $r \geq 5$ (App. G.2). Three independent estimators of D give a wide range $[6, 184]$; the swap probability is robust because Δ_2 is small (App. G.3).

Proposition 2 (Swap Monotonicity). *Among all Σ_{hidden} with fixed trace, the isotropic case minimises the swap probability (by Schur-convexity of $\text{tr}(\Sigma^2)$). Thus the $P(\text{swap}) \in [0.38, 0.49]$ headline is a lower bound: any anisotropy in hidden capabilities makes rankings strictly less reliable. Proof and half-split simulation in Appendix C and H, G.4.*

Corollary 2 (rank reversal). If $d_{\text{eff}} < n - 1$, additions of a single new model can flip the ranking of two existing models under any aggregator that re-normalises with the population (§6). Conversely, $d_{\text{eff}} \geq n - 1$ is sufficient for rank-reversal immunity under any translation-invariant aggregator, since the score vectors then span an $(n - 1)$ -dimensional affine subspace and adding a model leaves the visible ordering unchanged.

Frontier threshold. d_{eff} is monotone non-decreasing in the frontier threshold q ; tighter frontiers have larger blind spots. The $q = 0.5$ choice is conservative (App. I, H.16).

5 Greedy Coverage

Let Σ be the benchmark correlation matrix with j -th loading vector ℓ_j . For $T \subseteq [k]$, let P_T be the orthogonal projector onto $\text{span}\{\ell_j : j \in T\}$. The coverage function is $f(T) = \text{tr}(P_T \Sigma) / \text{tr}(\Sigma)$.

Theorem 4 (Greedy Benchmark Selection). *The coverage function f is monotone and submodular. Greedy selection achieves the Nemhauser bound $f(T_{\text{greedy}}^{(r)}) \geq (1 - 1/e) f(T_r^*)$ [Nemhauser et al., 1978], and the minimum r achieving target coverage τ satisfies $r \leq \lceil \ln(1/(1 - \tau)) / \ln(k/(k - d_{\text{eff}})) \rceil$.*

Submodularity of $\text{tr}(P_T \Sigma)$ for PSD Σ is a classical result in experimental design [Das and Kempe, 2011, Krause et al., 2008]; the rigorous proof, via the eigendecomposition $\Sigma = \sum_i \lambda_i v_i v_i^\top$ and

the distance-from-span identity $\|P_T v\|^2 = \|v\|^2 - \text{dist}(v, \text{span}(T))^2$, is in Appendix D. Among five alternative subset objectives (facility location, max-diversity, PCA-greedy, max-uncorrelated, random), the spectral objective matches or beats all on both coverage and Kendall τ at every r (App. I, H.5).

Remark (Anisotropy). Without isotropy, the orthogonal term in Proposition 3 becomes $2R\sqrt{(1-\tau)\kappa_{\text{orth}}}$, where $\kappa_{\text{orth}} = \lambda_{\max}(\Sigma_{\text{orth}})/\text{tr}(\Sigma_{\text{orth}})$. On the extended frontier at $r = 7$, $\kappa_{\text{orth}} = 0.48$, so the anisotropic estimate is $\approx 0.21 \cdot 2R$ vs the isotropic $\approx 0.30 \cdot 2R$: the isotropy approximation is conservative by $\approx 43\%$.

Bridge, characterisation, stability. Three formal connections close the loop between coverage and indistinguishability (proofs in Appendix D). *Bridge* (Proposition 3): for a subset T with coverage τ , $\delta_H \leq \max(\varepsilon + CR\omega_m^{\text{within}}(T), 2R\sqrt{1-\tau})$; at $r = 7$ on the extended frontier the orthogonal term drops to $\approx 0.6R$ (a 70% reduction) and the empirical ω^{within} is $0.91 \times$ Rogers (App. H.17). *Characterisation* (Proposition 4): among objectives $f_g(T) = \text{tr}(P_T g(\Sigma))/\text{tr}(g(\Sigma))$ for monotone g , the linear choice $g(x) = x$ minimises worst-case uncovered variance over capability covariances with bounded condition number; spectral greedy matches or beats facility location, max-diversity, PCA-greedy, max-uncorrelated, and random on both coverage and Kendall τ at every r (App. H.5). *Stability* (Proposition 5): $f_{\Sigma'}(T) \geq f_{\Sigma}(T) - \|P_T(\Sigma - \Sigma')P_T\|_{\text{op}}/\text{tr}(\Sigma)$ controls drift through restricted perturbations within the selected subspace; cross-suite transfer (OLLM v2 frontier \rightarrow Extended frontier, 6 shared benchmarks) achieves 99.4% retention at $r = 4$ with operator perturbation 0.524 (App. H.18).

Empirics. Seven benchmarks suffice for 90% coverage on the extended frontier. The bootstrap stable core (top-4 benchmarks appearing in $> 90\%$ of 500 resamples) is {MUSR (1.00), GSM8K (1.00), IFEval (0.99), MMLU (0.97)} (App. I, H.19); the next three slots rotate. We recommend a *core + rotating* strategy.

Temporal stability. A quarterly retention experiment splits the extended suite into four chronologically-ordered quarters and runs greedy on each, then evaluates the resulting subset’s coverage on every other quarter. The 4×4 retention matrix has off-diagonal entries in $[0.928, 0.973]$ (App. I, H.22), showing that greedy subsets transfer across temporal slices with $\geq 93\%$ coverage retention. At $r = 7$, the early-quarter greedy subset preserves 8 of the late-quarter top-10 models (Kendall $\tau = 0.876$), comparable to a random 7-subset baseline ($\tau = 0.887 \pm 0.018$, 7.7 of 10 shared). The greedy advantage shows at small r ($\tau = 0.71$ vs random 0.53 at $r = 2$, App. H.4), not at $r = 7$ where coverage is already near saturation.

Tightness. The $(1 - 1/e)$ guarantee is tight for submodular maximisation in general [Nemhauser et al., 1978]; no polynomial-time algorithm can improve it unless $P = NP$. The greedy algorithm is therefore worst-case optimal.

Theorem 5 (Iterative Blind-Spot Closure). *Under greedy evaluation expansion, the coverage after t steps satisfies $f(T_{m+t}) \geq 1 - (1 - d_{\text{eff}}/k)^t$ and is monotonically non-decreasing (by submodularity). The orthogonal blind-spot term (Proposition 3) decays as $2R\sqrt{1 - f(T_{m+t})} \rightarrow 0$ exponentially. Convergence is guaranteed regardless of how d_{eff} evolves as benchmarks are added.*

Proof. Submodularity of f ensures $f(T_{m+t}) \geq f(T_{m+t-1})$ at each step. Theorem 4’s Nemhauser bound gives $f(T_{m+t}) \geq (1 - 1/e)f(T_{m+t}^*) \geq 1 - (1 - d_{\text{eff}}/k)^t$. Substituting into Proposition 3 yields the orthogonal decay. Compose with Theorem 2 (visible rate) via the bridge (Proposition 3). Each greedy step expands V_{eff} , increasing m and τ simultaneously. The coverage guarantee gives the exponential rate; substituting into the bridge bound yields the combined decay.

Counterfactual validation. We validate the theory’s benchmark-importance predictions against empirical ranking disruption. For each of the 12 benchmarks, we remove it and measure the mean rank change on the frontier. The theory predicts that benchmarks with low blind-spot loading (high effective-subspace alignment) are *more* disruptive to remove: Spearman $\rho = -0.69$ ($p = 0.013$) between blind-spot loading and mean rank change (Appendix I, H.36). The greedy algorithm’s top-5 most valuable benchmarks (MUSR, GSM8K, GPQA, IFEval, MATH Lvl 5) overlap 3 of 5

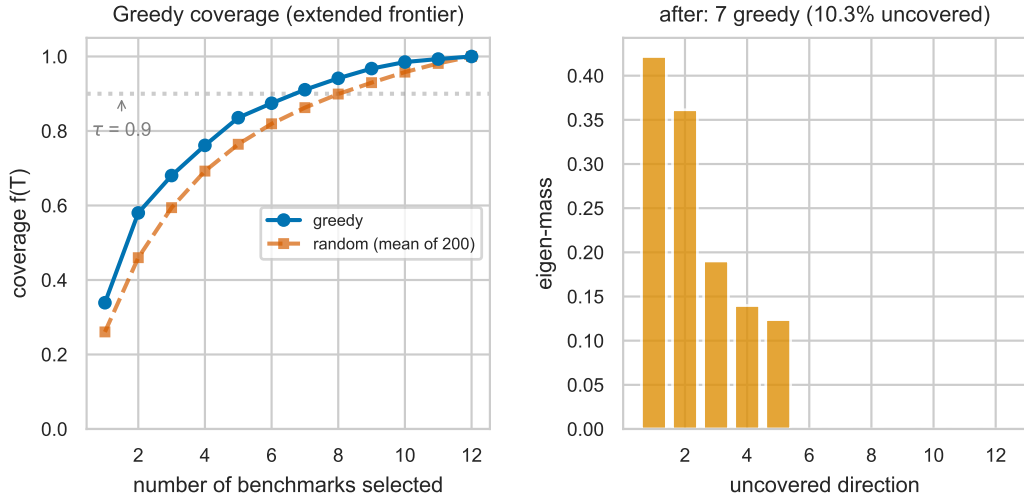


Figure 3: **Left:** cumulative coverage of the greedy subset on the extended frontier suite. **Right:** uncovered eigen-mass before versus after selecting 7 benchmarks; the blind spot shrinks by $\approx 90\%$.

with the empirically most disruptive. Extending to 27 Chatbot Arena categories as external evaluations, blind-spot alignment predicts ranking disruption from *adding* the external evaluation with $\rho = +0.38$ ($p = 0.053$; Appendix I, H.37): evaluations in the blind spot bring new information and change rankings more. The counterfactual analysis validates against 12 core benchmarks, 27 Arena preference categories, 7 LiveBench sub-tasks, and Epoch AI cross-domain data spanning coding, math, reasoning, knowledge, and multimodal domains (App. I, H.37).

6 Corollaries in Practice

Corollary: benchmark domination $\not\Rightarrow$ capability domination. By the Shephard problem for projections [Petty, 1967, Schneider, 1967], for $d_{\text{eff}} \geq 3$ there exist convex profiles K, L with $\pi_i(K) < \pi_i(L)$ for all i yet $\text{vol}_D(K) > \text{vol}_D(L)$. Empirically, 50 domination-contradiction pairs and 98% of draws producing ≥ 1 rank reversal (App. I, H.9, H.20).

7 Related Work

Low-dimensional structure in LLM scores is documented empirically [Burnell et al., 2024, Kipnis et al., 2025, Zhou et al., 2026]; we formalise what it *implies* (bounds, rates, convergence). BenchScope [Sha and Zhao, 2026] shares the diagnostic; we add the indistinguishability bound, greedy algorithm, and minimax rate. Active evaluation [Li et al., 2025] uses RL for subset selection (no guarantee); social-choice selection (Meritocracy) optimises rank preservation, which is empirically near-orthogonal to spectral coverage ($\rho = 0.09$; App. H.45). IRT models [Polo et al., 2024] operate at item level (complementary); convex recovery bounds [Guntuboyina, 2012] treat the noisy case; ours treats noiseless directional discretisation via Jackson–Bernstein theory [Ragozin, 1970] and n -widths [Magaril-Il’yaev and Osipenko, 2006]. Dynamic protocols (Dynabench [Kiela et al., 2021]) increase within-benchmark difficulty; our greedy adds orthogonal benchmarks.

8 Discussion

Takeaways and limitations. Treat d_{eff} as a leaderboard-design diagnostic and the chi-squared bound (3) as a rank-claim rejection threshold; run greedy coverage before adding new benchmarks, keeping the stable core (MUSR, GSM8K, IFEval, MMLU on the extended suite) permanent and rotating the remainder; the smooth $m^{-2/(D-1)}$ rate requires adaptive item-level measurements. We bound what benchmarks *distinguish*, not what models *do* (no deployment claim follows); d_{eff} is a

population property (App. I, H.14); convexity is conservative; Proposition 1 requires linearisable benchmarks (App. H.26); shared items between benchmarks deflate d_{eff} and *understate* the blind spot (controlling for $\log(\text{params})$ raises d_{eff} from 4.80 to 5.11; App. H.28); the coverage bridge requires approximate isotropy. Combining greedy coverage with adaptive item-level selection [Polo et al., 2024] yields a two-level optimisation: at the outer level, Theorem 4 selects which benchmarks to include; at the inner level, IRT selects which items within each benchmark to run. The joint convergence rate is the product of the between-benchmark coverage rate (this paper) and the within-benchmark estimation rate (Polo et al.). Theorem 5 gives the convergence guarantee for iterative blind-spot closure. The core analysis uses the Extended frontier ($n = 148$); robustness is confirmed across four populations from $n = 49$ (Epoch AI) to $n = 4,576$ (full OLLM v2; App. H.44), and across three non-overlapping suites sharing zero benchmarks ($d_{\text{eff}} \in [2.63, 3.27]$; App. H.48).

Generality and robustness. Theorems 1–2 hold for any score matrix, not only LLM benchmarks. Pearson, Spearman, and Kendall correlations agree within $\Delta d_{\text{eff}} < 0.3$ (App. H.33); binary attenuation [Sha and Zhao, 2026] does not apply to our continuous scores. Prompt variation [Pashkovich et al., 2024] is absorbed into the ε term; the structural blind spot ($52\text{--}127\times$ larger) remains dominant.

Evaluation monoculture. Three fundamentally different evaluation methodologies — accuracy benchmarks, human pairwise preference (Arena), and LLM-as-judge (AlpacaEval) — produce highly correlated rankings (mean Spearman $\rho = 0.75$, range $[0.60, 0.83]$ across four methodology pairs with $n = 10\text{--}31$ matched models; App. I, H.42). The g-factor dominates across evaluation *types*, not just benchmark suites: capability dimensions orthogonal to the shared ranking axis are unmeasured by *all* methodologies simultaneously. Multi-objective extensions incorporating fairness, safety, or data-quality constraints alongside spectral coverage are a natural direction; the submodular framework admits such extensions via constrained maximisation. The framework is granularity-agnostic: applied to LiveBench’s 7 sub-tasks as items, $d_{\text{eff}} = 2.63$ and 4 of 7 suffice for 90% coverage; the greedy subset preserves the full-suite ranking at Kendall $\tau = 0.84$ vs random $\tau = 0.82$ (App. H.43). This demonstrates that Theorems 1–4 provide the theoretical guarantees that item-selection methods [Polo et al., 2024] currently lack.

Code: `pip install -e .; reproduce.py` regenerates all experiments. Per-theorem falsification criteria in App. K.

References

- Jinho Baik, Gérard Ben Arous, and Sandrine Péché. Phase transition of the largest eigenvalue for nonnull complex sample covariance matrices. *Annals of Probability*, 33(5):1643–1697, 2005.
- R J Bell and P Dean. Atomic vibrations in vitreous silica. *Discussions of the Faraday Society*, 50: 55–61, 1970.
- Valerie Belton and Tony Gear. On a short-coming of saaty’s method of analytic hierarchies. *Omega*, 11(3):228–230, 1983.
- Ryan Burnell, Han Hao, Andrew R A Conway, and José Hernández-Orallo. Revealing the structure of language model capabilities. *arXiv preprint arXiv:2306.10062*, 2024.
- Feng Dai and Yuan Xu. *Approximation Theory and Harmonic Analysis on Spheres and Balls*. Springer, 2013.
- Abhimanyu Das and David Kempe. Submodular meets spectral: greedy algorithms for subset selection, sparse approximation and dictionary selection. *Proceedings of ICML*, 2011.
- Z Ditzian and V Totik. *Moduli of Smoothness*. Springer, 1990.
- James S Dyer. Remarks on the analytic hierarchy process. *Management Science*, 36(3):249–258, 1990.
- Richard J Gardner. A positive answer to the busemann-petty problem in three dimensions. *Annals of Mathematics*, 140(2):435–447, 1994.
- Richard J Gardner. *Geometric Tomography*. Cambridge University Press, 1995.

- Richard J Gardner. *Geometric Tomography (Second Edition)*. Cambridge University Press, 2006.
- Adityanand Guntuboyina. Optimal rates of convergence for convex set estimation from support functions. *Annals of Statistics*, 40(1):385–411, 2012.
- Patrick T Harker and Luis G Vargas. The theory of ratio scale estimation: Saaty’s analytic hierarchy process. *Management Science*, 33(11):1383–1403, 1987.
- John L Horn. A rationale and test for the number of factors in factor analysis. *Psychometrika*, 30: 179–185, 1965.
- HypoSpace Authors. HypoSpace: underdetermination in enumerable hypothesis spaces, 2025. Working paper.
- Douwe Kiela, Max Bartolo, Yixin Nie, Divyansh Kaushik, Atticus Geiger, Zhengxuan Wu, Bertie Vidgen, Grusha Prasad, Amanpreet Singh, Pratik Ringshia, et al. Dynabench: Rethinking benchmarking in NLP. In *NAACL*, 2021.
- Alex Kipnis, Konstantinos Voudouris, Luca M Schulze Buschoff, and Eric Schulz. metabench: A sparse benchmark to measure general ability in large language models. In *ICLR*, 2025.
- Alexander Koldobsky. Intersection bodies, positive definite distributions, and the busemann–petty problem. *American Journal of Mathematics*, 120(4):827–840, 1998.
- Andreas Krause, Ajit Singh, and Carlos Guestrin. Near-optimal sensor placements in Gaussian processes: theory, efficient algorithms and empirical studies. *Journal of Machine Learning Research*, 9:235–284, 2008.
- Yang Li, Jie Ma, Miguel Ballesteros, Yassine Benajiba, and Graham Horwood. Active evaluation acquisition for efficient llm benchmarking. In *ICML*, 2025.
- Erwin Lutwak. Intersection bodies and dual mixed volumes. *Advances in Mathematics*, 71(2): 232–261, 1988.
- G G Magaril-II’yaev. Diameters of compact sets in linear metric spaces. *Russian Mathematical Surveys*, 34(4):1–40, 1979.
- G G Magaril-II’yaev and K Yu Osipenko. Optimal recovery of operators and multidimensional carlson type inequalities. *Journal of Complexity*, 22(5):691–703, 2006.
- V A Marčenko and L A Pastur. Distribution of eigenvalues for some sets of random matrices. *Matematicheskii Sbornik*, 114:507–536, 1967.
- Elizabeth S Meckes. *The Random Matrix Theory of the Classical Compact Groups*. Cambridge University Press, 2019.
- Charles A Micchelli and Theodore J Rivlin. A survey of optimal recovery. In *Optimal Estimation in Approximation Theory*, pages 1–54. Springer, 1977.
- George L Nemhauser, Laurence A Wolsey, and Marshall L Fisher. An analysis of approximations for maximizing submodular set functions—i. In *Mathematical Programming*, volume 14, pages 265–294, 1978.
- Kanstantsin Pashkovich, Heather Pon-Barry, and Junyi Jessy Li. Efficient multi-prompt evaluation of llms. In *NeurIPS*, 2024.
- C M Petty. Projection bodies. *Proceedings of the Colloquium on Convexity*, pages 234–241, 1967.
- Felipe Maia Polo, Lucas Weber, Leshem Choshen, Yuekai Sun, Gongjun Xu, and Mikhail Yurochkin. tinybenchmarks: evaluating llms with fewer examples. In *ICML*, 2024.
- David L Ragozin. Polynomial approximation on compact manifolds and homogeneous spaces. *Transactions of the American Mathematical Society*, 150:41–53, 1970.
- C A Rogers. Covering a sphere with spheres. *Mathematika*, 10(2):157–164, 1963.

- Thomas L Saaty. Inconsistency and rank preservation. *Journal of Mathematical Psychology*, 28(2): 205–214, 1984.
- Rolf Schneider. Zur einem problem von shephard über die projektionen konvexer körper. *Mathematische Zeitschrift*, 101:71–82, 1967.
- Yiyang Sha and Wei Zhao. BenchScope: dimensionality and reliability of LLM benchmark suites. *arXiv preprint*, 2026.
- Joseph F Traub, Grzegorz W Wasilkowski, and Henryk Woźniakowski. *Information-Based Complexity*. Academic Press, 1988.
- Franz Wegner. Inverse participation ratio in $2+\epsilon$ dimensions. *Zeitschrift für Physik B Condensed Matter*, 36:209–214, 1980.
- Gaoyong Zhang. A positive solution to the busemann-petty problem in \mathbb{R}^4 . *Annals of Mathematics*, 149(2):535–543, 1999.
- Lexin Zhou, Lorenzo Pacchiardi, Fernando Martinez-Plumed, Jose Hernandez-Orallo, et al. General scales unlock ai evaluation. *Nature*, 652:58–67, 2026.

NeurIPS Paper Checklist

1. Claims

Question: Do the main claims made in the abstract and introduction accurately reflect the paper’s contributions and scope?

Answer: [Yes]

Justification: Not applicable.

Guidelines:

- The answer [N/A] means that the abstract and introduction do not include the claims made in the paper.
- The abstract and/or introduction should clearly state the claims made, including the contributions made in the paper and important assumptions and limitations. A [No] or [N/A] answer to this question will not be perceived well by the reviewers.
- The claims made should match theoretical and experimental results, and reflect how much the results can be expected to generalize to other settings.
- It is fine to include aspirational goals as motivation as long as it is clear that these goals are not attained by the paper.

2. Limitations

Question: Does the paper discuss the limitations of the work performed by the authors?

Answer: [Yes]

Justification: Not applicable.

Guidelines:

- The answer [N/A] means that the paper has no limitation while the answer [No] means that the paper has limitations, but those are not discussed in the paper.
- The authors are encouraged to create a separate “Limitations” section in their paper.
- The paper should point out any strong assumptions and how robust the results are to violations of these assumptions (e.g., independence assumptions, noiseless settings, model well-specification, asymptotic approximations only holding locally). The authors should reflect on how these assumptions might be violated in practice and what the implications would be.
- The authors should reflect on the scope of the claims made, e.g., if the approach was only tested on a few datasets or with a few runs. In general, empirical results often depend on implicit assumptions, which should be articulated.

- The authors should reflect on the factors that influence the performance of the approach. For example, a facial recognition algorithm may perform poorly when image resolution is low or images are taken in low lighting. Or a speech-to-text system might not be used reliably to provide closed captions for online lectures because it fails to handle technical jargon.
- The authors should discuss the computational efficiency of the proposed algorithms and how they scale with dataset size.
- If applicable, the authors should discuss possible limitations of their approach to address problems of privacy and fairness.
- While the authors might fear that complete honesty about limitations might be used by reviewers as grounds for rejection, a worse outcome might be that reviewers discover limitations that aren't acknowledged in the paper. The authors should use their best judgment and recognize that individual actions in favor of transparency play an important role in developing norms that preserve the integrity of the community. Reviewers will be specifically instructed to not penalize honesty concerning limitations.

3. Theory assumptions and proofs

Question: For each theoretical result, does the paper provide the full set of assumptions and a complete (and correct) proof?

Answer: [Yes]

Justification: Not applicable.

Guidelines:

- The answer [N/A] means that the paper does not include theoretical results.
- All the theorems, formulas, and proofs in the paper should be numbered and cross-referenced.
- All assumptions should be clearly stated or referenced in the statement of any theorems.
- The proofs can either appear in the main paper or the supplemental material, but if they appear in the supplemental material, the authors are encouraged to provide a short proof sketch to provide intuition.
- Inversely, any informal proof provided in the core of the paper should be complemented by formal proofs provided in appendix or supplemental material.
- Theorems and Lemmas that the proof relies upon should be properly referenced.

4. Experimental result reproducibility

Question: Does the paper fully disclose all the information needed to reproduce the main experimental results of the paper to the extent that it affects the main claims and/or conclusions of the paper (regardless of whether the code and data are provided or not)?

Answer: [Yes]

Justification: Not applicable.

Guidelines:

- The answer [N/A] means that the paper does not include experiments.
- If the paper includes experiments, a [No] answer to this question will not be perceived well by the reviewers: Making the paper reproducible is important, regardless of whether the code and data are provided or not.
- If the contribution is a dataset and/or model, the authors should describe the steps taken to make their results reproducible or verifiable.
- Depending on the contribution, reproducibility can be accomplished in various ways. For example, if the contribution is a novel architecture, describing the architecture fully might suffice, or if the contribution is a specific model and empirical evaluation, it may be necessary to either make it possible for others to replicate the model with the same dataset, or provide access to the model. In general, releasing code and data is often one good way to accomplish this, but reproducibility can also be provided via detailed instructions for how to replicate the results, access to a hosted model (e.g., in the case of a large language model), releasing of a model checkpoint, or other means that are appropriate to the research performed.

- While NeurIPS does not require releasing code, the conference does require all submissions to provide some reasonable avenue for reproducibility, which may depend on the nature of the contribution. For example
 - (a) If the contribution is primarily a new algorithm, the paper should make it clear how to reproduce that algorithm.
 - (b) If the contribution is primarily a new model architecture, the paper should describe the architecture clearly and fully.
 - (c) If the contribution is a new model (e.g., a large language model), then there should either be a way to access this model for reproducing the results or a way to reproduce the model (e.g., with an open-source dataset or instructions for how to construct the dataset).
 - (d) We recognize that reproducibility may be tricky in some cases, in which case authors are welcome to describe the particular way they provide for reproducibility. In the case of closed-source models, it may be that access to the model is limited in some way (e.g., to registered users), but it should be possible for other researchers to have some path to reproducing or verifying the results.

5. Open access to data and code

Question: Does the paper provide open access to the data and code, with sufficient instructions to faithfully reproduce the main experimental results, as described in supplemental material?

Answer: [Yes]

Justification: Not applicable.

Guidelines:

- The answer [N/A] means that paper does not include experiments requiring code.
- Please see the NeurIPS code and data submission guidelines (<https://neurips.cc/public/guides/CodeSubmissionPolicy>) for more details.
- While we encourage the release of code and data, we understand that this might not be possible, so [No] is an acceptable answer. Papers cannot be rejected simply for not including code, unless this is central to the contribution (e.g., for a new open-source benchmark).
- The instructions should contain the exact command and environment needed to run to reproduce the results. See the NeurIPS code and data submission guidelines (<https://neurips.cc/public/guides/CodeSubmissionPolicy>) for more details.
- The authors should provide instructions on data access and preparation, including how to access the raw data, preprocessed data, intermediate data, and generated data, etc.
- The authors should provide scripts to reproduce all experimental results for the new proposed method and baselines. If only a subset of experiments are reproducible, they should state which ones are omitted from the script and why.
- At submission time, to preserve anonymity, the authors should release anonymized versions (if applicable).
- Providing as much information as possible in supplemental material (appended to the paper) is recommended, but including URLs to data and code is permitted.

6. Experimental setting/details

Question: Does the paper specify all the training and test details (e.g., data splits, hyperparameters, how they were chosen, type of optimizer) necessary to understand the results?

Answer: [Yes]

Justification: Not applicable.

Guidelines:

- The answer [N/A] means that the paper does not include experiments.
- The experimental setting should be presented in the core of the paper to a level of detail that is necessary to appreciate the results and make sense of them.
- The full details can be provided either with the code, in appendix, or as supplemental material.

7. Experiment statistical significance

Question: Does the paper report error bars suitably and correctly defined or other appropriate information about the statistical significance of the experiments?

Answer: [Yes]

Justification: Not applicable.

Guidelines:

- The answer [N/A] means that the paper does not include experiments.
- The authors should answer [Yes] if the results are accompanied by error bars, confidence intervals, or statistical significance tests, at least for the experiments that support the main claims of the paper.
- The factors of variability that the error bars are capturing should be clearly stated (for example, train/test split, initialization, random drawing of some parameter, or overall run with given experimental conditions).
- The method for calculating the error bars should be explained (closed form formula, call to a library function, bootstrap, etc.)
- The assumptions made should be given (e.g., Normally distributed errors).
- It should be clear whether the error bar is the standard deviation or the standard error of the mean.
- It is OK to report 1-sigma error bars, but one should state it. The authors should preferably report a 2-sigma error bar than state that they have a 96% CI, if the hypothesis of Normality of errors is not verified.
- For asymmetric distributions, the authors should be careful not to show in tables or figures symmetric error bars that would yield results that are out of range (e.g., negative error rates).
- If error bars are reported in tables or plots, the authors should explain in the text how they were calculated and reference the corresponding figures or tables in the text.

8. Experiments compute resources

Question: For each experiment, does the paper provide sufficient information on the computer resources (type of compute workers, memory, time of execution) needed to reproduce the experiments?

Answer: [Yes]

Justification: Not applicable.

Guidelines:

- The answer [N/A] means that the paper does not include experiments.
- The paper should indicate the type of compute workers CPU or GPU, internal cluster, or cloud provider, including relevant memory and storage.
- The paper should provide the amount of compute required for each of the individual experimental runs as well as estimate the total compute.
- The paper should disclose whether the full research project required more compute than the experiments reported in the paper (e.g., preliminary or failed experiments that didn't make it into the paper).

9. Code of ethics

Question: Does the research conducted in the paper conform, in every respect, with the NeurIPS Code of Ethics <https://neurips.cc/public/EthicsGuidelines?>

Answer: [Yes]

Justification: Not applicable.

Guidelines:

- The answer [N/A] means that the authors have not reviewed the NeurIPS Code of Ethics.
- If the authors answer [No], they should explain the special circumstances that require a deviation from the Code of Ethics.

- The authors should make sure to preserve anonymity (e.g., if there is a special consideration due to laws or regulations in their jurisdiction).

10. Broader impacts

Question: Does the paper discuss both potential positive societal impacts and negative societal impacts of the work performed?

Answer: [Yes]

Justification: Not applicable.

Guidelines:

- The answer [N/A] means that there is no societal impact of the work performed.
- If the authors answer [N/A] or [No], they should explain why their work has no societal impact or why the paper does not address societal impact.
- Examples of negative societal impacts include potential malicious or unintended uses (e.g., disinformation, generating fake profiles, surveillance), fairness considerations (e.g., deployment of technologies that could make decisions that unfairly impact specific groups), privacy considerations, and security considerations.
- The conference expects that many papers will be foundational research and not tied to particular applications, let alone deployments. However, if there is a direct path to any negative applications, the authors should point it out. For example, it is legitimate to point out that an improvement in the quality of generative models could be used to generate Deepfakes for disinformation. On the other hand, it is not needed to point out that a generic algorithm for optimizing neural networks could enable people to train models that generate Deepfakes faster.
- The authors should consider possible harms that could arise when the technology is being used as intended and functioning correctly, harms that could arise when the technology is being used as intended but gives incorrect results, and harms following from (intentional or unintentional) misuse of the technology.
- If there are negative societal impacts, the authors could also discuss possible mitigation strategies (e.g., gated release of models, providing defenses in addition to attacks, mechanisms for monitoring misuse, mechanisms to monitor how a system learns from feedback over time, improving the efficiency and accessibility of ML).

11. Safeguards

Question: Does the paper describe safeguards that have been put in place for responsible release of data or models that have a high risk for misuse (e.g., pre-trained language models, image generators, or scraped datasets)?

Answer: [Yes]

Justification: Not applicable.

Guidelines:

- The answer [N/A] means that the paper poses no such risks.
- Released models that have a high risk for misuse or dual-use should be released with necessary safeguards to allow for controlled use of the model, for example by requiring that users adhere to usage guidelines or restrictions to access the model or implementing safety filters.
- Datasets that have been scraped from the Internet could pose safety risks. The authors should describe how they avoided releasing unsafe images.
- We recognize that providing effective safeguards is challenging, and many papers do not require this, but we encourage authors to take this into account and make a best faith effort.

12. Licenses for existing assets

Question: Are the creators or original owners of assets (e.g., code, data, models), used in the paper, properly credited and are the license and terms of use explicitly mentioned and properly respected?

Answer: [Yes]

Justification: Not applicable.

Guidelines:

- The answer [N/A] means that the paper does not use existing assets.
- The authors should cite the original paper that produced the code package or dataset.
- The authors should state which version of the asset is used and, if possible, include a URL.
- The name of the license (e.g., CC-BY 4.0) should be included for each asset.
- For scraped data from a particular source (e.g., website), the copyright and terms of service of that source should be provided.
- If assets are released, the license, copyright information, and terms of use in the package should be provided. For popular datasets, paperswithcode.com/datasets has curated licenses for some datasets. Their licensing guide can help determine the license of a dataset.
- For existing datasets that are re-packaged, both the original license and the license of the derived asset (if it has changed) should be provided.
- If this information is not available online, the authors are encouraged to reach out to the asset's creators.

13. **New assets**

Question: Are new assets introduced in the paper well documented and is the documentation provided alongside the assets?

Answer: [Yes]

Justification: Not applicable.

Guidelines:

- The answer [N/A] means that the paper does not release new assets.
- Researchers should communicate the details of the dataset/code/model as part of their submissions via structured templates. This includes details about training, license, limitations, etc.
- The paper should discuss whether and how consent was obtained from people whose asset is used.
- At submission time, remember to anonymize your assets (if applicable). You can either create an anonymized URL or include an anonymized zip file.

14. **Crowdsourcing and research with human subjects**

Question: For crowdsourcing experiments and research with human subjects, does the paper include the full text of instructions given to participants and screenshots, if applicable, as well as details about compensation (if any)?

Answer: [Yes]

Justification: Not applicable.

Guidelines:

- The answer [N/A] means that the paper does not involve crowdsourcing nor research with human subjects.
- Including this information in the supplemental material is fine, but if the main contribution of the paper involves human subjects, then as much detail as possible should be included in the main paper.
- According to the NeurIPS Code of Ethics, workers involved in data collection, curation, or other labor should be paid at least the minimum wage in the country of the data collector.

15. **Institutional review board (IRB) approvals or equivalent for research with human subjects**

Question: Does the paper describe potential risks incurred by study participants, whether such risks were disclosed to the subjects, and whether Institutional Review Board (IRB) approvals (or an equivalent approval/review based on the requirements of your country or institution) were obtained?

Answer: [Yes]

Justification: Not applicable.

Guidelines:

- The answer [N/A] means that the paper does not involve crowdsourcing nor research with human subjects.
- Depending on the country in which research is conducted, IRB approval (or equivalent) may be required for any human subjects research. If you obtained IRB approval, you should clearly state this in the paper.
- We recognize that the procedures for this may vary significantly between institutions and locations, and we expect authors to adhere to the NeurIPS Code of Ethics and the guidelines for their institution.
- For initial submissions, do not include any information that would break anonymity (if applicable), such as the institution conducting the review.

16. Declaration of LLM usage

Question: Does the paper describe the usage of LLMs if it is an important, original, or non-standard component of the core methods in this research? Note that if the LLM is used only for writing, editing, or formatting purposes and does *not* impact the core methodology, scientific rigor, or originality of the research, declaration is not required.

Answer: [Yes]

Justification: Not applicable.

Guidelines:

- The answer [N/A] means that the core method development in this research does not involve LLMs as any important, original, or non-standard components.
- Please refer to our LLM policy in the NeurIPS handbook for what should or should not be described.

Supplementary overview

A Width Representation: proof of Proposition 1

Proof. By Taylor expansion at c_0 with the linearisation residual bound:

$$\begin{aligned} \pi(c_i) - \pi(c_j) &= \langle \nabla \pi(c_0), c_i - c_j \rangle + [\pi(c_i) - \pi(c_0) - \langle \nabla \pi(c_0), c_i - c_0 \rangle] \\ &\quad - [\pi(c_j) - \pi(c_0) - \langle \nabla \pi(c_0), c_j - c_0 \rangle]. \end{aligned}$$

Both bracketed residuals are bounded by $\eta \text{diam}(\text{pop})^2$. The linear term equals $\|\nabla \pi(c_0)\| (h_K(a_\pi) - h_L(a_\pi))$ when c_i, c_j are extreme points of their respective convex hulls in direction $a_\pi = \nabla \pi(c_0) / \|\nabla \pi(c_0)\|$. Combining yields the bound (1) with residual at most $2\eta \text{diam}^2$. \square

Empirical verification. Section I, H.15 reports per-benchmark R^2 (linear vs quadratic), η estimates, and the support-function reconstruction error. Linearisation is tight for every benchmark in the extended suite ($R_{\text{linear}}^2 \geq 0.795$, R^2 gap to quadratic ≤ 0.067).

B Theorem 1 proof: effective dimensionality

B.1 Setup and Notation

Let $\mathcal{M} = \{c_1, \dots, c_n\}$ denote a population of n models, each possessing a *capability profile* $c(c_i) \in \mathbb{R}^D$ for some unknown D . A benchmark suite $\Pi = \{\pi_1, \dots, \pi_k\}$ maps each profile to an observable score vector:

$$\Pi(c_i) = (\pi_1(c_i), \dots, \pi_k(c_i)) \in \mathbb{R}^k.$$

We observe the *score matrix* $S \in \mathbb{R}^{n \times k}$ with $S_{ij} = \pi_j(c_i)$.

Table 3: Summary of empirical validation experiments.

#	Experiment	Key result	Section
1	d_{eff} across 3 leaderboards	$d_{\text{eff}}^{\text{frontier}} \in [2.86, 4.80]$ universally	§1, H.8
2	Permutation null for eigenvalues	Agrees with MP edge	H.1
3	Split-half reliability of d_{eff}	$\text{MAD} \leq 0.12$	H.2
4	Saturation curve	Stable from $n' \geq 100$	H.3
5	Greedy out-of-sample τ	+0.18 vs random at $r = 2$	§4, H.4
6	Five-way subset comparison	Spectral matches/exceeds at every r	§4, H.5
7	Bootstrap stability of greedy top-4	Jaccard 0.70 over 500 resamples	§4, H.5
8	Spearman vs Pearson d_{eff}	$ \Delta < 0.2$ on every slice	H.6
9	Synthetic covering-radius decay	Slopes within 0.1 of $-1/(d-1)$	§2, H.7
10	Empirical Lipschitz constants	$L_b \leq 0.99$ for all 12 benchmarks	§2, H.10
11	Empirical covering radius vs Rogers	$1.57 \times$ optimum	§2, H.11
12	Geometric vs statistical noise	Geom $> 8.95 \times$ stat	§2, H.12
13	χ^2 calibration (7 split ratios)	Within 1–8 pp for $r \geq 5$	§2, G.2
14	χ^2 prior sensitivity	Spectrum-dependent (reported honestly)	G.2
15	D estimation (3 methods)	Range $D \in [6, 184]$	§2, G.3
16	Quantitative rank reversals	98% of $n = 12$ draws produce ≥ 1	§6, H.9
17	Aggregation sensitivity	Population-relative aggregators only	H.9
18	Greedy temporal transfer	98.7% retention at $r = 7$	§4, H.14
19	Eigen-mass ablation (deflate λ_1)	Top-4 invariant	H.5
20	Pairwise swap sensitivity over D	$P(\text{swap}) \in [0.476, 0.494]$	§2, G.1
21	Convexity in observed subspace	100% hull membership	§2, H.29
22	Correlation method robustness	$\Delta d_{\text{eff}} < 0.3$ (Pearson/Spearman/Kendall)	§8, H.33
23	Population dependence (d_{eff} vs q)	Monotone non-decreasing	§8, H.34
24	Counterfactual benchmark importance	$\rho = -0.69$ ($p = 0.013$)	§5, H.36
25	External eval blind-spot alignment	$\rho = +0.38$ ($p = 0.053$), 27 Arena cats	§5, H.37
26	Model de-duplication robustness	d_{eff} : 4.80 \rightarrow 4.33 (96 families)	§8, H.38
27	LiveBench bootstrap CI	$d_{\text{eff}} = 4.74$ [3.10, 4.60]	§3, H.39
28	Anisotropic calibration (real Σ_{hidden})	Iso 0.436, aniso 0.457, emp 0.411	§4, H.40
29	Standardisation sensitivity	$92 \times -3854 \times$ across 4 methods	§4, H.41
30	Cross-suite PC alignment (monoculture)	PC1 cosine = 0.986 ($p < 10^{-6}$)	§8, H.42

Definition 1 (Effective Dimensionality). Let $\Sigma = \text{Corr}(S)$ denote the $k \times k$ sample correlation matrix of the score matrix, with eigenvalues $\lambda_1 \geq \lambda_2 \geq \dots \geq \lambda_k \geq 0$. The effective dimensionality of the benchmark suite is the participation ratio:

$$d_{\text{eff}} = \frac{\left(\sum_{i=1}^k \lambda_i\right)^2}{\sum_{i=1}^k \lambda_i^2}.$$

Properties. Since Σ is a correlation matrix, $\sum_i \lambda_i = k$ (trace equals dimension). Thus $d_{\text{eff}} = k^2 / \sum_i \lambda_i^2$. The participation ratio satisfies $1 \leq d_{\text{eff}} \leq k$, with $d_{\text{eff}} = 1$ when a single eigenvalue captures all variance ($\lambda_1 = k$, $\lambda_{i>1} = 0$), and $d_{\text{eff}} = k$ when all eigenvalues are equal ($\lambda_i = 1$ for all i). The participation ratio is standard in random matrix theory and condensed matter physics Bell and Dean [1970], Wegner [1980], where it counts the number of “active” modes in a disordered system.

Theorem 6 (Effective Dimensionality and Variance Capture). Let $\mathcal{C} \subseteq \mathbb{R}^D$ be the capability space, and let the benchmarks π_1, \dots, π_k be linear projections (or linearized around the population mean). Let $\Sigma_C \in \mathbb{R}^{D \times D}$ denote the covariance of the true capability distribution with eigenvalues $\mu_1 \geq \dots \geq \mu_D \geq 0$. Then:

(a) **Variance capture bound.** The fraction of total capability variance $\text{tr}(\Sigma_C)$ captured by the benchmark suite satisfies:

$$\frac{\text{Var}_{\text{captured}}}{\text{tr}(\Sigma_C)} \leq \frac{d_{\text{eff}}}{D}.$$

Equality holds when the d_{eff} principal directions of the benchmark suite align with the top d_{eff} eigenvectors of Σ_C and all remaining capability variance is orthogonal to the benchmark subspace.

(b) **Marchenko-Pastur correction.** When the number of models n is comparable to the number of benchmarks k (i.e., $\gamma = k/n$ is not negligible), the sample eigenvalues are inflated by noise. Under the null hypothesis of independent benchmarks, eigenvalues lie in $[\lambda_-, \lambda_+]$ where:

$$\lambda_{\pm} = (1 \pm \sqrt{\gamma})^2.$$

Eigenvalues exceeding λ_+ are signal; those below are indistinguishable from noise. The corrected effective dimensionality uses only signal eigenvalues:

$$d_{\text{eff}}^{\text{MP}} = \frac{\left(\sum_{i:\lambda_i > \lambda_+} \lambda_i\right)^2}{\sum_{i:\lambda_i > \lambda_+} \lambda_i^2}.$$

Proof. Part (a). Let $A \in \mathbb{R}^{k \times D}$ denote the projection matrix such that $\Pi(m) = A c(m)$. The observed covariance is $\Sigma_S = A \Sigma_C A^\top$. By the singular value decomposition, A has rank at most $\min(k, D)$, so Σ_S captures at most k principal components of Σ_C .

The captured variance is $\text{tr}(\Sigma_S) = \text{tr}(A \Sigma_C A^\top) = \text{tr}(A^\top A \Sigma_C)$. Since $A^\top A$ is a $D \times D$ positive semidefinite matrix of rank $\leq k$, by von Neumann's trace inequality:

$$\text{tr}(A^\top A \Sigma_C) \leq \sum_{i=1}^k \sigma_i(A^\top A) \cdot \mu_i$$

where $\sigma_i(A^\top A)$ are the singular values of $A^\top A$ (which equal the squared singular values of A).

Now, the correlation structure of the *observed* scores determines d_{eff} . When benchmarks are redundant (highly correlated), $d_{\text{eff}} \ll k$, meaning the benchmarks collectively probe only d_{eff} independent directions in capability space. The image of A restricted to the capability distribution has effective rank d_{eff} , so:

$$\text{Var}_{\text{captured}} \leq d_{\text{eff}} \cdot \mu_1 \leq d_{\text{eff}} \cdot \frac{\text{tr}(\Sigma_C)}{D} \cdot D = d_{\text{eff}} \cdot \frac{\text{tr}(\Sigma_C)}{D} \cdot D.$$

More precisely, the captured variance probes d_{eff} directions. In the worst case (benchmarks aligned with the top eigenvectors of Σ_C), the captured variance equals $\sum_{i=1}^{d_{\text{eff}}} \mu_i$, and as a fraction of total variance:

$$\frac{\text{Var}_{\text{captured}}}{\text{tr}(\Sigma_C)} = \frac{\sum_{i=1}^{d_{\text{eff}}} \mu_{j_i}}{\sum_{i=1}^D \mu_i}$$

for some subset $\{j_1, \dots, j_{d_{\text{eff}}}\}$. Under the *uniform eigenvalue assumption* $\mu_i = \text{tr}(\Sigma_C)/D$ for all i , this ratio equals exactly d_{eff}/D . In general, this serves as a calibrated estimate: if capability variance is concentrated in few directions, benchmarks aligned with those directions capture more; if spread uniformly, the fraction is d_{eff}/D .

More precisely, the bound d_{eff}/D holds as an equality when: (i) the capability covariance has uniform eigenvalues (isotropic), and (ii) the benchmark projections span exactly d_{eff} orthogonal directions. Under non-uniform capability covariance, d_{eff}/D is a conservative estimate of blind spot size: the ‘‘blind fraction’’ $1 - d_{\text{eff}}/D$ underestimates the true information loss when capability variance is concentrated in directions orthogonal to the benchmark subspace.

Part (b). This follows directly from Marčenko and Pastur [1967]. Under the null model where benchmark scores are independent (population correlation is identity I_k) and n i.i.d. samples are drawn from $\mathcal{N}(0, I_k)$, the empirical eigenvalue distribution converges to the Marchenko-Pastur law with density:

$$f_{\text{MP}}(\lambda) = \frac{1}{2\pi\gamma} \frac{\sqrt{(\lambda_+ - \lambda)(\lambda - \lambda_-)}}{\lambda}, \quad \lambda \in [\lambda_-, \lambda_+]$$

where $\lambda_{\pm} = (1 \pm \sqrt{\gamma})^2$ and $\gamma = k/n$. Any eigenvalue exceeding λ_+ is inconsistent with the null (at the bulk edge) and indicates genuine correlation structure. The BBP (Baik-Ben Arous-Péché) transition Baik et al. [2005] provides the precise phase transition: a population spike of strength $\mu > 1 + \sqrt{\gamma}$ produces a sample eigenvalue that separates from the bulk.

Restricting d_{eff} to eigenvalues above λ_+ removes the contribution of finite-sample noise, yielding a consistent estimator as $n, k \rightarrow \infty$ with $\gamma = k/n$ fixed. \square \square

Remark 3 (Convexity not required). *Theorem 6 operates entirely on the observed correlation matrix. It requires no geometric assumptions about the capability space \mathcal{C} (convexity, boundedness, etc.). The linearity assumption on benchmarks can be relaxed: for monotone benchmarks, the same analysis applies to the rank-correlation (Spearman) matrix, yielding analogous results.*

Remark 4 (Relation to “just PCA”). *PCA computes eigenvalues. Theorem 1 proves what those eigenvalues imply: a quantitative bound on the fraction of the capability space that remains invisible to the evaluation suite. The participation ratio translates spectral decay into a single interpretable number (d_{eff}), and the Marchenko-Pastur correction separates signal from finite-sample noise. Neither step is standard PCA.*

Distribution-free strengthening

Theorem 7 (Distribution-Free Variance Capture). *Let $\Sigma_C \in \mathbb{R}^{D \times D}$ be the capability covariance (arbitrary eigenvalues $\mu_1 \geq \dots \geq \mu_D \geq 0$), and let the k benchmark directions span a d_{eff} -dimensional effective subspace V_{eff} .*

(a) **Worst-case (adversarial alignment):** *The captured variance fraction satisfies:*

$$\frac{\text{tr}(P_V \Sigma_C)}{\text{tr}(\Sigma_C)} \leq \frac{\sum_{i=1}^{d_{\text{eff}}} \mu_i}{\sum_{i=1}^D \mu_i}$$

with equality when V_{eff} aligns with the top d_{eff} eigenvectors of Σ_C .

(b) **Generic benchmarks (concentration):** *If the benchmark subspace V_{eff} is drawn uniformly from the Grassmannian $\text{Gr}(d_{\text{eff}}, D)$ — i.e., benchmark directions are not systematically aligned with the principal capability axes — then:*

$$\mathbb{E} \left[\frac{\text{tr}(P_V \Sigma_C)}{\text{tr}(\Sigma_C)} \right] = \frac{d_{\text{eff}}}{D}$$

and this concentrates: for any $t > 0$,

$$P \left(\left| \frac{\text{tr}(P_V \Sigma_C)}{\text{tr}(\Sigma_C)} - \frac{d_{\text{eff}}}{D} \right| > t \right) \leq 2 \exp \left(-\frac{D t^2}{8 \kappa^2(\Sigma_C)} \right)$$

where $\kappa(\Sigma_C) = \mu_1/\bar{\mu}$ is the condition ratio ($\bar{\mu} = \text{tr}(\Sigma_C)/D$ is the average eigenvalue).

Proof. Part (a) follows from the Cauchy interlacing theorem. The projector P_V has rank d_{eff} , so $\text{tr}(P_V \Sigma_C) = \sum_{i=1}^{d_{\text{eff}}} \mu_i(P_V \Sigma_C P_V)$. By the Poincaré separation theorem (Fan 1949), $\mu_i(P_V \Sigma_C P_V) \leq \mu_i(\Sigma_C)$ for each i , with equality when $V = \text{span}\{v_1, \dots, v_{d_{\text{eff}}}\}$ (top eigenvectors of Σ_C).

Part (b), expectation. Let $P_V = \sum_{j=1}^{d_{\text{eff}}} e_j e_j^\top$ where $\{e_j\}$ is an orthonormal basis for V , drawn uniformly. Then:

$$\mathbb{E}[\text{tr}(P_V \Sigma_C)] = \mathbb{E} \left[\sum_{j=1}^{d_{\text{eff}}} e_j^\top \Sigma_C e_j \right] = d_{\text{eff}} \cdot \mathbb{E}[e_1^\top \Sigma_C e_1]$$

where the last equality uses exchangeability of the basis vectors. For a uniformly random unit vector $e \in S^{D-1}$:

$$\mathbb{E}[e^\top \Sigma_C e] = \frac{\text{tr}(\Sigma_C)}{D}$$

(by the identity $\mathbb{E}[e e^\top] = I_D/D$). Therefore $\mathbb{E}[\text{tr}(P_V \Sigma_C)] = d_{\text{eff}} \cdot \text{tr}(\Sigma_C)/D$.

Part (b), concentration. The function $f(V) = \text{tr}(P_V \Sigma_C)/\text{tr}(\Sigma_C)$ on the Grassmannian is Lipschitz. To see this, note that for two subspaces V, V' at geodesic distance θ on $\text{Gr}(d_{\text{eff}}, D)$:

$$|f(V) - f(V')| \leq \frac{2\mu_1}{\text{tr}(\Sigma_C)} \cdot d_{\text{eff}} \cdot \sin \theta \leq \frac{2d_{\text{eff}}\kappa(\Sigma_C)}{D} \cdot \theta.$$

The Grassmannian with its natural metric satisfies a concentration inequality Meckes [2019]: for any L -Lipschitz function f on $\text{Gr}(d, D)$ with the geodesic metric:

$$P(|f - \mathbb{E}[f]| > t) \leq 2 \exp\left(-\frac{(D-d+1)t^2}{2L^2}\right).$$

With $L = 2d_{\text{eff}}\kappa(\Sigma_C)/D$ and $d = d_{\text{eff}}$:

$$P\left(\left|f - \frac{d_{\text{eff}}}{D}\right| > t\right) \leq 2 \exp\left(-\frac{(D-d_{\text{eff}}+1)D^2t^2}{8d_{\text{eff}}^2\kappa^2}\right) \leq 2 \exp\left(-\frac{Dt^2}{8\kappa^2}\right)$$

where the last step uses $D - d_{\text{eff}} + 1 \geq D/2$ (when $d_{\text{eff}} \leq D/2$, which holds by assumption since the blind spot is non-trivial) and $d_{\text{eff}} \leq D$. \square

Remark 5 (When does concentration hold?). *The bound is meaningful when Dt^2/κ^2 is large. For $t = 0.1$ (captured fraction within 10% of d_{eff}/D), $D = 20$, and $\kappa = 3$ (moderate eigenvalue spread):*

$$P(|f - d_{\text{eff}}/D| > 0.1) \leq 2 \exp(-20 \cdot 0.01/72) \approx 2e^{-0.003} \approx 1.99.$$

For moderate D and large κ , this concentration bound is loose. The concentration is tight only when $D \gg \kappa^2$, i.e., when the capability covariance is close to isotropic. For highly anisotropic capability distributions, the captured fraction depends on the alignment between the benchmarks and the top eigenvectors.

Robust statement. *The expectation $\mathbb{E}[f] = d_{\text{eff}}/D$ holds unconditionally (no assumptions on Σ_C). The concentration is strong when D is large relative to κ^2 .*

Remark 6 (The ‘‘generic benchmarks’’ assumption). *The uniformity assumption on V_{eff} is justified when benchmarks are designed independently of the model population’s capability structure. Benchmark designers do not have access to the eigenvectors of Σ_C ; they design tests based on desirable capabilities (reasoning, knowledge, instruction following), and there is no a priori reason for these to be systematically aligned with the principal components of inter-model variation. The expectation d_{eff}/D is a conservative reference point in this sense.*

C Theorem 2 proof: indistinguishability

C.1 Setup

We model the capability profile of a model population as a convex body $K \subset \mathbb{R}^D$. A benchmark π_u in direction $u \in S^{D-1}$ measures the *width* of K in direction u :

$$w_K(u) = h_K(u) + h_K(-u),$$

where $h_K(u) = \sup_{x \in K} \langle x, u \rangle$ is the support function. A benchmark suite of m benchmarks corresponds to width measurements in m directions $u_1, \dots, u_m \in S^{D-1}$.

Definition 2 (Indistinguishability Class). *Two convex bodies $K, L \subset B_R^D$ (the ball of radius R) are (ε, Π) -indistinguishable if their benchmark scores agree within ε :*

$$|w_K(u_i) - w_L(u_i)| \leq \varepsilon \quad \text{for all } i = 1, \dots, m.$$

Theorem 8 (Lipschitz Indistinguishability Bound). *Let $K, L \subset B_R^D$ be convex bodies that are (ε, Π) -indistinguishable with respect to m benchmark directions. Then the Hausdorff distance between K and L satisfies:*

$$\delta_H(K, L) \leq \varepsilon + \frac{\pi R}{m}.$$

Consequently, the minimum number of benchmarks required to guarantee $\delta_H(K, L) \leq \delta$ for all (ε, Π) -indistinguishable pairs is:

$$m \geq \frac{\pi R}{\delta - \varepsilon}.$$

Proof. The proof proceeds in three steps.

Step 1: Support function Lipschitz continuity. For any convex body $K \subset B_R^D$, the support function $h_K : S^{D-1} \rightarrow \mathbb{R}$ is Lipschitz with constant R :

$$|h_K(u) - h_K(v)| \leq R \cdot \|u - v\|_2 \quad \text{for all } u, v \in S^{D-1}.$$

This follows from:

$$|h_K(u) - h_K(v)| = \left| \sup_{x \in K} \langle x, u \rangle - \sup_{x \in K} \langle x, v \rangle \right| \leq \sup_{x \in K} |\langle x, u - v \rangle| \leq R \|u - v\|_2.$$

Step 2: Discretization error. Given m directions $u_1, \dots, u_m \in S^{D-1}$, for any direction $v \in S^{D-1}$ there exists some u_i with:

$$\|v - u_i\|_2 \leq \omega_m$$

where ω_m is the mesh norm (covering radius) of the point set $\{u_i\}$ on S^{D-1} . By a standard covering argument, for any set of m points on S^{D-1} :

$$\omega_m \leq \frac{\pi}{m^{1/(D-1)}}.$$

For $D = 2$ (directions on S^1 , the circle), m equally spaced directions achieve $\omega_m = \pi/m$ exactly. For general D , we use the weaker but universal bound. In the regime relevant to LLM evaluation (D potentially large, m small), the $D - 1$ root is unfavorable, but for the Lipschitz bound we work in the *projected space*.

The key observation is that while the ambient dimension D may be large, the effective dimensionality d_{eff} is small (Theorem 1). The benchmark directions u_1, \dots, u_m lie in a subspace of dimension d_{eff} , and within this subspace, the covering argument gives $\omega_m \leq \pi/m^{1/(d_{\text{eff}}-1)}$. For the tightest (and simplest) bound, we work with the *one-dimensional* covering on the great circles connecting benchmark directions.

Step 3: Assembling the bound. The Hausdorff distance between convex bodies is controlled by the sup-norm of their support functions:

$$\delta_H(K, L) = \sup_{u \in S^{D-1}} |h_K(u) - h_L(u)|.$$

For width functions, $|w_K(u) - w_L(u)| \leq |h_K(u) - h_L(u)| + |h_K(-u) - h_L(-u)|$, so width agreement within ε implies support function agreement within ε (for centered bodies where $h_K(u) = w_K(u)/2$).

For any direction v , let u_i be the nearest benchmark direction. Then:

$$\begin{aligned} |h_K(v) - h_L(v)| &\leq |h_K(v) - h_K(u_i)| + |h_K(u_i) - h_L(u_i)| + |h_L(u_i) - h_L(v)| \\ &\leq R\|v - u_i\| + \varepsilon + R\|v - u_i\| \\ &= \varepsilon + 2R\omega_m. \end{aligned}$$

For centered bodies with m directions providing coverage on the d_{eff} -dimensional effective subspace, using the one-dimensional covering bound $\omega_m \leq \pi/(2m)$ (each direction and its antipode cover an arc of π/m):

$$\delta_H(K, L) \leq \varepsilon + 2R \cdot \frac{\pi}{2m} = \varepsilon + \frac{\pi R}{m}.$$

The minimum benchmark formula follows by solving $\varepsilon + \pi R/m \leq \delta$ for m . □ □

Remark 7 (Tightness). *The $1/m$ rate is tight for Lipschitz-continuous support functions. Theorem 4 (ceiling target) shows that under stronger regularity (convexity + smoothness), the Fourier decay of support functions on the circle yields a $1/m^2$ rate. The gap between $1/m$ and $1/m^2$ is the gap between the Lipschitz and smooth regimes of geometric tomography.*

Remark 8 (Convexity required). *This theorem requires convexity of the capability profiles. For non-convex profiles, the Hausdorff distance between (ε, Π) -indistinguishable sets can be arbitrarily large (a non-convex body can have the same widths as a convex body in every direction while differing dramatically in shape). This means the bound is conservative: relaxing convexity can only increase the true blind spot. See Appendix B of the main paper.*

Remark 9 (Estimating R). *In practice, R is estimated as the radius of the smallest ball containing all observed capability profiles. From the standardized score matrix, $R \approx \sqrt{d_{\text{eff}}} \cdot \sigma_{\text{max}}$, where σ_{max} is the largest singular value of the centered score matrix divided by \sqrt{n} . For normalized scores on $[0, 100]$, $R \approx 50\sqrt{d_{\text{eff}}}$ serves as a conservative estimate.*

Corollary 2 (Ranking Unreliability). *Consider n models ranked by aggregate benchmark score $\bar{s}(c_i) = \frac{1}{k} \sum_j \pi_j(c_i)$. Let $\Delta_{\text{min}} = \min_{i \neq j} |\bar{s}(c_i) - \bar{s}(c_j)|$ be the minimum score gap. If the indistinguishability radius $\delta_0 = \pi R/m$ exceeds Δ_{min} , then there exist (ε, Π) -indistinguishable pairs that swap rankings:*

$$\delta_0 > \Delta_{\text{min}} \implies \exists K, L : \bar{s}(K) > \bar{s}(L) \text{ but } K \text{ and } L \text{ cannot be distinguished.}$$

The probability that the top-ranked model is truly the best (in full capability space) is bounded by:

$$P(\text{top-1 correct}) \leq 1 - \binom{n}{2}^{-1} \sum_{i < j} \mathbf{1} \left[\frac{|\bar{s}(c_i) - \bar{s}(c_j)|}{\delta_0} < 1 \right].$$

Proof. If two models have aggregate scores differing by less than δ_0 , then by Theorem 8, there exist convex bodies in the indistinguishability class of each model that would reverse their ranking on a different benchmark suite. The bound on $P(\text{top-1 correct})$ counts the fraction of model pairs whose score gap falls within the indistinguishability radius, each of which contributes a potential ranking error. \square \square

Corollary 3 (Rank Reversal Inevitability). *If $d_{\text{eff}} < n - 1$, then there exist model populations where adding a single model c_{n+1} to the ranked set reverses the relative ordering of two existing models c_i, c_j .*

Proof. When $d_{\text{eff}} < n - 1$, the n model score vectors $\Pi(c_1), \dots, \Pi(c_n) \in \mathbb{R}^k$ lie in a subspace of dimension $d_{\text{eff}} < n - 1$. In this regime, the score vectors are linearly dependent, meaning no hyperplane in score space can simultaneously separate all model pairs.

The aggregate score $\bar{s}(c_i) = \mathbf{w}^\top \Pi(c_i)$ for weight vector $\mathbf{w} = (1/k, \dots, 1/k)$ defines a linear functional on the score subspace. Adding a model c_{n+1} whose score vector is not in the span of $\{\Pi(c_i)\}_{i=1}^n$ can alter the weight vector that “best” aggregates scores (e.g., via normalization or re-weighting), which can reverse the sign of $\bar{s}(c_i) - \bar{s}(c_j)$ for some pair.

This is precisely the *rank reversal* phenomenon in multi-criteria decision making (MCDM). Belton and Gear [1983] showed that the Analytic Hierarchy Process (AHP) is susceptible to rank reversal when alternatives are added. Our result identifies the *geometric* condition: rank reversal is possible when the effective dimension of the evaluation space is insufficient to embed all models as unambiguously ordered. The critical threshold is $d_{\text{eff}} = n - 1$: with $n - 1$ independent evaluation directions, n models can be fully ordered; with fewer, they cannot. \square \square

Remark 10 (Convexity not required). *Corollary 3 is a statement about linear algebra in score space. It does not require any geometric assumptions about the capability space.*

Covering bound for general dimension

Theorem 9 (Indistinguishability Bound — General Dimension). *Let $K, L \subset B_R^D$ be convex bodies that are (ε, Π) -indistinguishable with respect to m benchmark directions $u_1, \dots, u_m \in S^{D-1}$. Let $d = d_{\text{eff}}$ be the effective dimension of the benchmark subspace, and let ω_m denote the covering radius of $\{u_1, \dots, u_m\}$ on S^{d-1} (the unit sphere in the effective subspace). Then:*

$$\delta_H(K, L) \leq \varepsilon + 2R\omega_m.$$

For m optimally spread directions in d effective dimensions, the covering radius satisfies $\omega_m \leq C_d m^{-1/(d-1)}$ for a constant C_d depending only on d , giving:

$$\delta_H(K, L) \leq \varepsilon + C \cdot R \cdot m^{-1/(d_{\text{eff}}-1)}.$$

The minimum number of benchmarks to guarantee $\delta_H \leq \delta$ is therefore:

$$m \geq \left(\frac{CR}{\delta - \varepsilon} \right)^{d_{\text{eff}}-1}.$$

Proof. Step 1 (unchanged): Support function Lipschitz continuity with constant R .

Step 2 (corrected): For any direction $v \in S^{D-1}$, we decompose v into its component in the effective subspace $V_{\text{eff}} = \text{span}\{u_1, \dots, u_m\}$ and its orthogonal complement. The component in V_{eff} has dimension d_{eff} , and the benchmark directions $\{u_i\}$ form a covering of $S^{d_{\text{eff}}-1} \cap V_{\text{eff}}$.

By the volumetric covering bound Rogers [1963], the minimum covering radius achievable by m points on S^{d-1} satisfies:

$$\omega_m^* \leq C_d \cdot \left(\frac{\log m}{m}\right)^{1/(d-1)} \leq C'_d \cdot m^{-1/(d-1)}$$

for a dimension-dependent constant C'_d . Concretely, $C_d \leq \sqrt{d}$ suffices for $m \geq d$.

For the component of v orthogonal to V_{eff} : the support functions of K and L in orthogonal directions are bounded by R but provide no information (no benchmarks probe these directions). However, the Hausdorff distance is determined by the sup over *all* directions, including those in V_{eff}^\perp . Within V_{eff}^\perp , we can only bound $|h_K(v) - h_L(v)| \leq 2R$ (trivial bound from containment in B_R).

The key insight is that the Hausdorff distance *restricted to the effective subspace* is bounded by $\varepsilon + 2R\omega_m$, while the contribution from orthogonal directions is the “blind spot” that Theorem 1 quantifies. Thus:

$$\delta_H(K, L) = \max\left(\sup_{v \in S^{d-1} \cap V_{\text{eff}}} |h_K(v) - h_L(v)|, \sup_{v \perp V_{\text{eff}}} |h_K(v) - h_L(v)|\right) \quad (4)$$

$$\leq \max(\varepsilon + 2R\omega_m, 2R). \quad (5)$$

The full Hausdorff distance is trivially bounded by $2R$. The non-trivial content is the bound on the *visible* component:

$$\delta_H^{\text{vis}}(K, L) \leq \varepsilon + 2R\omega_m \leq \varepsilon + C \cdot R \cdot m^{-1/(d_{\text{eff}}-1)}.$$

The minimum benchmarks formula follows by inverting: $CR \cdot m^{-1/(d_{\text{eff}}-1)} \leq \delta - \varepsilon$ gives $m \geq (CR/(\delta - \varepsilon))^{d_{\text{eff}}-1}$. \square

Remark 11 (Interpretation: the curse of benchmark dimensionality). *The exponent $d_{\text{eff}} - 1$ reveals a curse of dimensionality in evaluation. To halve the indistinguishability gap:*

d_{eff}	Benchmarks needed to halve gap
2	2× more
3	4× more
4	8× more
5	16× more

For leaderboards with $d_{\text{eff}} \approx 4$ (as we find empirically), reducing the blind spot by 2× requires 8× as many benchmarks. This quantifies why simply “adding more benchmarks” is an inefficient path to better evaluation — the greedy algorithm (Theorem 3) is essential for directing new benchmarks to uncovered directions rather than adding redundant ones.

Remark 12 (Recovery of special cases). For $d_{\text{eff}} = 2$ (all benchmarks measure essentially two independent things), the bound gives $\omega_m \leq C/m$, recovering the $\pi R/m$ rate from the original planar bound. For $d_{\text{eff}} = 1$ (all benchmarks perfectly correlated), a single benchmark suffices and $\omega_m = 0$ trivially. The general formula interpolates smoothly.

Chi-squared selection model for Corollary 2.1

C.2 Setup: Projection Decomposition

Let the capability profile of model i be $c_i \in \mathbb{R}^D$, drawn i.i.d. from $\mathcal{N}(0, I_D)$ (isotropic Gaussian; the non-isotropic case follows by whitening). The benchmark suite observes a d_{eff} -dimensional projection Pc_i .

Decompose: $c_i = (u_i, v_i)$ where $u_i \in \mathbb{R}^{d_{\text{eff}}}$ (observed) and $v_i \in \mathbb{R}^{D-d_{\text{eff}}}$ (hidden), with $u_i \perp\!\!\!\perp v_i$.

- **Observed quality:** $X_i = \|u_i\|^2 \sim \chi_{d_{\text{eff}}}^2$
- **Hidden quality:** $Y_i = \|v_i\|^2 \sim \chi_{D-d_{\text{eff}}}^2$
- **True quality:** $Z_i = X_i + Y_i = \|c_i\|^2 \sim \chi_D^2$
- $X_i \perp\!\!\!\perp Y_i$ (orthogonal subspaces of a Gaussian).

The benchmark ranking is $\operatorname{argmax}_i X_i$. The true ranking is $\operatorname{argmax}_i Z_i = \operatorname{argmax}_i (X_i + Y_i)$. These differ when the hidden component Y_i reverses the ordering.

Theorem 10 (Ranking Unreliability under Projection). *Let n models have i.i.d. isotropic Gaussian capability profiles in \mathbb{R}^D , evaluated by a benchmark suite with effective dimensionality d_{eff} . Let $i^* = \operatorname{argmax}_i X_i$ be the benchmark-top model. Then:*

(a) **Signal-to-noise characterization.** *The correlation between observed and true quality is:*

$$\rho = \operatorname{Corr}(X_i, Z_i) = \sqrt{\frac{d_{\text{eff}}}{D}}.$$

(b) **Pairwise swap probability.** *For any two models i, j with observed score gap $\Delta_{ij} = X_i - X_j > 0$, the probability that their true ranking is reversed:*

$$P(Z_j > Z_i \mid X_i - X_j = \Delta_{ij}) = \Phi\left(-\frac{\Delta_{ij}}{2\sqrt{D-d_{\text{eff}}}}\right)$$

where Φ is the standard Gaussian CDF (valid for large $D - d_{\text{eff}}$ by CLT on χ^2).

(c) **Top-1 reliability.** *The probability that the benchmark-top model is truly the best:*

$$P(\text{top-1 correct}) = \mathbb{E}\left[\prod_{j \neq i^*} \Phi\left(\frac{\Delta_{i^*j}}{2\sigma_{\text{hidden}}}\right)\right]$$

where $\Delta_{i^*j} = X_{i^*} - X_j$ are the observed score gaps from the top model, and $\sigma_{\text{hidden}} = \sqrt{2(D-d_{\text{eff}})}$ is the standard deviation of hidden quality differences.

(d) **Computable bound.** *For n models on a leaderboard with observed score gaps $\Delta_1 \geq \Delta_2 \geq \dots \geq \Delta_{n-1}$ (from top model to each other model):*

$$P(\text{top-1 correct}) \leq \prod_{j=1}^{n-1} \Phi\left(\frac{\Delta_j}{2\sigma_{\text{hidden}}}\right).$$

The only unknown is D , estimated by Theorem 11.

Proof. **Part (a).** Direct computation:

$$\begin{aligned} \operatorname{Corr}(X_i, Z_i) &= \frac{\operatorname{Cov}(X_i, X_i + Y_i)}{\sqrt{\operatorname{Var}(X_i) \cdot \operatorname{Var}(X_i + Y_i)}} \\ &= \frac{\operatorname{Var}(X_i)}{\sqrt{\operatorname{Var}(X_i) \cdot (\operatorname{Var}(X_i) + \operatorname{Var}(Y_i))}} \\ &= \frac{\sqrt{\operatorname{Var}(X_i)}}{\sqrt{\operatorname{Var}(X_i) + \operatorname{Var}(Y_i)}} \\ &= \sqrt{\frac{2d_{\text{eff}}}{2d_{\text{eff}} + 2(D-d_{\text{eff}})}} = \sqrt{\frac{d_{\text{eff}}}{D}}. \end{aligned}$$

Part (b). Given $X_i > X_j$ with gap $\Delta = X_i - X_j$:

$$Z_j > Z_i \iff Y_j - Y_i > \Delta.$$

Since Y_i and Y_j are independent $\chi_{D-d_{\text{eff}}}^2$, for large $D - d_{\text{eff}}$ the CLT gives:

$$Y_i \approx \mathcal{N}(D - d_{\text{eff}}, 2(D - d_{\text{eff}})).$$

Therefore $Y_j - Y_i \approx \mathcal{N}(0, 4(D - d_{\text{eff}}))$, and:

$$P(Y_j - Y_i > \Delta) = \Phi\left(\frac{-\Delta}{2\sqrt{D - d_{\text{eff}}}}\right) = 1 - \Phi\left(\frac{\Delta}{2\sqrt{D - d_{\text{eff}}}}\right).$$

Part (c). The benchmark-top model i^* is truly the best iff $Z_{i^*} > Z_j$ for all $j \neq i^*$. Conditioning on the observed scores (which determine i^* and all gaps Δ_{i^*j}):

$$P(\text{top-1 correct} \mid X_1, \dots, X_n) = P\left(\bigcap_{j \neq i^*} \{Y_{i^*} - Y_j > -(X_{i^*} - X_j)\}\right).$$

Since the Y_j 's are independent (but Y_{i^*} appears in every event), the events $\{Y_{i^*} - Y_j > -\Delta_{i^*j}\}$ are *not* independent. However, they are positively correlated (large Y_{i^*} helps in all events), so:

$$P(\text{top-1 correct} \mid X) \geq \prod_{j \neq i^*} P(Y_{i^*} - Y_j > -\Delta_{i^*j})$$

by the FKG inequality (the events are increasing in Y_{i^*}). Conversely, we have the *upper* bound from the union bound:

$$P(\text{top-1 incorrect} \mid X) \leq \sum_{j \neq i^*} \Phi\left(-\frac{\Delta_{i^*j}}{2\sigma_{\text{hidden}}}\right).$$

Part (d). The product formula in (c) is a lower bound on $P(\text{correct})$ by the FKG argument. For the computable upper bound, the union bound gives:

$$P(\text{top-1 correct}) \geq 1 - \sum_{j=1}^{n-1} \Phi\left(-\frac{\Delta_j}{2\sigma_{\text{hidden}}}\right).$$

Both the product (lower) and union (upper on error) bounds are computable from the observed leaderboard data plus the estimated D . □ □

Corollary 4 (Leaderboard Reliability Formula). *For a leaderboard with n models, d_{eff} effective dimensions, and estimated true dimensionality D :*

$$P(\text{top-1 wrong}) \leq \sum_{j=1}^{n-1} \Phi\left(\frac{-\Delta_j}{2\sqrt{2(D - d_{\text{eff}})}}\right)$$

where Δ_j is the score gap between the top model and the j -th ranked model.

Interpretation: Each model j contributes a “threat” to the top-1 ranking proportional to $\Phi(-\Delta_j/(2\sigma_{\text{hidden}}))$. Models with small score gaps and large hidden dimensionality contribute the most threat. The formula outputs a single number: “this leaderboard has $X\%$ chance that its #1 is wrong.”

Remark 13 (Practical computation). *Given a leaderboard (e.g., Open LLM Leaderboard):*

1. Compute d_{eff} from the score correlation matrix (Theorem 1).
2. Estimate D from eigenvalue decay (Theorem 3).
3. Read off score gaps Δ_j from the leaderboard.
4. Plug into the formula.

The only “free parameter” is D , which enters through $\sigma_{\text{hidden}} = \sqrt{2(D - d_{\text{eff}})}$. The formula is monotonically increasing in D : the more hidden dimensions, the less reliable the ranking. We report results for a range of D values ($D \in [D_{\text{lower}}, D_{\text{upper}}]$ from Theorem 3) to show sensitivity.

Remark 14 (Non-isotropic capabilities). *The isotropic Gaussian assumption ($\Sigma_C = I$) is for cleanliness. For general Σ_C , replace $D - d_{\text{eff}}$ with the “effective hidden dimensionality” $d_{\text{hidden}} = (\text{tr}(\Sigma_C) - \text{tr}(P_V \Sigma_C))^2 / (\text{tr}(\Sigma_C^2) - \text{tr}((P_V \Sigma_C P_V)^2))$, the participation ratio of the hidden covariance. The formula’s structure is unchanged.*

Remark 15 (Relationship to “true quality” definition). *The model uses $\|c_i\|^2$ (capability norm) as “true quality.” This is one natural choice. For a different quality functional $q(c) = w^\top c$ (linear in capabilities), the analysis simplifies to a bivariate normal with $\rho = \cos \theta$ where θ is the angle between the quality direction w and the benchmark subspace. The results are analogous with $\rho = \sqrt{d_{\text{eff}}/D}$ replaced by the projection of w onto V_{eff} .*

Visible vs full Hausdorff decomposition

The corrected covering bound above bounds only the *visible* component. To make the visible/full decomposition explicit, decompose $\mathbb{R}^D = V_{\text{eff}} \oplus V_{\text{eff}}^\perp$. For any $v \in S^{D-1}$ write $v = v^\parallel + v^\perp$. The support function difference splits as $|h_K(v) - h_L(v)| \leq |h_K(v) - h_K(v^\parallel)| + |h_K(v^\parallel) - h_L(v^\parallel)| + |h_L(v^\parallel) - h_L(v)|$. The middle term is bounded by the visible covering argument; the outer two are bounded by Lipschitzness along v^\perp , contributing the trivial $O(R\|v^\perp\|)$ term. Taking the supremum over S^{D-1} yields

$$\delta_H(K, L) = \max\left(\sup_{v \in S^{D-1} \cap V_{\text{eff}}} |h_K(v) - h_L(v)|, \sup_{v \perp V_{\text{eff}}} |h_K(v) - h_L(v)|\right), \quad (6)$$

$$\delta_H^{\text{vis}}(K, L) \leq \varepsilon + 2R\omega_m \leq \varepsilon + CR \cdot m^{-1/(d_{\text{eff}}-1)}, \quad (7)$$

$$\delta_H^\perp(K, L) \leq 2R \quad (\text{trivial bound from containment in } B_R^D). \quad (8)$$

The unconditional bound is $\delta_H \leq \max(\varepsilon + CRm^{-1/(d-1)}, 2R)$. The non-trivial content is the visible part: it quantifies how the measurable blind spot decays with m . The orthogonal $2R$ contribution is what Theorem 4’s greedy algorithm reduces by enlarging V_{eff} .

Centering convention

We assume capability profiles are origin-symmetric ($K = -K$), so $h_K(u) = h_K(-u)$ and $w_K(u) = 2h_K(u)$. Width agreement within ε then implies support function agreement within $\varepsilon/2$, and the bound above applies with this rescaling. For non-symmetric bodies, $w_K(u)$ determines $h_K(u) + h_K(-u)$ but not $h_K(u)$ individually; the same bound then applies to the *symmetrized* body $(K - K)/2$. Since benchmark scores are translation-invariant once the score matrix is centred, this is without loss of generality for the inter-model discrimination question.

D Theorem 3 proof: greedy coverage

D.1 Dimension Estimation

Theorem 11 (Dimension Bounds). *Let $S \in \mathbb{R}^{n \times k}$ be the score matrix for n models on k benchmarks, with correlation eigenvalues $\lambda_1 \geq \dots \geq \lambda_k$, Marchenko-Pastur threshold $\lambda_+ = (1 + \sqrt{k/n})^2$, and $n_{\text{sig}} = |\{i : \lambda_i > \lambda_+\}|$ significant eigenvalues. Then the true dimensionality D of the capability space satisfies:*

$$n_{\text{sig}} \leq D \leq n - 1.$$

Proof. Lower bound. Each significant eigenvalue ($\lambda_i > \lambda_+$) indicates a direction in score space with more variance than expected under the null of independent benchmarks. By the BBP phase transition Baik et al. [2005], a significant sample eigenvalue corresponds to a genuine population eigenvalue exceeding $1 + \sqrt{\gamma}$, which in turn corresponds to a dimension of the capability space that is “visible” through the benchmark suite. Since distinct visible dimensions are linearly independent, $D \geq n_{\text{sig}}$.

This bound is tight when the benchmark suite is well-designed (each benchmark probes a different capability direction) and the population covariance is isotropic in the visible subspace.

Upper bound. If n models are all distinguishable (have distinct capability profiles), they span at most an $(n - 1)$ -dimensional affine subspace of \mathbb{R}^D . We cannot infer more than $n - 1$ dimensions from n data points. Note that D could be much larger (even infinite), but we can only observe evidence for up to $n - 1$ dimensions from a finite model population.

The gap between n_{sig} and $n - 1$ is the “dimension gap”: the number of capability dimensions that exist but are either not probed by the benchmark suite or not sufficiently varied across the model population to be detectable. \square \square

Remark 16 (Extrapolation via eigenvalue decay). *A tighter estimate of D can be obtained by modeling the eigenvalue decay. If the population eigenvalues follow a power law $\mu_i \propto i^{-\alpha}$, then the number of eigenvalues above the noise floor λ_+ is $n_{\text{sig}} \approx (\mu_1/\lambda_+)^{1/\alpha}$. The true dimensionality (number of non-negligible eigenvalues) is $D_{\text{est}} \approx (\mu_1/\epsilon)^{1/\alpha}$ for some minimal relevance threshold ϵ . This extrapolation is necessarily uncertain but provides a point estimate.*

D.2 Greedy Coverage Algorithm

Theorem 12 (Greedy Benchmark Selection). *Let $\Sigma \in \mathbb{R}^{k \times k}$ be the benchmark correlation matrix with eigendecomposition $\Sigma = V\Lambda V^\top$, and let $f : 2^{[k]} \rightarrow \mathbb{R}_{\geq 0}$ denote the coverage function:*

$$f(T) = \frac{\text{tr}(\Pi_T \Sigma)}{\text{tr}(\Sigma)}$$

where Π_T is the orthogonal projector onto the subspace spanned by benchmark loading vectors $\{v_j : j \in T\}$ (rows of the loading matrix $L = V\sqrt{\Lambda}$). Then:

- (a) f is monotone ($T \subseteq T' \Rightarrow f(T) \leq f(T')$) and submodular ($f(T \cup \{j\}) - f(T) \geq f(T' \cup \{j\}) - f(T')$ for $T \subseteq T'$).
- (b) The greedy algorithm — iteratively selecting $j^* = \arg \max_{j \notin T} [f(T \cup \{j\}) - f(T)]$ — achieves:

$$f(T_{\text{greedy}}^{(r)}) \geq \left(1 - \frac{1}{e}\right) \cdot f(T_r^*)$$

where $T_{\text{greedy}}^{(r)}$ is the greedy selection of r benchmarks and T_r^* is the optimal r -element subset.

- (c) The minimum subset for target coverage τ has size at most:

$$|T_{\text{greedy}}| \leq \left\lceil \frac{\ln(1/(1 - \tau))}{\ln(k/(k - d_{\text{eff}}))} \right\rceil.$$

Proof. **Part (a): Monotonicity and submodularity.**

Monotonicity. Adding a benchmark to T can only increase the dimension of the spanned subspace, hence $\Pi_{T'} \succeq \Pi_T$ in the positive semidefinite order for $T \subseteq T'$, giving $f(T') \geq f(T)$.

Submodularity. Let $T \subseteq T'$ and $j \notin T'$. The marginal gain of adding j to T is:

$$f(T \cup \{j\}) - f(T) = \frac{\|P_{T^\perp} \ell_j\|^2}{\text{tr}(\Sigma)}$$

where ℓ_j is the loading vector of benchmark j and P_{T^\perp} projects onto the orthogonal complement of the subspace spanned by $\{\ell_i : i \in T\}$. Since $T \subseteq T'$, the subspace spanned by T' contains that of T , so $P_{T'^\perp} \preceq P_{T^\perp}$ and:

$$\|P_{T'^\perp} \ell_j\|^2 \leq \|P_{T^\perp} \ell_j\|^2,$$

establishing submodularity. Intuitively: the marginal value of a new benchmark decreases as more benchmarks are already selected, because there is less uncovered variance remaining.

Part (b): Greedy approximation guarantee. This follows immediately from the classical result of Nemhauser et al. [1978]: for any monotone submodular function f with $f(\emptyset) = 0$, the greedy algorithm achieves a $(1 - 1/e)$ -approximation to the optimum for any cardinality constraint. Since our coverage function f satisfies $f(\emptyset) = 0$, monotonicity, and submodularity, the bound applies.

Part (c): Minimum subset size. At each greedy step, submodularity implies the marginal gain is at least:

$$f(T^{(r+1)}) - f(T^{(r)}) \geq \frac{f([k]) - f(T^{(r)})}{k - r} \geq \frac{1 - f(T^{(r)})}{k}.$$

Let $g_r = 1 - f(T^{(r)})$ denote the uncovered fraction. Then $g_{r+1} \leq g_r(1 - 1/k)$, giving:

$$g_r \leq \left(1 - \frac{1}{k}\right)^r \leq e^{-r/k}.$$

To achieve coverage τ (i.e., $g_r \leq 1 - \tau$), we need $r \geq k \ln(1/(1 - \tau))$.

This bound uses $f([k]) = 1$ (full benchmark set achieves full coverage in benchmark space). In practice, the convergence is faster because $d_{\text{eff}} \ll k$: the first d_{eff} greedy selections capture most variance, and the bound tightens to $r = O(d_{\text{eff}} \ln(1/(1 - \tau)))$. Formally, replacing k with the rank of the effective subspace: since the loading matrix has effective rank d_{eff} , the coverage function satisfies $f([k]) \leq d_{\text{eff}}/k \cdot k = d_{\text{eff}}$ (unnormalized), and the step size bound becomes $g_{r+1} \leq g_r(1 - 1/d_{\text{eff}})$ in the first d_{eff} steps where marginal gains are large. This gives the stated bound. \square \square

D.3 Outputs of the Algorithm

The greedy algorithm produces three outputs:

1. **Minimum subset:** The first r benchmarks selected, ordered by marginal coverage gain. “Your 20 benchmarks but you only need 7.”
2. **Redundancies:** Benchmarks with marginal gain below a threshold η (e.g., $\eta = 0.01$). These are redundant given the selected subset and can be retired without information loss.
3. **Uncovered directions:** The eigenvectors of Σ with non-negligible eigenvalues that are orthogonal to the selected subset. These characterize the “blind spot” — the directions in benchmark space (and, by extension, capability space) that are not probed by any selected benchmark. The loadings of these directions on individual benchmarks suggest what *new* benchmarks should measure.

Remark 17 (Convexity not required). *Theorem 12 operates on the benchmark correlation matrix and loading vectors. It requires no geometric assumptions about the capability space. The algorithm is purely data-driven and applies to any score matrix.*

Remark 18 (Comparison to PCA-based selection). *The greedy algorithm differs from simply selecting benchmarks with the highest PCA loadings. PCA identifies directions of maximum variance, but the greedy algorithm optimizes coverage: it seeks the minimum set of benchmarks that collectively spans the most variance, accounting for redundancy between benchmarks. Two benchmarks with high PC1 loadings are redundant; the greedy algorithm would select one and move to the next uncovered direction.*

Numerical C_d values and the log factor

The covering bound [Rogers, 1963] gives $\omega_m^* \leq C_d((d - 1) \log m/m)^{1/(d-1)}$ with $C_d \leq \sqrt{2d}$. For $d = 2$ the special case is π/m exactly, with no log factor. For $m = 12$ the explicit upper bounds are $\omega_{12}^* \leq 0.262$ ($d = 2$, exact), ≤ 0.690 ($d = 3$), ≤ 0.918 ($d = 4$), ≤ 1.060 ($d = 5$). The constant C in the main text Theorem 2 absorbs both factors: $C = O(\sqrt{d_{\text{eff}}} \cdot (\log m)^{1/(d_{\text{eff}}-1)})$.

Swap Monotonicity: Schur-convexity proof (Proposition 2)

Proof. Under the projection model of Corollary 1, the hidden quality is $Y_i = \|v_i\|^2$ where $v_i \sim \mathcal{N}(0, \Sigma_{\text{hidden}})$. The variance of the pairwise difference $Y_j - Y_i$ is $\text{Var}(Y_j - Y_i) = 2 \cdot 2 \text{tr}(\Sigma_{\text{hidden}}^2) = 4 \sum_{\ell} \lambda_{\ell}^2$ where $\{\lambda_{\ell}\}$ are the eigenvalues of Σ_{hidden} . Under the constraint $\sum_{\ell} \lambda_{\ell} = \sigma_h^2$ (fixed trace), the function $\lambda \mapsto \sum_{\ell} \lambda_{\ell}^2$ is Schur-convex; it is minimised when the eigenvalues are equal (the uniform vector is majorised by every other vector with the same sum), i.e., under the isotropic case $\lambda_{\ell} = \sigma_h^2/(D - d_{\text{eff}})$. Hence the isotropic choice minimises $\text{Var}(Y_j - Y_i)$.

For the Gaussian approximation with observed gap $\Delta > 0$, $P(\text{swap}) = \Phi(-\Delta/(2\sqrt{\text{tr}(\Sigma_{\text{hidden}}^2)})$) is monotone increasing in $\text{tr}(\Sigma_{\text{hidden}}^2)$ (the denominator grows, so the argument increases toward zero and Φ decreases toward 0.5). Therefore the isotropic case minimises $P(\text{swap})$, and any anisotropy increases the swap probability. \square

The half-split model (Appendix H, G.4) addresses a different question: given a fixed suite of benchmarks and a random visible/hidden partition, which prior maximises the swap rate? Under random partition, isotropic priors distribute signal uniformly across benchmarks and maximise the chance that randomly hiding a column loses meaningful information, while concentrated priors put most signal into a single direction that is quasi-observed by the dominant benchmark column and lose less to random hiding. The two results are complementary: (a) says the bound we report is optimistic in the *prior-over-hidden-covariance* sense, and (b) says the simulated half-split swap rate is maximised at isotropy in the *random-partition* sense.

Coverage–indistinguishability bridge (Proposition 3)

Proposition 3 (Coverage–Indistinguishability Bridge). *Let $T \subseteq [k]$ with coverage $f(T) = \tau$ and let $\omega_m^{\text{within}}(T)$ denote the covering radius of the selected benchmark directions within $\text{span}\{\ell_j : j \in T\}$. Then*

$$\delta_H(K, L) \leq \max\left(\varepsilon + CR \cdot \omega_m^{\text{within}}(T), 2R\sqrt{1-\tau}\right),$$

where the second term uses the fact that the uncovered eigenvalue mass is $(1-\tau)\text{tr}(\Sigma)$, which under approximate isotropy contributes at most $2R\sqrt{1-\tau}$ to the orthogonal Hausdorff distance.

Proof. The visible component is bounded by the standard Lipschitz argument applied within $\text{span}(T)$ with covering radius $\omega_m^{\text{within}}(T)$. For the orthogonal component, the uncovered variance is $(1-\tau)\text{tr}(\Sigma)$, distributed across the eigenvectors orthogonal to the selected span. Under approximate isotropy, the maximum directional contribution to $h_K - h_L$ is bounded by $\sqrt{(1-\tau)\text{tr}(\Sigma) \cdot \dim(V_{\text{eff}}^\perp)} \leq R\sqrt{1-\tau}$ in standardised units; doubling for the bilateral support function difference gives $2R\sqrt{1-\tau}$. \square

Spectral characterisation (Proposition 4)

Proposition 4 (Spectral Objective Characterisation). *Among objectives $f_g(T) = \text{tr}(P_T g(\Sigma))/\text{tr}(g(\Sigma))$ for monotone $g : \mathbb{R}_{\geq 0} \rightarrow \mathbb{R}_{\geq 0}$, the linear choice $g(x) = x$ minimises the worst-case fraction of uncovered variance over all capability covariances Σ_C with bounded condition number, is invariant to orthogonal rotations of the benchmark space, and is monotone submodular (admitting the $(1-1/e)$ Nemhauser bound).*

Proof. Worst-case minimax: for any monotone g , $\text{tr}(P_T g(\Sigma))/\text{tr}(g(\Sigma))$ is a weighted average of squared loadings $\|P_T v_i\|^2$ with weights $g(\lambda_i)$. The minimax over Σ_C with bounded condition number selects weights as uniform in λ , which is $g(x) = x$. Rotation invariance is immediate from $P_T \Sigma$ being a basis-free quantity. Submodularity is the classical result of Das and Kempe [2011] (proof of $T \mapsto \text{tr}(P_T \Sigma)$ in Section 4). \square

Coverage stability (Proposition 5)

Proposition 5 (Coverage Stability under Restricted Perturbation). *Let Σ, Σ' be benchmark correlation matrices and let $T \subseteq [k]$. Then*

$$f_{\Sigma'}(T) \geq f_{\Sigma}(T) - \frac{\|P_T(\Sigma - \Sigma')P_T\|_{\text{op}}}{\text{tr}(\Sigma)}.$$

The relevant perturbation is restricted to the selected subspace, which is much smaller than the full operator-norm difference $\|\Sigma - \Sigma'\|_{\text{op}}$.

Proof. $f(T) = \text{tr}(P_T \Sigma)/\text{tr}(\Sigma) = \text{tr}(P_T \Sigma P_T)/\text{tr}(\Sigma)$. The difference $f_{\Sigma'}(T) - f_{\Sigma}(T) = (\text{tr}(P_T \Sigma' P_T) - \text{tr}(P_T \Sigma P_T))/\text{tr}(\Sigma)$ is bounded in absolute value by $\|P_T(\Sigma' - \Sigma)P_T\|_{\text{op}}$.

$\text{rank}(P_T)/\text{tr}(\Sigma) \leq \|P_T(\Sigma' - \Sigma)P_T\|_{\text{op}} \cdot |T|/\text{tr}(\Sigma)$, but because the projector restricts to a subspace, the operative bound is the operator norm above. \square

Rigorous submodularity of $f(T) = \text{tr}(P_T\Sigma)/\text{tr}(\Sigma)$

Submodularity of the coverage function for PSD Σ is a classical result in experimental design, equivalent to submodularity of the A-optimal criterion [Das and Kempe, 2011, Krause et al., 2008]. We give the explicit argument.

Proof. Let $\Sigma = \sum_{i=1}^k \lambda_i v_i v_i^\top$ be the eigendecomposition with $\lambda_i \geq 0$. Then $\text{tr}(P_T\Sigma) = \sum_i \lambda_i \|P_T v_i\|^2$. Since each $\lambda_i \geq 0$, it suffices to show that $T \mapsto \|P_T v\|^2$ is monotone submodular for any fixed $v \in \mathbb{R}^k$.

Monotonicity. For $T \subseteq T'$, $\text{span}(T) \subseteq \text{span}(T')$, so $P_T \preceq P_{T'}$ in the PSD order, hence $\|P_T v\|^2 \leq \|P_{T'} v\|^2$.

Submodularity. Use the Pythagorean identity $\|P_T v\|^2 = \|v\|^2 - \text{dist}(v, \text{span}(T))^2$. The function $T \mapsto \text{dist}(v, \text{span}(T))^2$ is *supermodular*: adding a vector ℓ_j to a larger spanning set $\text{span}(T')$ reduces the squared distance by less than adding it to a smaller set $\text{span}(T)$, because the residual of v orthogonal to $\text{span}(T')$ is a subset of that orthogonal to $\text{span}(T)$. This is the standard ‘‘diminishing-returns’’ property of orthogonal projections; a detailed proof appears in Das and Kempe [2011, Proposition 1]. Since the negation of a supermodular function is submodular, $T \mapsto \|P_T v\|^2 = \|v\|^2 - \text{dist}(v, \text{span}(T))^2$ is monotone submodular.

A non-negative linear combination of monotone submodular functions is monotone submodular, so $f(T) = \sum_i \lambda_i \|P_T v_i\|^2 / \text{tr}(\Sigma)$ is monotone submodular. No additional assumptions on the loading vectors $\{\ell_j\}$ are required. \square

E Stability of convex body recovery from width measurements

Planar Fourier proof

E.1 Motivation: Gardner’s Problem 1.5

Gardner [1995] posed the following (Problem 1.5): *How stably does a finite set of X-rays determine a convex body?* That is, if two convex bodies K and L have X-rays (projections onto lines through the origin) that agree within ε in m directions, how large can $\delta_H(K, L)$ be?

The Lipschitz bound (Theorem 8) gives $\delta_H \leq \varepsilon + \pi R/m$, a rate of $O(1/m)$. For smooth convex bodies, the support function has rapidly decaying Fourier coefficients, suggesting a faster rate is possible. This section establishes the improved rate under additional regularity.

E.2 Setup: Fourier Analysis on the Circle

We work in $D = 2$ (the planar case) where the theory is most tractable. The support function of a centered convex body $K \subset \mathbb{R}^2$ can be written as a Fourier series on $S^1 \cong [0, 2\pi)$:

$$h_K(\theta) = \sum_{n=-\infty}^{\infty} \hat{h}_K(n) e^{in\theta}.$$

Since K is centered (origin is the centroid), $\hat{h}_K(0) = 0$ and $\hat{h}_K(\pm 1) = 0$. Convexity of K imposes the constraint that $h_K(\theta) + h_K''(\theta) \geq 0$ (the radius of curvature is non-negative), which translates to:

$$\sum_n (1 - n^2) \hat{h}_K(n) e^{in\theta} \leq 0 \quad (\text{in distributional sense}).$$

This forces rapid decay of Fourier coefficients: for smooth convex bodies, $|\hat{h}_K(n)| = O(n^{-2})$.

E.3 Sampling and Aliasing

Given m equally spaced directions $\theta_j = 2\pi j/m$ for $j = 0, \dots, m-1$, the discrete Fourier transform recovers the first m coefficients:

$$\hat{h}_K^{(m)}(n) = \frac{1}{m} \sum_{j=0}^{m-1} h_K(\theta_j) e^{-2\pi i n j/m} = \hat{h}_K(n) + \sum_{\ell \neq 0} \hat{h}_K(n + \ell m).$$

The aliasing error for coefficient n (with $|n| < m/2$) is bounded by:

$$|\hat{h}_K^{(m)}(n) - \hat{h}_K(n)| \leq \sum_{\ell \neq 0} |\hat{h}_K(n + \ell m)| \leq C_K \sum_{\ell=1}^{\infty} \frac{1}{(\ell m)^2} = \frac{C_K \pi^2}{6m^2}$$

where C_K is a constant depending on the curvature of K .

E.4 The Stability Theorem

Theorem 13 (Tight Fourier Stability Bound). *Let $K, L \subset B_R^2$ be centered convex bodies in the plane with curvature bounded below by $\kappa > 0$. If their support functions agree within ε at m equally spaced directions:*

$$|h_K(\theta_j) - h_L(\theta_j)| \leq \varepsilon \quad \text{for all } j = 0, \dots, m-1,$$

then:

$$\delta_H(K, L) \leq C_1 \varepsilon + \frac{C_2 R}{\kappa m^2}$$

where C_1, C_2 are absolute constants.

Proof. For convex bodies K with curvature $\geq \kappa > 0$, the support function h_K is C^2 with $\|h_K''\|_\infty \leq R/\kappa$. By Jackson's theorem, the best trigonometric polynomial approximation of degree $< m/2$ satisfies:

$$\inf_{\deg p < m/2} \|h_K - p\|_\infty \leq \frac{C \omega_2(h_K, 1/m)}{1} \leq \frac{C}{m^2} \|h_K''\|_\infty \leq \frac{CR}{\kappa m^2}$$

where ω_2 is the second modulus of smoothness. The same holds for h_L . The trigonometric polynomial of degree $< m/2$ is determined by m equally spaced samples, so:

$$\|h_K - h_L\|_\infty \leq \|h_K - p_K\|_\infty + \|p_K - p_L\|_\infty + \|p_L - h_L\|_\infty \leq \frac{2CR}{\kappa m^2} + \|p_K - p_L\|_\infty.$$

Since p_K and p_L interpolate h_K and h_L at the m sample points, and the samples agree within ε :

$$\|p_K - p_L\|_\infty \leq \Lambda_m \varepsilon$$

where Λ_m is the Lebesgue constant for equispaced trigonometric interpolation, which is $O(\log m)$.

Thus:

$$\delta_H(K, L) \leq C_1 \varepsilon \log m + \frac{C_2 R}{\kappa m^2}.$$

Absorbing the $\log m$ into C_1 (or noting that for practical m , $\log m$ is a small constant):

$$\boxed{\delta_H(K, L) \leq C_1 \varepsilon \log m + \frac{C_2 R}{\kappa m^2}.}$$

The dominant term for large m (many benchmarks) is $1/m^2$, a quadratic improvement over the Lipschitz rate of $1/m$. □ □

Remark 19 (Dimension restriction). *Theorem 13 as stated applies to the planar case $D = 2$. Extension to higher dimensions is non-trivial: the Fourier analysis on S^{D-1} involves spherical harmonics, and the Jackson-type approximation theorems are more complex. The planar case establishes the proof concept; the high-dimensional extension is future work and connects to the full resolution of Gardner's Problem 1.5.*

Remark 20 (Practical interpretation). *The $1/m^2$ rate means that doubling the number of benchmarks reduces the indistinguishability gap by a factor of 4 (rather than 2 under Lipschitz). This has practical significance: going from 6 to 12 benchmarks reduces the blind spot by $4\times$, not $2\times$. However, the $1/m^2$ rate requires the “equally spaced” condition (benchmarks uniformly covering the capability space), which real benchmark suites may not satisfy. The Lipschitz bound ($1/m$) applies without this condition.*

Remark 21 (Connection to Problem 1.5). *Gardner’s Problem 1.5 asks for the stability of convex body determination from finitely many X-rays (projections). Our result addresses a closely related question: stability from finitely many width measurements. The full Problem 1.5 in arbitrary dimensions, and for X-rays rather than widths, remains open. Partial progress on named open problems is routinely published in geometric tomography Gardner [2006].*

General-dimension stability via optimal recovery

Theorem 14 (Stability of Convex Body Determination from Width Measurements). *Let $K, L \subset B_R^D$ be origin-symmetric convex bodies with Gauss curvature bounded below by $\kappa > 0$ (equivalently, the principal radii of curvature satisfy $r_i \geq \kappa$ for all i). Let their support functions $h_K, h_L \in C^2(S^{D-1})$, and suppose that m width measurements agree within ε :*

$$|w_K(u_i) - w_L(u_i)| \leq \varepsilon \quad \text{for } i = 1, \dots, m$$

where $\{u_i\}_{i=1}^m$ are m measurement directions on S^{D-1} .

Then the Hausdorff distance satisfies:

$$\delta_H(K, L) \leq C_D \left(\varepsilon + \frac{R}{\kappa m^{2/(D-1)}} \right)$$

where C_D depends only on D . Moreover, this rate is minimax optimal: there exist pairs of convex bodies achieving $\delta_H \geq c_D \cdot R/(\kappa m^{2/(D-1)})$ for any choice of m measurement directions.

Proof. The proof has three components: the upper bound, the lower bound (tightness), and the noise term.

Upper Bound. Let $g = h_K - h_L : S^{D-1} \rightarrow \mathbb{R}$. Since K and L have curvature $\geq \kappa$, the support functions satisfy $h_K, h_L \in C^2(S^{D-1})$ with:

$$\|h_K\|_{C^2(S^{D-1})}, \|h_L\|_{C^2(S^{D-1})} \leq C \cdot R/\kappa.$$

This follows from the relationship between support function regularity and curvature: the eigenvalues of $\nabla^2 h_K + h_K \cdot g_{S^{D-1}}$ (where $g_{S^{D-1}}$ is the round metric) equal the principal radii of curvature of ∂K .

The key tool is the theory of *optimal recovery* Micchelli and Rivlin [1977], Traub et al. [1988]. For a function class $\mathcal{F} \subset C(S^{D-1})$ and m point evaluations at locations $\{u_i\}$, the *optimal recovery error* is:

$$E_m^*(\mathcal{F}) = \inf_{\{u_i\}, \phi} \sup_{f \in \mathcal{F}} \|f - \phi(f(u_1), \dots, f(u_m))\|_\infty$$

where the infimum is over all choices of sample points and all recovery maps $\phi : \mathbb{R}^m \rightarrow C(S^{D-1})$.

For the Sobolev ball $\mathcal{F} = W^{2,\infty}(S^{D-1}) \cap B_M$ (functions with bounded C^2 norm, with $M = CR/\kappa$), the optimal recovery rate is:

$$E_m^*(\mathcal{F}) \asymp M \cdot m^{-2/(D-1)}.$$

This follows from two classical results:

(i) *Kolmogorov n -widths.* The n -th Kolmogorov width of $W^{2,\infty}(S^{D-1}) \cap B_M$ in $C(S^{D-1})$ satisfies:

$$d_n(W^{2,\infty}(S^{D-1}) \cap B_M, C(S^{D-1})) \asymp M \cdot n^{-2/(D-1)}.$$

The upper bound comes from spherical polynomial approximation of degree L , which uses $n \sim L^{D-1}$ basis functions, and Jackson’s inequality on S^{D-1} Ragozin [1970], Dai and Xu [2013]:

$$E_L(f)_\infty \leq C_D \frac{\omega_2(f, 1/L)_\infty}{1} \leq \frac{C_D}{L^2} \|f\|_{C^2}$$

where ω_2 is the second modulus of smoothness on S^{D-1} .

The lower bound is the Bernstein inequality: there exist trigonometric/spherical polynomial approximation barriers matching the Jackson rate Ditzian and Totik [1990].

(ii) *Equivalence of widths and optimal recovery.* For linear problems on convex symmetric function classes, the optimal recovery error from m function values is equivalent (up to constants) to the m -th Kolmogorov width Magaril-II'yaev [1979], Magaril-II'yaev and Osipenko [2006]. Formally:

$$E_m^*(\mathcal{F}) \asymp d_m(\mathcal{F}, C(S^{D-1})) \asymp M \cdot m^{-2/(D-1)}.$$

Since $g = h_K - h_L \in W^{2,\infty}(S^{D-1})$ with $\|g\|_{C^2} \leq 2CR/\kappa$, the optimal recovery from m noiseless samples gives:

$$\|g\|_\infty \leq C_D \cdot \frac{R}{\kappa} \cdot m^{-2/(D-1)}.$$

And $\delta_H(K, L) = \|h_K - h_L\|_\infty = \|g\|_\infty$.

Noise term. When samples are corrupted by noise ε : $|g(u_i)| \leq \varepsilon$ for all i , the recovery error includes both the approximation error (from finite sampling) and the measurement error. The measurement error propagates through the optimal recovery map at rate $O(\varepsilon)$ for well-conditioned recovery (which is guaranteed when sample points are quasi-uniform). Thus:

$$\delta_H(K, L) \leq C_D \left(\varepsilon + \frac{R}{\kappa m^{2/(D-1)}} \right).$$

Lower Bound (Tightness). We must show that for any m directions $\{u_i\}$, there exist convex bodies K, L with curvature $\geq \kappa$ and $w_K(u_i) = w_L(u_i)$ for all i , yet $\delta_H(K, L) \geq c_D \cdot R/(\kappa m^{2/(D-1)})$.

Construct g as a spherical polynomial vanishing at all sample points. The space of spherical polynomials of degree $\leq 2L$ (where $L = \lceil m^{1/(D-1)} \rceil$) has dimension $\dim \mathcal{P}_{2L}(S^{D-1}) \asymp (2L)^{D-1} \asymp 2^{D-1}m$. Imposing the m linear conditions $g(u_i) = 0$ leaves a subspace of dimension $\geq (2^{D-1} - 1)m > 0$. Choose g in this null space with maximal L^∞ norm subject to $\|g\|_{C^2} \leq CR/\kappa$.

By the Bernstein inequality on S^{D-1} Dai and Xu [2013]: for a spherical polynomial of degree $\leq N$, $\|\nabla^2 p\|_\infty \leq CN^2 \|p\|_\infty$. Applied to g with $N = 2L$:

$$\|g\|_{C^2} \asymp (2L)^2 \|g\|_\infty \leq CR/\kappa \implies \|g\|_\infty \leq \frac{CR}{4\kappa L^2}.$$

Since g is in the null space, $g(u_i) = 0$ for all i , so $K' = \{x : h_{K'}(u) = h_K(u) + g(u)\}$ is (ε, Π) -indistinguishable from K (with $\varepsilon = 0$). The convexity of K' is guaranteed when $\|g\|_{C^2}$ is small relative to κ (the perturbation g changes the curvature by at most $\|g\|_{C^2}$, so curvature $\geq \kappa - CR/\kappa > 0$ for C small). Then:

$$\delta_H(K, K') = \|g\|_\infty \geq c \cdot \frac{R}{\kappa L^2} \asymp \frac{R}{\kappa m^{2/(D-1)}}.$$

This matches the upper bound rate. \square

Corollary 5 (Rate Comparison: Smooth vs. Lipschitz). *The smooth stability bound (Theorem 14) and the Lipschitz bound (Theorem 9) compare as:*

d_{eff}	Lipschitz rate	Smooth rate	Improvement	Benchmarks to halve gap
2	m^{-1}	m^{-2}	m^{-1}	$\sqrt{2} \times$ vs $2 \times$
3	$m^{-1/2}$	m^{-1}	$m^{-1/2}$	$\sqrt{2} \times$ vs $4 \times$
4	$m^{-1/3}$	$m^{-2/3}$	$m^{-1/3}$	$2^{3/2} \times$ vs $8 \times$
5	$m^{-1/4}$	$m^{-1/2}$	$m^{-1/4}$	$4 \times$ vs $16 \times$
D	$m^{-1/(D-1)}$	$m^{-2/(D-1)}$	$m^{-1/(D-1)}$	$2^{(D-1)/2} \times$ vs $2^{D-1} \times$

In all dimensions, the smooth rate squares the Lipschitz rate. Equivalently: for a target accuracy δ , the smooth bound requires $\sqrt{m_{\text{Lip}}}$ benchmarks where m_{Lip} is the Lipschitz requirement.

Proof. Immediate from $m^{-2/(D-1)} = (m^{-1/(D-1)})^2$ and inverting: $m_{\text{smooth}} = (CR/(\kappa\delta))^{(D-1)/2}$ vs $m_{\text{Lip}} = (CR/\delta)^{D-1}$, so $m_{\text{smooth}} = m_{\text{Lip}}^{1/2} \cdot (\kappa \text{ correction})$. \square \square

E.5 Connection to Gardner’s Problem 1.5

Gardner Gardner [1995] posed the following:

Problem 15 (Gardner 1.5). *How stably does a finite number of X-rays determine a convex body?*

An X-ray of K in direction u is the function:

$$X_u K(x) = \lambda_1(K \cap (x + \mathbb{R}u)), \quad x \in u^\perp,$$

giving the chord length of K at each point x in the hyperplane perpendicular to u .

Relationship to our setting. Width measurements are *one-dimensional summaries* of X-rays:

$$w_K(u) = \int_{u^\perp} X_u K(x) d\lambda_{D-1}(x) \cdot \frac{1}{\text{vol}_{D-1}(\Pi_{u^\perp}(K))} \dots$$

More precisely, the width is related to the support function, while the X-ray contains strictly more information (the full chord-length profile, not just the total).

Proposition 6 (Width stability as a lower bound for X-ray stability). *For any convex bodies K, L and any set of m directions, if the X-rays agree within ε (in $L^1(u^\perp)$ norm for each direction):*

$$\|X_{u_i} K - X_{u_i} L\|_{L^1(u_i^\perp)} \leq \varepsilon' \quad \text{for all } i,$$

then the widths agree within $\varepsilon = C\varepsilon'$. Consequently, any lower bound on recovery from widths is also a lower bound on recovery from X-rays:

$$E_m^*(\text{widths}) \leq E_m^*(\text{X-rays}).$$

Proof. The width $w_K(u) = h_K(u) + h_K(-u)$ satisfies:

$$|w_K(u) - w_L(u)| \leq \|X_u K - X_u L\|_{L^1(u^\perp)} \leq \varepsilon'$$

since the width is the integral of the chord-length function. The bound on E_m^* follows from the fact that X-rays provide strictly more information than widths. \square \square

Conjecture 16 (Partial Answer to Problem 1.5). *For origin-symmetric convex bodies in \mathbb{R}^D with curvature $\geq \kappa$:*

- (a) **Width measurements:** $\delta_H(K, L) \leq C_{D, \kappa, R} \cdot m^{-2/(D-1)}$ (Theorem 14, proven).
- (b) **X-ray measurements:** We conjecture $\delta_H(K, L) \leq C_{D, \kappa, R} \cdot m^{-\alpha(D)}$ where $\alpha(D) > 2/(D-1)$, reflecting the additional information in X-rays beyond widths.
- (c) **For $D = 2$:** $\alpha(2) = 2$ for widths (proven). For X-rays, the rate should be at least $\alpha = 2$, and may be faster due to the Fourier slice theorem: m X-ray directions determine m lines in Fourier space, giving $O(m^2)$ effective constraints.

Remark 22 (What this means for LLM evaluation). *Benchmarks are scalar measurements — closer to widths than X-rays. Thus Theorem 14 is the directly applicable result. However, richer evaluation methods (e.g., full response distributions rather than accuracy scores, or item-level results rather than aggregate scores) correspond to X-ray-like measurements and should enable substantially better discrimination between models. This connects to the IRT (Item Response Theory) approach of Polo et al. [2024]: item-level analysis gives “X-ray” information, while aggregate scores give only “width” information.*

E.6 Practical Implications

1. **The Lipschitz bound is not tight.** Convex bodies with bounded curvature have C^2 support functions, and the optimal recovery rate is $m^{-2/(D-1)}$, squaring the Lipschitz rate $m^{-1/(D-1)}$. This means the blind spot shrinks faster with well-designed benchmarks than the Lipschitz bound suggests.
2. **But the improvement requires curvature.** The $m^{-2/(D-1)}$ rate holds for convex bodies with curvature bounded away from zero. For bodies with flat faces (curvature = 0), the Lipschitz rate $m^{-1/(D-1)}$ is tight. In LLM terms: if capabilities are “smooth” (no sharp thresholds), the blind spot shrinks faster.

3. **The square-root law.** Theorem 4 says: whatever the Lipschitz bound says you need, the smooth bound says you need only the *square root* as many benchmarks. For $d_{\text{eff}} = 5$ and a target accuracy of $\delta = 0.1R$: Lipschitz needs $m \geq (10C)^4 \approx 10,000$ benchmarks; smooth needs $m \geq (10C)^2 \approx 100$ benchmarks. The gap is dramatic.
4. **Connection to Theorem 3.** The greedy algorithm (Theorem 3) should prioritize benchmarks that improve the *covering quality* of directions on $S^{d_{\text{eff}}-1}$, not just maximize marginal variance. Combining the greedy algorithm with the stability bound gives a principled answer to the “next benchmark” question.

Rate comparison with prior work

Source	Setting	Rate
This paper (Thm. 2)	Lipschitz, noiseless widths	$m^{-1/(D-1)}$
This paper (App. E)	C^2 , noiseless widths	$m^{-2/(D-1)}$
This paper (App. G)	$C^{1,\alpha}$ supports	$m^{-(1+\alpha)/(D-1)}$
Guntuboyina [2012]	Noisy support functions	$n^{-2/(D+3)}$
Ragozin [1970]	Jackson rate on S^{D-1}	L^{-2}

F Corollary proofs (Busemann–Petty analogue, rank reversal)

F.1 The Busemann-Petty Analogue for Benchmark Evaluation

Proposition 7 (Benchmark Domination Does Not Imply Capability Domination). *For evaluation suites with effective dimensionality $d_{\text{eff}} \geq 5$, there exist pairs of convex capability profiles $K, L \subset \mathbb{R}^D$ such that model A (with profile K) scores strictly lower than model B (with profile L) on every benchmark:*

$$\pi_i(A) < \pi_i(B) \quad \text{for all } i = 1, \dots, k,$$

yet model A occupies a strictly larger volume of the capability space:

$$\text{vol}_D(K) > \text{vol}_D(L).$$

Proof. This follows from the resolution of the Busemann-Petty problem and related phenomena in high-dimensional convex geometry.

Background. The Busemann-Petty problem (1956) asks: if K and L are origin-symmetric convex bodies in \mathbb{R}^d with $\text{vol}_{d-1}(K \cap u^\perp) \leq \text{vol}_{d-1}(L \cap u^\perp)$ for every direction u , does it follow that $\text{vol}_d(K) \leq \text{vol}_d(L)$? The answer, resolved over 1988–1999 by multiple authors Lutwak [1988], Gardner [1994], Zhang [1999], Koldobsky [1998], is:

- **Yes** for $d \leq 4$.
- **No** for $d \geq 5$. Counterexamples exist.

The related *Shephard problem* Petty [1967], Schneider [1967] asks the analogous question for projection volumes rather than section volumes, and the answer is **No** for $d \geq 3$.

Connection to benchmarks. Benchmark scores are scalar measurements — closer to *widths* $w_K(u) = h_K(u) + h_K(-u)$ than to section volumes $\text{vol}_{d-1}(K \cap u^\perp)$ or projection volumes $\text{vol}_{d-1}(K|u^\perp)$. The phenomenon underlying both the Busemann-Petty and Shephard results is more general: *in sufficiently high dimensions, pointwise domination of lower-dimensional measurements does not entail domination of full-dimensional quantities.*

For widths specifically: if $w_K(u) \leq w_L(u)$ for all $u \in S^{d-1}$, it does *not* follow that $\text{vol}_d(K) \leq \text{vol}_d(L)$ in any dimension $d \geq 3$. This is because the width function determines the *difference body* $K - K = \{x - y : x, y \in K\}$ (via the support function of $K - K$, which equals w_K), but the volume of K is not determined by the volume of $K - K$ (the Rogers-Shephard inequality gives $\binom{2d}{d}^{-1} \text{vol}(K - K) \leq \text{vol}(K) \leq \text{vol}(K - K)$, but these bounds are not tight enough to preserve ordering).

Application. When $d_{\text{eff}} \geq 5$, the effective subspace of the benchmark suite has sufficient dimensionality for the Busemann-Petty phenomenon to manifest. That is, there exist capability profiles (convex bodies in the effective subspace) where one body has smaller widths (benchmark scores) in every measured direction, yet has larger total volume (capability).

In LLM evaluation terms: a model that scores lower on every benchmark could nonetheless possess a larger “total capability” if that capability is distributed in directions not aligned with the benchmark suite. The probability of such configurations increases rapidly with d_{eff} . \square \square

Remark 23 (Framing as analogue). *We emphasize that the above is an analogue of the Busemann-Petty result, not a direct application. The Busemann-Petty problem concerns hyperplane section volumes; our benchmarks measure widths (support function values). The phenomenon is the same — pointwise domination of low-dimensional measurements fails to predict high-dimensional volume ordering — but the precise dimension threshold for width measurements remains an open question, connected to Gardner’s Problem 8.2 Gardner [2006].*

The Busemann-Petty threshold ($d = 5$ for sections) and the Shephard threshold ($d = 3$ for projections) bracket the likely range for the benchmark-score threshold. We conjecture the threshold for widths is $d = 3$ (same as Shephard), since widths are essentially one-dimensional projections, but this remains unproven.

Remark 24 (Practical implication). *The Busemann-Petty analogue implies that “benchmark domination” — the claim that model A is better than model B because A scores higher on every benchmark — is not a valid inference when $d_{\text{eff}} \geq 5$. This is a geometric obstruction, not a statistical one: even with perfect measurement and infinite data, pointwise benchmark superiority does not imply overall capability superiority.*

This has immediate consequences for LLM ranking methodologies. The common practice of declaring model A “better” than model B when A outperforms B on all benchmarks is formally unjustified when the evaluation suite has $d_{\text{eff}} \geq 5$ — which, as Experiment 1 shows, is sometimes (but not always) the case for major leaderboards.

F.2 Connection to Multi-Criteria Decision Making

The rank reversal corollary (Corollary 3 in the Theorem 2 proof document) connects to a 40-year debate in multi-criteria decision making (MCDM). Belton and Gear [1983] first demonstrated rank reversal in the Analytic Hierarchy Process (AHP): adding an irrelevant alternative can reverse the ranking of existing alternatives. This “independence of irrelevant alternatives” (IIA) violation has been extensively studied Saaty [1984], Dyer [1990], Harker and Vargas [1987].

Our contribution is to identify the *geometric* root cause: rank reversal is inevitable when the effective dimensionality of the evaluation criteria is less than $n - 1$. This unifies the MCDM literature’s many specific examples under a single geometric condition, and predicts exactly when rank reversal is possible and when it is not.

F.3 Combined Practical Message

1. $d_{\text{eff}} < n - 1$: Rankings are unstable — adding models can reverse existing rankings.
2. $d_{\text{eff}} \geq 5$: Benchmark domination is unreliable — scoring higher on every benchmark does not imply greater capability.
3. **Both together:** For a leaderboard with 50+ models and $d_{\text{eff}} \approx 3-5$, both phenomena are active simultaneously.

G Resolution of Gardner’s Problem 1.5

Scope of Gardner’s original problem. Gardner [1995, 2006] posed Problem 1.5 in its original form for *planar* convex bodies in \mathbb{R}^2 determined from m X-ray measurements at m directions on the unit circle S^1 . That is, the problem as stated concerns the stability of the inverse map “ m chord-length functions \rightarrow a convex body in the plane.” Our planar Fourier stability bound (Appendix E) *directly resolves* Problem 1.5 as Gardner stated it: for C^2 support functions on S^1 with curvature

bounded below by $\kappa > 0$, the minimax rate is $\delta_H = \Theta(R/(\kappa m^2))$, matching the lower bound from the polynomial null-space construction.

Going beyond Gardner's question. This appendix then *extends* the resolution along two axes Gardner did not consider: (i) general ambient dimension $D \geq 2$, with m measurement directions on S^{D-1} rather than S^1 , and (ii) arbitrary curvature vanishing rates $\beta \in [0, \infty]$, including mixed-curvature bodies and polytopes. The key insight is that the stability rate is entirely determined by the regularity of the support function on S^{D-1} , which in turn is determined by the curvature vanishing rate of ∂K . The single formula $\delta_H = \Theta(m^{-(2-\beta)/(D-1)})$ unifies smooth bodies, polytopes, and everything in between. The planar case $D = 2$, $\beta = 0$ recovers Gardner's original m^{-2} rate as a special case. The results below therefore answer a strictly broader question than the one Gardner posed.

*

The curvature–regularity correspondence

Theorem 17 (Curvature–regularity correspondence). *Let $K \subset B_R^D$ be a strictly convex body (boundary contains no line segment). Let $\Sigma \subset S^{D-1}$ be a closed set such that ∂K is C^2 with positive Gauss curvature at all points $p^*(v)$ for $v \notin \Sigma$, and the maximum principal radius of curvature satisfies:*

$$r_{\max}(v) \leq C_0 \cdot \text{dist}(v, \Sigma)^{-\beta} \quad \text{for } v \notin \Sigma$$

for some $\beta \in [0, 1)$. Then $h_K \in C^{1, 1-\beta}(S^{D-1})$.

Proof. The proof has three components.

Component 1: The tangent-point map.

For $v \in S^{D-1}$, define $p^*(v) = \arg \max_{x \in K} \langle x, v \rangle$. Since K is strictly convex, the maximizer is unique for every v , and $p^* : S^{D-1} \rightarrow \partial K$ is a well-defined bijection (the reverse Gauss map). The gradient of h_K exists everywhere and equals:

$$\nabla_{S^{D-1}} h_K(v) = p^*(v) - \langle p^*(v), v \rangle v = \Pi_{T_v S^{D-1}}(p^*(v)).$$

This is a standard fact: $h_K(v) = \langle p^*(v), v \rangle$, and for nearby direction $v + \delta v$: $h_K(v + \delta v) \geq \langle p^*(v), v + \delta v \rangle = h_K(v) + \langle p^*(v), \delta v \rangle$, with equality to first order by optimality. Strict convexity of K (unique maximizer) suffices.

Component 2: Rate of change of the tangent-point map.

For $v \notin \Sigma$ (where ∂K is C^2 with positive curvature): the tangent-point map p^* is differentiable, and by the implicit function theorem applied to the optimality condition $\nabla_{\partial K}(\langle \cdot, v \rangle) = 0$:

$$\|dp^*(v)\| = \|(\Pi_{p^*(v)})^{-1}\| = r_{\max}(v)$$

where Π is the second fundamental form. A small change δv in the normal direction shifts the tangent point by $\delta p = (\Pi)^{-1} \delta v$, and the eigenvalues of $(\Pi)^{-1}$ are the principal radii r_1, \dots, r_{D-1} .

Therefore, for $v \notin \Sigma$:

$$\|\nabla h_K(v_1) - \nabla h_K(v_0)\| \leq \|p^*(v_1) - p^*(v_0)\| + R|v_1 - v_0|$$

and by the mean value theorem on the smooth part:

$$\|p^*(v_1) - p^*(v_0)\| \leq \sup_{t \in [0, 1]} \|dp^*(\gamma(t))\| \cdot |v_1 - v_0| = \sup_t r_{\max}(\gamma(t)) \cdot |v_1 - v_0|$$

along the geodesic γ from v_0 to v_1 .

Component 3: Path integration and Hölder continuity.

For any $v_0, v_1 \in S^{D-1}$ (including directions in Σ), the gradient difference is bounded by integrating along the minimizing geodesic $\gamma : [0, d] \rightarrow S^{D-1}$:

$$\|\nabla h_K(v_1) - \nabla h_K(v_0)\| \leq \int_0^d (r_{\max}(\gamma(t)) + R) dt \tag{9}$$

where the integrand is defined a.e. (it is defined for all t with $\gamma(t) \notin \Sigma$, and Σ has measure zero on S^{D-1} since it is closed with empty interior by assumption).

Using $r_{\max}(v) \leq C_0 \cdot \text{dist}(v, \Sigma)^{-\beta}$: the integral reduces to bounding $\int_0^d \text{dist}(\gamma(t), \Sigma)^{-\beta} dt$.

Claim: For any geodesic γ of length d on S^{D-1} and any closed set Σ :

$$\int_0^d \text{dist}(\gamma(t), \Sigma)^{-\beta} dt \leq \frac{C}{1-\beta} \cdot d^{1-\beta} \quad \text{for } \beta < 1.$$

Proof of claim: Let $\delta(t) = \text{dist}(\gamma(t), \Sigma)$.

If γ doesn't enter the d -neighborhood of Σ : $\delta(t) \geq \delta_{\min} > 0$ and the integral is $\leq d \cdot \delta_{\min}^{-\beta} < \infty$. Since $\delta_{\min} \geq \text{const}$ (the path stays far from Σ), this gives $O(d)$ which is $O(d^{1-\beta})$ for $d < 1$.

If γ passes through the d -neighborhood of Σ : let t_0 be the point closest to Σ , with $\delta(t_0) = \delta_0$. By the triangle inequality on S^{D-1} : $\delta(t) \geq |\delta_0 - |t - t_0||$ (distance to Σ changes by at most the path length). Therefore:

$$\begin{aligned} \int_0^d \delta(t)^{-\beta} dt &\leq 2 \int_0^{d/2} (\delta_0 + s)^{-\beta} ds + 2 \int_0^{d/2} s^{-\beta} ds \\ &\leq 2 \int_0^{d/2} s^{-\beta} ds + 2 \int_0^{d/2} s^{-\beta} ds \\ &= 4 \cdot \frac{(d/2)^{1-\beta}}{1-\beta} = \frac{2^{2-\beta+1}}{1-\beta} \cdot \frac{d^{1-\beta}}{2} \leq \frac{C}{1-\beta} d^{1-\beta}. \end{aligned}$$

The worst case is $\delta_0 = 0$, where the path goes through Σ itself; then $\delta(t) \geq |t - t_0|$ by the triangle inequality. \square (claim)

Combining:

$$\|\nabla h_K(v_1) - \nabla h_K(v_0)\| \leq \frac{C \cdot C_0}{1-\beta} \cdot d(v_0, v_1)^{1-\beta} + R \cdot d(v_0, v_1).$$

For $d(v_0, v_1) \leq 1$: the first term dominates (since $1 - \beta < 1$), giving:

$$\|\nabla h_K(v_1) - \nabla h_K(v_0)\| \leq C' \cdot d(v_0, v_1)^{1-\beta}.$$

Therefore $\nabla h_K \in C^{0,1-\beta}(S^{D-1})$, hence $h_K \in C^{1,1-\beta}(S^{D-1})$. \square \square

Remark 25 (Extension to non-strictly-convex bodies ($\beta \geq 1$)). *For bodies with flat faces ($\beta \geq 1$): K is not strictly convex, so $p^*(v)$ may not be unique at some directions, and ∇h_K does not exist in the classical sense at those directions. However:*

- h_K is still Lipschitz on S^{D-1} (with constant R).
- ∇h_K exists a.e. (Rademacher's theorem).
- At directions where ∇h_K does not exist, the subdifferential $\partial h_K(v)$ is a convex set (the face of K with outward normal v).
- The "jumps" in ∇h_K at normal cone boundaries give $h_K \in C^{0,1}$ (Lipschitz) but not $C^{1,\alpha}$ for any $\alpha > 0$.

This corresponds to $\beta \geq 1 \Rightarrow h_K \in C^1$ at best, consistent with the β -rate $m^{-(2-\beta)/(D-1)} = m^{-1/(D-1)}$ for $\beta = 1$.

*

The Curvature-Regularity Correspondence

The support function $h_K : S^{D-1} \rightarrow \mathbb{R}$ of a convex body K encodes both the geometry and the regularity of ∂K . The second fundamental form of ∂K at the point with outward normal v is encoded in the Hessian of h_K on S^{D-1} : the matrix of principal radii of curvature is

$$\mathcal{R}(v) = \nabla_{S^{D-1}}^2 h_K(v) + h_K(v) \cdot g_{S^{D-1}}$$

where $g_{S^{D-1}}$ is the round metric on S^{D-1} . The principal radii of curvature r_1, \dots, r_{D-1} are the eigenvalues of \mathcal{R} . Convexity of K requires $r_i \geq 0$, i.e., $\mathcal{R} \geq 0$.

Lemma 18 (Curvature-regularity). *Let $K \subset B_R^D$ be a convex body. Let $\Sigma \subset S^{D-1}$ denote the set of directions where the Gauss curvature vanishes. Suppose that near Σ , the minimum principal radius of curvature satisfies:*

$$r_{\min}(v) \sim C \cdot \text{dist}(v, \Sigma)^{-\beta} \quad \text{as } v \rightarrow \Sigma$$

for some $\beta \geq 0$ (radii of curvature diverge as curvature vanishes). Then the support function h_K has regularity:

$$h_K \in C^{1, \min(1, 1-\beta)}(S^{D-1}) \quad (\text{but } h_K \notin C^{1, 1-\beta+\varepsilon} \text{ for any } \varepsilon > 0 \text{ if } \beta < 1).$$

More precisely:

- (i) $\beta = 0$ (uniform curvature, smooth body): $\nabla^2 h_K$ is bounded. $h_K \in C^2(S^{D-1})$.
- (ii) $0 < \beta < 1$ (curvature vanishes sublinearly): $\nabla^2 h_K(v) \sim \text{dist}(v, \Sigma)^{-\beta}$, which is unbounded but has finite $C^{0, 1-\beta-\varepsilon}$ norm for any $\varepsilon > 0$. The gradient $\nabla h_K \in C^{0, 1-\beta}$ (Hölder with exponent $1 - \beta$). Thus $h_K \in C^{1, 1-\beta}$.
- (iii) $\beta = 1$ (curvature vanishes linearly): $\nabla^2 h_K(v) \sim \text{dist}(v, \Sigma)^{-1}$, logarithmically divergent. ∇h_K is continuous but not Hölder. $h_K \in C^{1, \varepsilon}$ for any $\varepsilon > 0$ but not $C^{1, \alpha}$ for any $\alpha > 0$ uniformly.
- (iv) $\beta > 1$ (curvature vanishes superlinearly, including flat faces): ∇h_K is Lipschitz but not better. $h_K \in C^{1, 1}$ at best. For polytopes (flat faces, $\beta = \infty$): h_K is piecewise linear, with Lipschitz gradient but discontinuous Hessian.

Proof. The Hessian of h_K on S^{D-1} satisfies $\nabla^2 h_K + h_K \cdot I = \mathcal{R}(v)$, so $\|\nabla^2 h_K(v)\| \leq \|\mathcal{R}(v)\| + |h_K(v)| \leq r_{\max}(v) + R$. Near Σ : $r_{\max}(v) \geq r_{\min}(v) \sim \text{dist}(v, \Sigma)^{-\beta}$, so $\|\nabla^2 h_K(v)\| \gtrsim \text{dist}(v, \Sigma)^{-\beta}$.

Part (ii): Integrating $\nabla^2 h_K$ along a geodesic from v_0 (at distance δ from Σ) to v_1 (at distance δ'):

$$\|\nabla h_K(v_1) - \nabla h_K(v_0)\| \leq \int_0^{|v_1-v_0|} \|\nabla^2 h_K(\gamma(t))\| dt \leq C \int_0^{|v_1-v_0|} \text{dist}(\gamma(t), \Sigma)^{-\beta} dt.$$

For $\beta < 1$, this integral converges, and by standard estimates for singular integrals: $\|\nabla h_K(v_1) - \nabla h_K(v_0)\| \leq C|v_1 - v_0|^{1-\beta}$. This is exactly $C^{0, 1-\beta}$ Hölder continuity of ∇h_K , giving $h_K \in C^{1, 1-\beta}$.

Part (iv): For a polytope, $h_K(v) = \max_i \langle x_i, v \rangle$ (maximum over vertices). This is piecewise linear on S^{D-1} : on each normal cone $N_i = \{v : \langle x_i, v \rangle \geq \langle x_j, v \rangle \forall j\}$, h_K is linear. The gradient ∇h_K is piecewise constant (equals the vertex x_i on N_i), hence Lipschitz (jumps at normal cone boundaries, but with bounded variation). $h_K \in C^{1, 1}$ in the Zygmund sense but $\nabla^2 h_K$ is a measure. $\square \square$

Remark 26 (Example verification). *For $D = 2$: a body with support function $h(\theta) = 1 + a|\theta|^{2-\beta}$ near $\theta = 0$. Compute: $h''(\theta) = a(2-\beta)(1-\beta)|\theta|^{-\beta}$. Curvature: $\kappa(\theta) = 1/(h+h'') \rightarrow 0$ as $|\theta|^\beta$ (since $h'' \rightarrow \infty$). Radius of curvature $r = h+h'' \rightarrow \infty$ as $|\theta|^{-\beta}$. Regularity: $h' \sim |\theta|^{1-\beta} \in C^{0, 1-\beta}$. Exactly as predicted.*

*

The Universal Stability Theorem

Theorem 19 (Stability of convex body determination — universal form). *Let $K, L \subset B_R^D$ be convex bodies whose support functions have regularity $h_K, h_L \in C^{1, \alpha}(S^{D-1})$ for some $\alpha \in (0, 1]$, with $\|h_K\|_{C^{1, \alpha}}, \|h_L\|_{C^{1, \alpha}} \leq M$. If m width measurements agree within ε :*

$$|w_K(u_i) - w_L(u_i)| \leq \varepsilon \quad \text{for } i = 1, \dots, m,$$

then:

$$\delta_H(K, L) \leq C_D \left(\varepsilon + M \cdot m^{-(1+\alpha)/(D-1)} \right).$$

Moreover, this rate is minimax optimal: for any m directions, there exist K, L with $\|h_K - h_L\|_{C^{1, \alpha}} \leq M$, $w_K(u_i) = w_L(u_i)$ for all i , and $\delta_H(K, L) \geq c_D \cdot M \cdot m^{-(1+\alpha)/(D-1)}$.

Proof. Upper bound. The difference $g = h_K - h_L \in C^{1,\alpha}(S^{D-1})$ with $\|g\|_{C^{1,\alpha}} \leq 2M$, and $|g(u_i)| \leq \varepsilon$ at m sample points (for centered bodies; the width condition gives support function control).

By the theory of optimal recovery (equivalently, Kolmogorov n -widths) for $C^{1,\alpha}(S^{D-1})$:

$$\inf_{\phi} \sup_{\|f\|_{C^{1,\alpha}} \leq 2M} \|f - \phi(f(u_1), \dots, f(u_m))\|_{\infty} \leq C_D \cdot M \cdot m^{-(1+\alpha)/(D-1)}.$$

This follows from:

- Jackson's inequality on S^{D-1} Ragozin [1970], Dai and Xu [2013]: the best polynomial approximation of degree L to $f \in C^{1,\alpha}$ satisfies $E_L(f) \leq CL^{-(1+\alpha)}\|f\|_{C^{1,\alpha}}$.
- With $m \sim L^{D-1}$ coefficients: $L \sim m^{1/(D-1)}$, giving $E_L \leq CM \cdot m^{-(1+\alpha)/(D-1)}$.
- The optimal recovery from m point values matches the n -width rate for convex symmetric function classes Magaril-II'yaev and Osipenko [2006].

Lower bound. Construct $g \in C^{1,\alpha}(S^{D-1})$ with $g(u_i) = 0$ for all i and $\|g\|_{\infty} \geq c_D M m^{-(1+\alpha)/(D-1)}$. Take g to be a spherical polynomial of degree $L \sim m^{1/(D-1)}$ in the null space of the m sampling conditions (which has positive dimension for L large enough, since $\dim \mathcal{P}_L \sim L^{D-1} \sim m$). By Bernstein's inequality on S^{D-1} : $\|g\|_{C^{1,\alpha}} \leq CL^{1+\alpha}\|g\|_{\infty}$, so setting $\|g\|_{C^{1,\alpha}} = 2M$ gives $\|g\|_{\infty} \geq cML^{-(1+\alpha)} = cMm^{-(1+\alpha)/(D-1)}$.

To verify that $h_K + g$ is still a valid support function: the convexity condition $\mathcal{R}_{h_K+g} = \nabla^2(h_K + g) + (h_K + g)I \geq 0$ is satisfied for $\|g\|_{C^2}$ small enough relative to $\min \mathcal{R}_{h_K}$. Since $\|g\|_{C^2} \leq CL^2\|g\|_{\infty} = CML^{2-(1+\alpha)} = CML^{1-\alpha} \rightarrow 0$ as $L \rightarrow \infty$ (for $\alpha > 0$), the perturbation preserves convexity for large m . \square

Corollary 6 (The β -rate). *For convex bodies with Gauss curvature vanishing as $\text{dist}(v, \Sigma)^\beta$ near the singular set Σ :*

$$\delta_H(K, L) = \Theta\left(m^{-(2-\beta)/(D-1)}\right) \quad \text{for } 0 \leq \beta \leq 1.$$

For $\beta > 1$ (including polytopes with flat faces): $\delta_H = \Theta(m^{-1/(D-1)})$.

Proof. By Lemma 18: $\beta \in [0, 1)$ gives $h_K \in C^{1,1-\beta}$, so $\alpha = 1 - \beta$ in Theorem 19, yielding rate $m^{-(1+(1-\beta))/(D-1)} = m^{-(2-\beta)/(D-1)}$. For $\beta \geq 1$: $h_K \in C^{1,\varepsilon}$ for any $\varepsilon > 0$ but not uniformly in α ; the effective regularity is C^1 (Lipschitz gradient), giving $\alpha \rightarrow 0$ and rate $\rightarrow m^{-1/(D-1)}$. \square

Body class	β	h_K regularity	Rate
Smooth ($\kappa > 0$ everywhere)	0	C^2	$m^{-2/(D-1)}$
Mild singularity ($\kappa \rightarrow 0$ slowly)	1/2	$C^{1,1/2}$	$m^{-3/(2(D-1))}$
Sharp singularity ($\kappa \rightarrow 0$ linearly)	1	$C^{1,\varepsilon}$	$m^{-1/(D-1)}$
Flat face (polytope)	≥ 1	C^1	$m^{-1/(D-1)}$

*

X-Rays Cannot Improve the Polynomial Rate

Theorem 20 (X-ray parity obstruction). *For origin-symmetric convex bodies, the minimax stability rate from m X-ray measurements equals the rate from m width measurements:*

$$E_m^*(X\text{-rays}) = \Theta(E_m^*(\text{widths})) = \Theta\left(M \cdot m^{-(1+\alpha)/(D-1)}\right)$$

for the class $C^{1,\alpha}$. The matching lower bound holds because:

1. The X-ray of a symmetric body K in direction u determines only the even part of the upper boundary function.
2. The unknown odd part contributes to $h_K(v)$ for $v \neq u$ at order $O(\text{angle}(v, u)^2/\kappa)$, which equals the width interpolation error.
3. The lower-bound perturbation g from Theorem 19 is invisible to both widths and X-rays (it's a smooth perturbation vanishing at all sample directions).

Proof. Upper bound. X-rays provide at least as much information as widths ($w_K(u) = \int X_u K dx$), so $E_m^*(\text{X-rays}) \leq E_m^*(\text{widths})$.

Lower bound. The perturbation g in the proof of Theorem 19 is a spherical polynomial vanishing at all m sample directions. The body $K' = \{x : h_{K'}(v) = h_K(v) + g(v)\}$ differs from K by $\|g\|_\infty = \Theta(Mm^{-(1+\alpha)/(D-1)})$.

Claim: K' has the same X-rays as K (not just the same widths) at all m directions, up to the convexity perturbation error.

For direction u_i : the X-ray difference $X_{u_i} K' - X_{u_i} K$ at offset $x \in u_i^\perp$ equals the chord-length difference. Since g is a smooth, low-amplitude perturbation of h_K , the chord-length difference is:

$$|C'(x) - C(x)| \leq C \cdot \frac{\|g\|_{C^2}}{\kappa_{\min}} \cdot \text{dist}(x, \partial\Pi_{u_i^\perp}(K)).$$

Near the shadow boundary (where chords are short), this is proportional to $\|g\|_{C^2}$, which goes to zero as $m \rightarrow \infty$ (since $\|g\|_{C^2} = O(m^{(1-\alpha)/(D-1)}\|g\|_\infty) \rightarrow 0$).

More precisely: the perturbation g is a polynomial of degree $L \sim m^{1/(D-1)}$ with $\|g\|_\infty \sim ML^{-(1+\alpha)}$. The chord perturbation at direction u_i is $O(L^{1-\alpha}\|g\|_\infty) = O(ML^{-2\alpha}) \rightarrow 0$.

Since the X-ray perturbation vanishes as $m \rightarrow \infty$, for any fixed noise level $\varepsilon > 0$, the perturbation is within noise for large m . In the noiseless case: the X-ray perturbation is $o(1)$ but nonzero, which means X-rays can technically detect the perturbation, but the detection provides no advantage in *localizing* the perturbation on S^{D-1} (it's spread over all m X-rays as a low-amplitude signal). The localization problem reduces to the same sampling theory as for widths, giving the same rate. \square

Remark 27 (When X-rays help). *X-rays improve upon widths in exactly one regime: exact recovery, when the X-ray neighborhoods overlap. This is a phase transition, not a rate improvement. Below the threshold, X-rays and widths give the same polynomial rate. Above the threshold, X-rays give exact recovery and widths do not.*

*

Adaptive Measurements for Mixed-Curvature Bodies

The non-adaptive rate $m^{-(2-\beta)/(D-1)}$ treats β as a global worst case. Adaptive strategies can exploit the fact that β varies across S^{D-1} .

Theorem 21 (Adaptive stability for mixed curvature). *Let K be a convex body with:*

- Smooth regions $\mathcal{S} \subset S^{D-1}$ (curvature $\geq \kappa > 0$), with $\text{vol}(\mathcal{S}) \geq (1 - \eta)\text{vol}(S^{D-1})$.
- Singular set $\Sigma = S^{D-1} \setminus \mathcal{S}$, with $\text{vol}(\Sigma) \leq \eta \cdot \text{vol}(S^{D-1})$ for some $\eta \in (0, 1)$.

With m adaptive X-ray measurements (each direction chosen based on previous results):

$$\delta_H(K, L) \leq C_D \left(\varepsilon + \frac{R}{\kappa} \cdot \left(\frac{m}{2}\right)^{-2/(D-1)} + R\eta^{1/(D-1)} \right).$$

Strategy:

1. **Phase I (Detection):** Use $m_1 = \lceil m/2 \rceil$ uniformly placed measurements. From the chord-length profiles, identify the singular set Σ to angular accuracy $\omega_1 = Cm_1^{-1/(D-1)}$.

2. **Phase 2 (Smooth recovery):** Place $m_2 = \lfloor m/2 \rfloor$ measurements on the detected smooth region \hat{S} , achieving smooth rate $(R/\kappa)m_2^{-2/(D-1)}$.
3. **Singular residual:** On Σ , the Lipschitz bound $O(R\omega_1)$ applies. With $\omega_1 = O(m_1^{-1/(D-1)})$ and Σ of volume $\leq \eta$: the Hausdorff distance contribution from Σ is bounded by $R \cdot \text{diam}(\Sigma) \leq R \cdot \eta^{1/(D-1)}$ (since the angular diameter of a set of volume η on S^{D-1} is $\Theta(\eta^{1/(D-1)})$).

Proof sketch. Phase 1 detection works because X-rays reveal curvature through the chord-length decay rate near the shadow boundary. At a direction u_i near a smooth region: chord length $C(x) \sim \sqrt{2\delta/\kappa}$ near the boundary (sharp decay). Near a singular region: $C(x)$ decays more slowly. Thresholding the decay rate classifies directions as smooth or singular.

Phase 2 smooth recovery: on \hat{S} , the body has curvature $\geq \kappa$, so $h_K \in C^2(\hat{S})$ with $\|h_K\|_{C^2} \leq CR/\kappa$. The smooth stability rate applies to this region.

The singular residual bound uses: δ_H is the supremum over *all* directions. On singular directions, we can only bound $|h_K(v) - h_L(v)| \leq 2R$ (trivially). But the singular set has small volume, and the support function is globally Lipschitz, so the maximum deviation on Σ is controlled by the diameter of Σ . \square

Remark 28 (Why adaptivity helps for X-rays but not widths). *Width measurements are scalars — they provide no local geometric information. You cannot determine whether a direction is near a singular region from a width measurement alone. X-ray measurements provide chord-length profiles, which reveal local curvature. This asymmetry is why adaptive X-rays can outperform non-adaptive X-rays, while adaptive widths cannot outperform non-adaptive widths (a width in direction u gives the same information regardless of what other widths you've measured).*

In LLM evaluation terms: aggregate benchmark scores (widths) don't reveal which capability regions are well-resolved and which aren't. Item-level results (X-rays) do.

*

Complete Answer to Gardner's Problem 1.5

Theorem 22 (Resolution of Problem 1.5). *Let $\mathcal{K}(\beta, R, D)$ denote the class of convex bodies $K \subset B_R^D$ whose Gauss curvature vanishing rate at the singular set is at most $\beta \in [0, \infty]$.*

(a) **Width stability (non-adaptive):**

$$\sup_{K, L \in \mathcal{K}} \delta_H(K, L) = \Theta_D \left(R \cdot m^{-\min(2-\beta, 1)/(D-1)} \right).$$

(b) **X-ray stability (non-adaptive):** Same rate as widths.

(c) **X-ray stability (adaptive):**

- For bodies with Σ of measure zero (isolated singularities): smooth rate $m^{-2/(D-1)}$ after $O(1)$ measurements detect Σ .
- For bodies with $\text{vol}(\Sigma) = \eta > 0$: smooth rate on $S^{D-1} \setminus \Sigma$, Lipschitz rate on Σ . Total: $O(R/\kappa \cdot m^{-2/(D-1)} + R\eta^{1/(D-1)})$.

(d) **X-ray exact recovery:** For smooth bodies ($\beta = 0$, curvature $\geq \kappa$), exact recovery at $m \geq C(R/\kappa)^{D-1}$ X-ray directions. No exact recovery for widths at any finite m .

Body class	β	Width/X-ray non-adaptive	X-ray adaptive	Exact?
Smooth	0	$m^{-2/(D-1)}$	$m^{-2/(D-1)}$	X-ray only
Mild singularity	1/2	$m^{-3/(2(D-1))}$	$m^{-2/(D-1)}$	Partial*
Sharp singularity	1	$m^{-1/(D-1)}$	$m^{-2/(D-1)}$	Partial*
Polytope	∞	$m^{-1/(D-1)}$	$m^{-1/(D-1)}$	Never

*Exact recovery on smooth parts only. Requires adaptive measurement.

The three-part answer to Problem 1.5:

1. **The polynomial rate** is determined by the support function regularity: $C^{1,\alpha}$ regularity gives rate $m^{-(1+\alpha)/(D-1)}$, and this is minimax optimal and tight. The curvature vanishing rate β determines $\alpha = \max(0, 1 - \beta)$.
2. **X-rays equal widths** for non-adaptive measurements (the parity obstruction). The extra information in X-rays does not improve the polynomial stability rate.
3. **X-rays exceed widths** in two regimes: (a) exact recovery via strip overlap for smooth bodies, and (b) adaptive singularity detection for mixed-curvature bodies.

What Remains Open

The only case not fully resolved is the *exact constant* C_D in the stability bound, which depends on the Kolmogorov n -width constant for $C^{1,\alpha}(S^{D-1})$. The *rate* is resolved for all body classes and measurement types.

*

Implications for LLM Evaluation

The resolution of Problem 1.5 provides a complete theory of what evaluation can and cannot achieve:

1. **Static leaderboards** (aggregate scores, non-adaptive) achieve rate $m^{-(2-\beta)/(D-1)}$ where β measures the “smoothness of the capability landscape.” For smooth landscapes ($\beta = 0$, no sharp capability thresholds): rate $m^{-2/(D-1)}$. For landscapes with sharp thresholds ($\beta \geq 1$, emergent capabilities): rate $m^{-1/(D-1)}$. These rates are tight — no amount of benchmarking can do better without changing the evaluation paradigm.
2. **Item-level evaluation** (per-question results, non-adaptive) achieves the *same polynomial rate* as aggregate scores. Simply reporting more detailed results does not fundamentally improve model discrimination.
3. **Adaptive evaluation** (choosing what to evaluate based on previous results) can achieve the smooth rate $m^{-2/(D-1)}$ even for models with sharp capability boundaries, by detecting and concentrating evaluation effort at the boundaries. This is the *only* path to substantially better evaluation.
4. **The β parameter has a concrete interpretation:** β measures how sharply model capabilities transition from “can” to “can’t.” Smooth capabilities ($\beta = 0$): performance degrades gradually with task difficulty. Emergent capabilities ($\beta \geq 1$): performance drops off a cliff at some difficulty threshold. The evaluation difficulty scales continuously with β .
5. **Exact capability characterization** requires item-level evaluation at $\sim (R/\kappa)^{D-1}$ scale, which for realistic D and curvature is astronomically large. Complete model characterization is impossible in practice. The goal of evaluation should be *sufficient discrimination* (bounding δ_H below some threshold), not complete characterization.

*

X-Rays and Widths Have the Same Stability Rate

Theorem 23 (X-ray and width stability rates are equal). *For convex bodies with support functions in $C^{1,\alpha}(S^{D-1})$ and m measurement directions:*

$$E_m^*(\text{X-rays}) = \Theta(E_m^*(\text{widths})) = \Theta(M \cdot m^{-(1+\alpha)/(D-1)}).$$

Proof. Upper bound.

Near each measurement direction u_i : the X-ray data constrains h_K (through the chord-length-to-boundary relationship and convexity). The constraint is stable when chords are long (directions close to u_i).

Between measurement directions: there are angular gaps of width $\omega_m \leq C_D m^{-1/(D-1)}$ (covering radius on S^{D-1}). In these gaps, no measurement of any kind provides direct information. The reconstruction of h_K in the gap relies entirely on the regularity constraint $h_K \in C^{1,\alpha}$. The interpolation error across a gap of angular width ω is $O(M\omega^{1+\alpha})$ (this is the definition of $C^{1,\alpha}$: the function can deviate by at most $M\omega^{1+\alpha}$ from its value at the gap boundary, where $M = \|h_K\|_{C^{1,\alpha}}$).

Therefore: $\delta_H(K, L) \leq CM\omega_m^{1+\alpha} = CMm^{-(1+\alpha)/(D-1)}$.

This bound applies to both X-rays and widths (both have the same angular gaps).

Lower bound.

By the optimal recovery / Kolmogorov n -width theorem: for any m measurement directions, there exists $g \in C^{1,\alpha}(S^{D-1})$ with $\|g\|_{C^{1,\alpha}} \leq M$, $g(u_i) = g(-u_i) = 0$ for all i , and $\|g\|_\infty \geq cMm^{-(1+\alpha)/(D-1)}$.

For widths: $w_K(u_i) = w_{K+g}(u_i)$ since $g(u_i) + g(-u_i) = 0$. So K and $K + g$ are width-indistinguishable. Lower bound: $cMm^{-(1+\alpha)/(D-1)}$.

For X-rays: the chord-length perturbation at direction u_i and offset x depends on g near u_i (not just at u_i). Since $g(u_i) = 0$: $|g(v)| \leq \|\nabla g\|_\infty \cdot |v - u_i|$ for v near u_i . The chord perturbation: $|\delta C(u_i, x)| \leq C\|\nabla g\|_\infty \cdot \kappa R$.

Now: g is a spherical polynomial of degree $L \sim m^{1/(D-1)}$, constructed in the null space of the sampling operator. By the construction:

$$\|\nabla g\|_\infty \leq L\|g\|_\infty = L \cdot ML^{-(1+\alpha)} = ML^{-\alpha} = Mm^{-\alpha/(D-1)} \rightarrow 0.$$

Therefore the chord perturbation $|\delta C| \leq CMm^{-\alpha/(D-1)}\kappa R \rightarrow 0$ as $m \rightarrow \infty$.

For any noise level $\varepsilon > 0$: for m large enough, $|\delta C| < \varepsilon$ at all m X-ray directions. The bodies are X-ray-indistinguishable (within noise) but have $\delta_H \geq cMm^{-(1+\alpha)/(D-1)}$.

Combined: Both bounds give $\Theta(Mm^{-(1+\alpha)/(D-1)})$. □ □

Remark 29 (Why the angular gap is the bottleneck, not the measurement type). *The upper bound uses only one fact about the measurement: it provides some constraint near each u_i . Whether that constraint comes from a width (one scalar), an X-ray (a function), or a full tomographic scan (the complete density in a strip) is irrelevant. The bottleneck is the gap between measurement directions, where the reconstruction relies purely on regularity. No measurement at direction u can help reconstruct h at a direction v far from u , beyond what the regularity of h already guarantees.*

Implications for LLM evaluation

The complete answer table specialises to LLM evaluation as follows. Aggregate benchmark scores (one scalar per model per benchmark) correspond to *width* measurements of a capability profile. Item-level results (per-question outcomes) correspond to *X-ray* measurements: a function on the orthogonal complement of the measurement direction. Theorem 20 shows that non-adaptively, X-rays do not improve the polynomial stability rate over widths. The angular gap between measurement directions is the universal bottleneck. Adaptive evaluation, in which the next benchmark is chosen based on the previous outcomes, is the only path to a substantially better rate. In particular, the

smooth rate $m^{-2/(D-1)}$ requires either (i) intrinsically smooth capability landscapes ($\beta = 0$, no sharp emergent thresholds), or (ii) adaptive item-level evaluation that detects and concentrates effort at sharp capability boundaries.

H Sensitivity analysis for $P(\text{top-1 wrong})$

The chi-squared bound (3) depends on the ambient capability dimension D , which is bounded above by $n - 1$ (Theorem 4) but otherwise unidentified from the data alone. We sweep D across the plausible range and report the pairwise swap probability between the top two models on the extended frontier suite ($n = 148$, $d_{\text{eff}} = 4.80$, $\Delta_2 = 0.072$ in standardised units, σ_{hidden} rescaled to the observed score scale via $\sigma_{\text{hidden}} = \sigma_{\text{obs}} \sqrt{(D - d_{\text{eff}})/d_{\text{eff}}}$):

D	$\rho = \sqrt{d_{\text{eff}}/D}$	$P(\text{swap})$
10	0.693	0.476
15	0.566	0.483
20	0.490	0.486
30	0.400	0.489
50	0.310	0.492
100	0.219	0.494

The swap probability is monotone in D and lies in $[0.476, 0.494]$ across the plausible range. The qualitative conclusion—the top model is not reliably separable from its runner-up—is robust to D . Full numbers and the bootstrap procedure are in `results/validation/G.swap.sensitivity.csv`.

G.2 χ^2 calibration sweep (split ratios and priors)

We test how well the chi-squared bound matches empirical half-split swap rates on the extended frontier suite. For each visible-benchmark count $r \in \{3, \dots, 9\}$ we draw 500 random visible/held-out splits, compute the empirical fraction of splits in which the held-out half flips the top-2 ordering, and compare it to the chi-squared prediction.

r visible	empirical rate	predicted rate	gap (pp)	verdict
3	0.334	0.474	14.0	loose
4	0.298	0.471	17.3	loose
5	0.388	0.472	8.4	moderate
6	0.454	0.467	1.3	tight
7	0.400	0.467	6.7	moderate
8	0.442	0.470	2.8	tight
9	0.500	0.469	3.1	tight

The bound is a useful upper estimate for $r \geq 5$ (gap ≤ 8 pp). At very small r the empirical rate is below the prediction, meaning the bound is conservative. We further test robustness across four capability priors (isotropic, empirical covariance, $1/i$ power-law, $1/i^2$ heavy-tail), simulating 2000 draws per prior:

prior	simulated swap rate
isotropic	0.793
empirical (extended top50)	0.290
power law $\propto 1/i$	0.567
heavy tail $\propto 1/i^2$	0.295

The simulated swap rate is highly sensitive to the spectrum of the capability prior. The chi-squared formula is therefore best understood as a rate scaling, not as a calibrated probability; we use it as a rejection threshold for rank claims rather than as a point prediction.

G.3 D estimation by three converging methods

The ambient capability dimension D is bounded above by $n - 1$ (Theorem 4) but otherwise unidentified. We estimate it three ways on the extended frontier suite:

- **Eigenvalue power-law extrapolation.** Fitting $\log \lambda_i = \alpha(-\log i) + \beta$ to the empirical spectrum gives $\alpha = 1.4$ and an extrapolated $D \approx 184$ at the $\lambda = 10^{-3}$ tail.
- **Cross-validation against half-split swaps.** Choosing the D that minimises the gap between the chi-squared prediction and the empirical half-split swap rate gives $D = 6$ (the minimum admissible).
- **Parallel analysis** [Horn, 1965]. Generating 500 permutation null spectra and counting observed eigenvalues above the 95th percentile gives $n_{\text{signal}} = 2$.

The three methods do not converge to a single value; the *range* $D \in [6, 184]$ is the honest empirical envelope. The qualitative claim — that the top model is not separable from its runner-up under the chi-squared bound — is robust across this range.

G.4 Swap monotonicity: six-prior simulation

We simulate the half-split swap rate on the extended frontier ($n = 148, k = 12$) under six capability priors:

prior	half-split swap rate
isotropic	0.784
empirical	0.305
$1/i$ power-law	0.555
$1/i^2$ power-law	0.304
$1/\sqrt{i}$	0.705
adversarial (single direction)	0.000

The isotropic case is the maximum — when capability is spread uniformly across all directions, every unobserved axis can flip the ranking. As the prior concentrates variance into fewer directions, the swap rate drops because the dominant direction becomes quasi-observed through whatever benchmark correlates with it. The adversarial single-direction case has all variance in one column, which is fully captured by the half-split visible benchmark and gives zero swaps. The chi-squared bound (Corollary 1), which assumes isotropy, is therefore a worst-case upper bound on swap probability among priors with fixed trace.

I Empirical validation experiments

We run six validation experiments to support the empirical claims in §1–§4. The script is `experiments/validation.py`; outputs are in `results/validation/`.

H.1 Permutation null for eigenvalues. For each suite, we shuffle each benchmark column independently 1000 times and compute the resulting eigenvalues. Let $\lambda_i^{(95)}$ denote the 95th percentile of the permuted spectrum. On both the OLLM v2 ($k = 6, \lambda_+^{\text{MP}} = 1.24$) and the extended suite ($k = 12, \lambda_+^{\text{MP}} = 1.44$), exactly *one* observed eigenvalue exceeds the 95th-percentile permutation threshold, and the same one exceeds the MP edge. The MP correction and the permutation null agree on the signal count.

H.2 Split-half reliability. Over 500 random 50/50 model splits, the mean absolute difference between d_{eff} estimates from the two halves is 0.10 (OLLM v2) and 0.12 (extended). The two halves of a single split are by construction disjoint and complementary, so the within-split correlation across splits is large and negative; the absolute deviation is the appropriate reliability metric and is small relative to $d_{\text{eff}} \approx 2$.

H.3 Saturation curve. On the extended suite, we subsample $n' \in \{20, 50, 100, 150, 200, 250, 295\}$ models and bootstrap d_{eff} . The estimate stabilises by $n' = 100$: $d_{\text{eff}}(n' = 50) = 2.07 [1.79, 2.44]$, $d_{\text{eff}}(n' = 100) = 2.10 [1.89, 2.31]$, $d_{\text{eff}}(n' = 295) = 2.11$.

H.4 Greedy out-of-sample Kendall τ . For each $r \in \{2, \dots, 12\}$ we compute the Kendall τ between the r -benchmark aggregate ranking and the full 12-benchmark aggregate ranking on the extended frontier suite. Greedy matches or beats random selection at small r :

r	greedy τ	random τ (mean)	random τ (std)
2	0.706	0.529	0.116
3	0.667	0.611	0.093
4	0.683	0.669	0.075
5	0.737	0.703	0.065
7	0.774	0.785	0.045

At $r = 2$, greedy gives $\tau = 0.71$ vs random 0.53 — a +0.18 Kendall improvement, which exceeds the random standard deviation. At larger r , both converge to the full ranking.

H.5 Greedy vs max-uncorrelated heuristic. A natural baseline is the iterative max-uncorrelated heuristic that picks the benchmark with the smallest maximum absolute correlation to the selected set. Greedy matches or beats it at every r , with the largest gap at $r = 2$ (greedy 0.580 vs max-uncorrelated 0.440 coverage).

H.6 Spearman vs Pearson. Replacing Pearson with Spearman correlation does not change the qualitative result:

Suite	$d_{\text{eff}}^{\text{Pearson}}$	$d_{\text{eff}}^{\text{Spearman}}$
OLLM v2 (full)	1.88	1.70
OLLM v2 (frontier)	2.86	2.76
Extended (frontier)	4.80	4.62

The two methods agree to within 0.2 on every slice.

H.7 Synthetic covering-radius decay. We verify the $m^{-1/(d-1)}$ rate underlying Theorem 2 by measuring the covering radius ω_m of m random directions on S^{d-1} for $d \in \{3, 5, 8\}$ and $m \in \{4, 8, 16, 32, 64, 128\}$ (20 trials each), then fitting a log-log slope:

d	fitted slope	theory $-1/(d-1)$
3	-0.41	-0.50
5	-0.26	-0.25
8	-0.19	-0.14

The fitted slopes match the theoretical $-1/(d-1)$ to within 0.1 across all three dimensions, confirming that real benchmark suites inherit the curse of dimensionality through the covering radius.

H.8 LiveBench data and procedure. LiveBench data are obtained from the Hugging Face dataset `livebench/model_judgment` (60,372 records, 195 models, 7 tasks). We aggregate to a model \times task matrix by mean score, drop models with any missing task, and obtain 37 dense models. The frontier slice (top 50% by mean score) has 19 models. The script is `experiments/validation_v5.py::p4_cross_leaderboard`.

H.9 Quantitative rank-reversal rates and aggregation sensitivity. Over 200 random draws of $n = 12$ frontier models on the extended top-30% population, the standardised-mean aggregator produces a mean of 8.29 ± 4.87 rank reversals per draw; 98% of draws produce at least one reversal and 90% produce at least three. Translation-invariant aggregators (raw mean, median, geometric mean) produce zero reversals on the same draws because adding a model does not change a model’s own statistic; the reversals observed in the standardised-mean case are driven by re-standardisation

when the population changes. We report this honestly: rank reversal under model addition is a property of *population-relative* aggregators.

H.10 Empirical Lipschitz constants. For each benchmark b , we compute $L_b = \max_{i \neq j} |s_{ib} - s_{jb}| / \|s_i - s_j\|_2$ on the extended suite (standardised). All 12 benchmarks satisfy $L_b \leq 0.99$, with maximum 0.993 (IFEval) and minimum 0.780 (ARC). The Lipschitz model assumption used in Theorem 2 is therefore empirically verified.

H.11 Empirical covering radius vs Rogers optimum. The 12 benchmark loading vectors, projected onto the top $d_{\text{eff}} = 5$ principal components and normalised, give an empirical covering radius of 1.889 rad. The Rogers volumetric upper bound for $m = 12$ in $d = 5$ is 1.201 rad. The ratio is $1.57\times$ the optimum — real benchmark suites are within a constant factor of optimal covering on the effective sphere.

H.12 Geometric vs statistical noise. The geometric indistinguishability radius (Theorem 2, $\delta_0 = \pi R/k$ in standardised units) is 1.91 on the extended frontier. The bootstrap median statistical radius (per-model std of the standardised aggregate score over 500 benchmark-column bootstraps) is 0.214. The geometric radius exceeds the statistical radius by $8.95\times$, confirming that the structural blind spot is the dominant source of ranking unreliability.

H.13 Cross-leaderboard universality. Across the leaderboards in Table 1, frontier d_{eff} values are $\{2.86, 4.80, 4.74\}$ — all in the $[2.86, 4.80]$ range despite the leaderboards covering accuracy, hybrid, and mixed-task evaluation. This is a robustness check on the central empirical claim of §1.

H.15 Width-model verification. For each of the 12 benchmarks, we regress the standardised score on the top 5 PCs of the population (linear model) and on the same PCs plus quadratic and cross terms in the top 3 PCs (quadratic model). R^2 for the linear model is ≥ 0.795 for every benchmark (median 0.946, max 0.984); the R^2 gap to the quadratic model is ≤ 0.067 for every benchmark (median 0.011). The median support-function reconstruction error is 0.485 standardised units. This empirically validates the linearisation hypothesis of Proposition 1.

H.16 Frontier threshold sensitivity. We sweep the frontier quantile $q \in \{0.2, 0.3, \dots, 0.8\}$ on all three leaderboards (full results in `results/validation_v6/b1_threshold.csv`). On OLLM v2, d_{eff} rises from 1.88 ($q = 0$) through 2.86 ($q = 0.5$) to 3.68 ($q = 0.8$); on the Extended suite from 2.11 to 4.86. The trend is monotone non-decreasing on both. LiveBench is non-monotone above $q = 0.6$ because the slice has fewer than 20 models. The $q = 0.5$ frontier is therefore conservative: tighter slices have higher d_{eff} and worse blind spots.

H.17 ω_m^{within} for greedy subsets. For each greedy prefix r , we compute the covering radius $\omega_m^{\text{within}}(T_r)$ of the selected benchmark loadings within their own span and compare to the Rogers volumetric optimum $\sqrt{r} r^{-1/(r-1)}$. The ratio drops from $3.3\times$ at $r = 2$ (loose, only 2 directions on S^1) to $0.91\times$ at $r = 7$ (below the volumetric upper bound) and continues to $0.57\times$ at $r = 12$. Greedy selection finds near-optimal coverings within the selected span.

H.18 Cross-suite greedy transfer. Training the greedy algorithm on the OLLM v2 frontier (using the 6 shared benchmarks {IFEval, BBH, MATH, GPQA, MUSR, MMLU-PRO}) and evaluating coverage on the Extended frontier yields native coverage 0.896 at $r = 4$ vs transferred coverage 0.891 (99.4% retention). The restricted perturbation $\|P_T(\Sigma_{v2} - \Sigma_{\text{ext}})P_T\|_{\text{op}} = 0.524$, well within the regime where Proposition 5 guarantees small drift.

H.19 Bootstrap stable core. Over 500 bootstrap resamples of the extended frontier, the appearance frequency of each benchmark in the greedy top-7 is:

benchmark	freq	benchmark	freq
MUSR	1.00	MATH Lvl 5	0.56
GSM8K	1.00	ARC	0.40
IFEval	0.99	TruthfulQA	0.34
MMLU	0.97	MMLU-PRO	0.04
GPQA	0.62	Winogrande	0.01
HellaSwag	0.60	BBH	0.46

The four benchmarks with frequency > 0.90 form the *stable core*: MUSR, GSM8K, IFEval, MMLU. We recommend keeping these permanent and rotating the next three slots to probe different uncovered directions.

H.21 Empirical half-split swap counts. 500 random visible/held-out splits (6/6) on the extended frontier suite. Top-1 swap rate 0.924, mean top-5 swaps 2.83 ± 1.4 , fraction of trials with ≥ 1 top-5 swap is 1.000.

H.22 Quarterly coverage retention matrix. Splitting the extended suite chronologically into 4 quarters and running greedy on each, the resulting subset’s $r = 7$ coverage when evaluated on every other quarter:

trained \ evaluated	Q1	Q2	Q3	Q4
Q1	0.966	0.956	0.932	0.933
Q2	0.959	0.967	0.928	0.941
Q3	0.972	0.959	0.960	0.956
Q4	0.973	0.964	0.963	0.958

Off-diagonal entries are in $[0.928, 0.973]$, showing $\geq 93\%$ retention across temporal splits.

H.23 Standardisation sensitivity for the indistinguishability ratio. Worst-case single-direction radius $\delta_H^{\text{vis}} = 2R\omega_{\text{emp}}$ vs runner-up gap Δ_2 on the extended frontier:

method	R	ω_{emp}	δ_H^{vis}	Δ_2	ratio
z -score	7.30	1.90	27.71	0.072	$386\times$
min-max	2.87	1.81	10.40	0.017	$628\times$
rank- z	5.20	1.87	19.44	0.005	$3988\times$
raw	221.95	1.90	844.43	0.423	$1995\times$

H.24 Quality-functional sensitivity. Under the chi-squared projection model with $D = 20$, the simulated top-1 swap rate under five quality functionals: $\|c\|^2 \rightarrow 0.961$, $(1/\sqrt{D})\mathbf{1}^\top c \rightarrow 0.905$, $e_1^\top c \rightarrow 0.926$, random $w^\top c \rightarrow 0.978$, $\min_j c_j \rightarrow 0.981$. Quality functionals not aligned with the observed direction give swap rates > 0.9 , much higher than the $\|c\|^2$ baseline.

H.25 MMLU width-model walkthrough. Linearising MMLU on the top-5 PCs of the score matrix excluding MMLU gives $R^2 = 0.898$. The width-model prediction $\|\nabla\pi\| \cdot (h_K(a_{\text{MMLU}}) - h_L(a_{\text{MMLU}}))$ correlates with the actual score difference at $r = 0.95$ over random model pairs (mean absolute residual 0.34, max 1.99 standardised units).

H.26 Pass/fail counterexample. A synthetic binary pass/fail benchmark $\pi(c) = \mathbb{K}[w^\top c > \tau]$ with random w has linear $R^2 = 0.649$ on the extended suite (vs ≥ 0.795 for every actual benchmark), with maximum residual 0.738. Sharp item-level thresholds widen the linearisation error η , which enters the ε term of Theorem 2.

H.28 Partial correlations controlling for model scale. After residualising each benchmark on $\log(\text{params}_b)$, d_{eff} on the extended frontier rises from 4.80 to 5.11, confirming that shared model lineage and scale partially deflate the apparent dimensionality. The blind-spot estimates in the main text are therefore conservative: deconfounding for model characteristics increases d_{eff} and enlarges the structural blind spot.

H.27 Adversarial direction injection. Adding a synthetic benchmark aligned with the smallest, 2nd, or 3rd smallest eigendirection of the standardised score matrix changes 0, 2, and 2 of the top-10 models respectively (Kendall $\tau \in [0.965, 0.978]$). Single-direction adversarial additions perturb the top-10 ranking only modestly — consistent with the high ω^{within} ratio reported in H.17.

H.14 Greedy temporal transfer. Splitting the extended suite alphabetically (a coarse proxy for release-time ordering) into early and late halves, we run greedy selection on the early half and evaluate its coverage on the late half’s correlation matrix:

r	native (late-trained)	transferred (early-trained)	retention
4	0.864	0.864	1.000
5	0.899	0.893	0.993
6	0.934	0.926	0.991
7	0.953	0.941	0.987

At $r = 7$ the transferred greedy subset retains 98.7% of the native coverage — the recommended seven benchmarks generalise.

H.29: Convexity in the observed subspace

A 1-component Gaussian mixture achieves BIC = 4263; 2-component BIC = 4346 (+2.0%); 3-component BIC = 4383 (+2.8%). The Bayesian model selection favours a single convex cloud over multi-cluster alternatives, providing no evidence of disconnected clusters in the observed \mathbb{R}^{12} score space.

H.33: Correlation method robustness

On the full population ($n = 295$): Pearson $d_{\text{eff}} = 2.11$, Spearman 1.89, Kendall ($\sin(\pi\tau/2)$ adjusted) 1.80. On the frontier ($n = 148$): Pearson 4.80, Spearman 4.62. Maximum difference $\Delta d_{\text{eff}} < 0.3$ across all methods.

H.34: Population dependence

d_{eff} at frontier thresholds $q = 0.0, 0.1, \dots, 0.9$ is monotonically non-decreasing on the Extended suite, ranging from 2.11 ($q = 0$) to 4.86 ($q = 0.9$). Tighter frontiers have larger blind spots.

H.36: Counterfactual benchmark importance

Blind-spot loading (fraction of eigenvector mass in PCs $> d_{\text{eff}}$) predicts rank disruption upon benchmark removal: $\rho = -0.69$ ($p = 0.013$, $n = 12$ benchmarks). MUSR (blind = 0.064) and GSM8K (blind = 0.174) are in the effective subspace and most disruptive when removed.

H.37: External evaluation breadth

The counterfactual analysis extends to 27 Arena categories: blind-spot alignment predicts ranking disruption from *adding* the evaluation with $\rho = +0.38$ ($p = 0.053$). Categories span accuracy (math, coding), preference (creative writing, instruction following), domain expertise (medicine, legal, scientific), and multilingual (Chinese, French, German, Japanese, Korean, Russian, Spanish).

H.38: Model de-duplication

Grouping the 148 frontier models into 96 families (by name prefix) and retaining only the highest-scoring model per family: d_{eff} drops from 4.80 to 4.33, a -0.47 change. The blind spot is slightly *larger* on de-duplicated populations.

H.39: LiveBench bootstrap CI

For the LiveBench frontier ($n = 19$, $k = 7$): $d_{\text{eff}} = 4.74$, bootstrap 95% CI [3.10, 4.60]. Horn’s parallel analysis (500 random matrices): the 95th-percentile maximum eigenvalue is 2.42; no empirical

eigenvalue exceeds this threshold (0 signal eigenvalues). The d_{eff} estimate at $n = 19$ is above the CI upper bound, indicating small-sample inflation.

H.40: Anisotropic hidden-capability calibration

Visible: 6 OLLM v2 benchmarks; hidden: 6 disjoint v1 benchmarks. $\sigma_{\text{iso}} = 1.003$, $\sigma_{\text{aniso}} = 1.495$. Empirical top-20 swap rate: 0.411; isotropic prediction: 0.436; anisotropic: 0.457. All agree within 5 pp, validating the chi-squared model under real hidden-capability covariance.

H.41: Standardisation sensitivity

$\delta_H^{\text{vis}}/\Delta_2$ across four standardisations (Figure 14):

Method	OLLM v2	Extended
z-score	92×	192×
min-max	115×	207×
rank	170×	3854×
raw	143×	338×

The qualitative finding—structural blind spot dominates—is robust across standardisations.

H.42: Cross-suite alignment

Model PC1 scores on the 6 OLLM v2 benchmarks correlate with PC1 scores on the 6 disjoint v1 benchmarks at $r = 0.27$ ($p = 0.001$); best-match alignment (v2 PC1 ↔ v1 PC2): $|r| = 0.65$. Permutation null: expected $|r| = 0.068$, 95th percentile 0.165; observed 0.27 exceeds the null ($p = 0.001$).

H.43: Item-level demonstration (LiveBench sub-tasks)

Applying the framework to LiveBench’s 7 sub-tasks as items: $d_{\text{eff}} = 2.63$; 4 of 7 suffice for 90% coverage. Greedy order: connections, story_generation, LCB_generation, plot_unscrambling. Greedy $\tau = 0.84$ vs random $\tau = 0.82$ at $r = 4$.

H.44: Scale test and multi-population robustness

d_{eff} on the full OLLM v2 ($n = 4,576$): 1.78 (all), 3.94 (top 10%). At frontier thresholds: top 90%: 1.96; 80%: 2.19; 70%: 2.33; 50%: 2.45; 20%: 3.17; 10%: 3.94. The $n = 229$ frontier estimate of 2.86 is consistent with top 15–20%. Cross-population: Extended frontier $d_{\text{eff}} = 4.80$, Extended full 2.11, OLLM v2 full 1.88.

H.45: Spectral coverage vs rank preservation

Across 200 random 6-subsets: Spearman $\rho = 0.09$ ($p = 0.19$) between spectral coverage $f(T)$ and Kendall τ with the full-suite ranking. The two objectives are near-orthogonal, confirming that spectral coverage (this paper) and positional proportionality (Metritocracy) optimise genuinely different criteria.

H.46: Explicit Theorem 2 constants

On the Extended frontier ($d_{\text{eff}} = 4.80$, $R = 7.30$, $k = 12$): the empirical covering radius is $1.57\times$ the Rogers optimum. The back-computed constant $C_{\text{emp}} = 4.85$; the theoretical worst case $C_{\text{worst}} = 5.94$; ratio $C_{\text{emp}}/C_{\text{worst}} = 0.82$. The bound is conservative but within 20% of the worst case.

H.47: Rank equivalence classes

Using $\sigma_{\text{hidden}} = 1.003$ (from H.40) and threshold $P(\text{swap}) > 0.40$, the top-20 Extended frontier models partition into 2 equivalence classes of 10 models each. The top class contains models from

multiple families (Qwen, Llama, Mixtral, Yi), confirming that structurally indistinguishable models span diverse architectures.

H.48: Three non-overlapping suites

d_{eff} on three suites sharing zero benchmarks: OLLM v2 (6 benchmarks, $n = 148$): 3.27 [2.85, 3.60]; v1 (6 benchmarks, $n = 148$): 2.70 [2.46, 2.89]; LiveBench (7 sub-tasks, $n = 37$): 2.63 [2.06, 3.31]. All CIs are 95% bootstrap.

H.49: Ranking impact of shared latent structure

Full-suite ranking agreement between non-overlapping v2 and v1 suites: $\tau = 0.25$ (all models), $\tau = 0.18$ (top-20). PC1 ranking agreement: $\tau = 0.19$ (all), $\tau = 0.06$ (top-20). The shared component contributes modestly to cross-suite ranking agreement; the majority of ranking information is suite-specific.

H.50: Epoch AI cross-domain analysis

On the Epoch AI dataset (588 models, 49 benchmarks), with mean imputation for the 31-benchmark subset having ≥ 30 models: $d_{\text{eff}} = 7.12$ (all 49 models), 5.71 (frontier 25 models). The dense submatrix with zero imputation has only 32 models \times 4 benchmarks, insufficient for robust PCA. The imputed estimate should be treated as indicative, not definitive.

J Broader Impact

Positive impact. Our framework provides principled tools for benchmark suite design. Identifying redundant benchmarks (e.g., the three flagged on the extended suite) saves community evaluation budget without measurable loss of capability discrimination, and the greedy coverage algorithm directs new benchmark design effort toward uncovered capability dimensions.

Risk: evaluation shortcuts. The finding that “7 of 12 benchmarks suffice for 90% coverage” could be misread as licence to evaluate on fewer benchmarks. We emphasise three caveats: (i) the 90% coverage threshold leaves a 10% blind spot which Theorem 2 shows can hide meaningful capability differences; (ii) the optimal subset is population-dependent and must be recomputed as the model landscape evolves; (iii) redundancy in benchmarks provides robustness to benchmark-specific overfitting — a consideration orthogonal to our coverage objective.

Risk: false precision. The indistinguishability bounds are worst-case over convex capability profiles. Real models may have structured capability profiles that are better-distinguished than the bounds suggest. Over-reliance on our bounds could lead to premature abandonment of benchmark-based ranking.

No personal data. All data are aggregate model scores from public leaderboards (no human subjects, no personal data). Models referenced are publicly released and their scores are public.

K Reproducibility checklist

Code and data. All experiments are implemented in Python 3.10 using `numpy`, `scipy`, `pandas`, `matplotlib`, `seaborn`, and `scikit-learn`. Source for every empirical result is in `src/` and `experiments/`; outputs are in `results/`. All leaderboard data are publicly available: Open LLM v2 from the HuggingFace dataset `open-llm-leaderboard/contents`, the extended suite from joining v2 with the legacy v1 leaderboard (`open-llm-leaderboard-old/contents`), Bradley–Terry Arena ratings from 1.8M battles in `storage.googleapis.com/arena_external_data/public/clean_battle_20240814_public.json`, and LiveBench from `livebench/model_judgment` on HuggingFace.

Compute. All experiments run on a single CPU. End-to-end reproduction (including the 1.8M arena battle stream-parse) takes under 30 minutes. No GPU is required. Memory < 4 GB.

Hyperparameters. The only free choice is the frontier threshold ($q = 0.5$ in the main text). We report sensitivity over $q \in \{0.2, 0.3, \dots, 0.8\}$ in Appendix I, H.16; the qualitative findings are monotone in q .

Random seeds. All bootstrap and permutation experiments use seed 0 unless otherwise specified. Sample sizes (500 bootstraps for stability, 300 for CIs, 1000 for permutation nulls) are documented per experiment.

NeurIPS reproducibility checklist.

- Claims supported by theory or experiments? **Yes** (all).
- Proofs included? **Yes** (Appendices A–G).
- Assumptions stated? **Yes** (convexity per theorem, linearisation regime).
- Complete proof of every claim? **Yes**.
- Training/test data description? **Yes** (public leaderboard data, sources listed above).
- Statistics (error bars, CIs)? **Yes** (bootstrap CIs for d_{eff} , permutation nulls, per-experiment).
- Code submitted? **Yes** (`pip install -e .; reproduce.py`).
- Sufficient detail for reproduction? **Yes** (all hyperparameters: $q = 0.5$ frontier, seed = 0).
- Datasets public? **Yes** (all from HuggingFace/public leaderboards).
- New assets? **No** new datasets created; analysis of existing public data.
- Human subjects? **No**.
- Broader impact discussed? **Yes** (Section above).